Isis Galia Zazueta Martinez

Modelling vortex-induced vibrations with a single wake oscillator coupled to both cross-flow and in-line motions

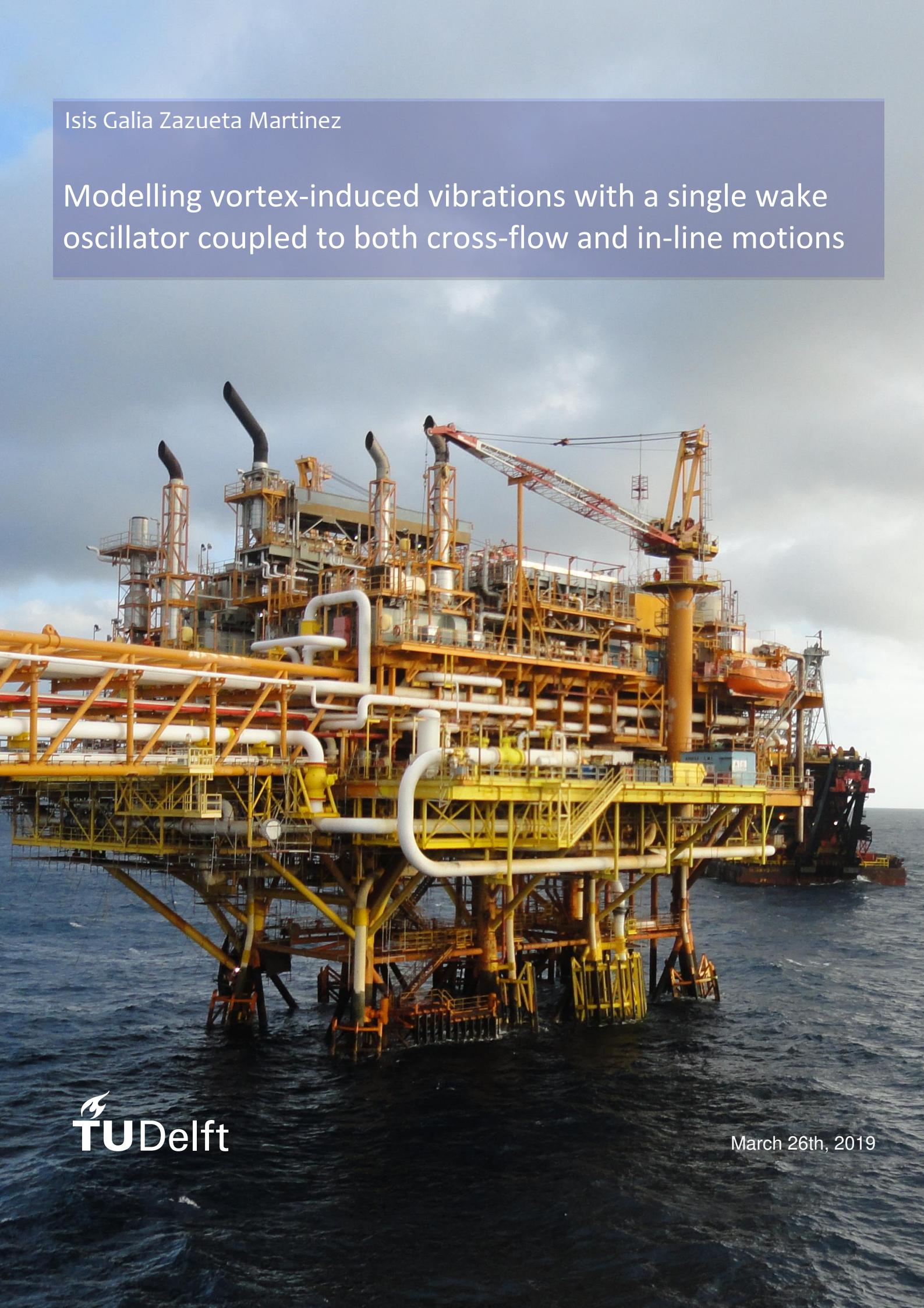

TU Delft

March 26th, 2019

Picture: Marine Platform in the Gulf of Mexico: E-KU-A2.
Photographer: I.G. Zazueta Martinez.
Date: 10/September/2014.

Modelling vortex-induced vibrations with a single wake oscillator coupled to both cross-flow and in-line motions

By

Isis Galia Zazueta Martinez

in partial fulfilment of the requirements for the degree of

Master of Science
in Offshore and Dredging Engineering

at the Delft University of Technology,
to be defended publicly on Tuesday March 26th, 2019 at 1:00 PM.

Thesis duration:	April 20th, 2018 - March 1st, 2019	
Thesis committee:	Prof. dr. A. Metrikine,	TU Delft – Chairman
	MSc. Yang Qu	TU Delft – Thesis Supervisor
	Dr. ir. K.N. van Dalen	TU Delft

An electronic version of this thesis is available at http://repository.tudelft.nl/.

March 26th,2019

TU Delft CONACYT Consejo Nacional de Ciencia y Tecnología SENER SECRETARÍA DE ENERGÍA

Preface

This thesis is about vortex induced vibration also known as VIV. VIV is a phenomenon very common in engineering. It can cause severe problems to the structures because it amplifies the amplitude of the movement in the structure, and the frequency of oscillation can cause fatigue in the structure.

This master thesis goes deeper in different ways of modelling VIV. It is especially focus on the wake oscillator model coupled to both cross-flow and in-line motions.

This report is written in a way that tries to clarify doubts to the not so expertise students in VIV phenomenon, and to those who want knowledge for the beginning of their research in modelling VIV.

Isis Galia Zazueta Martinez
Delft, March 2019

If you can't explain it simply, you don't understand it well enough.
Albert Einstein

Acknowledgements

The conclusion of my studies at TU Delft would not be possible without the support of my family: my mom Malenita, my dad Evaristo, my brother Nadir and my partner Felipe, who had the courage to come to the Netherlands leaving our life in Mexico.

Gracias papás por no cortarme las alas, y dejarme volar. Nadir gracias por tu apoyo sin titubeo. Y Felipe gracias por todo lo que me has dado.

Furthermore, I would like to thank to CONACYT and SENER, because with their trust and support I was able to study at TU Delft.

Also, I would like to thank to my daily supervisor Yang Qu and to the prof. A. Metrikine for their support and patience with my doubts.

Isis Galia Zazueta Martinez
Delft, March 2019

Index

Chapter 1

Introduction

Vortex-induced vibration (VIV) is a phenomenon that has attracted the attention of many researchers, especially during the last three decades. The reason for this is that this phenomenon may lead to significant fatigue of various structures. Until the present day the phenomenon is not completely understood, despite of significant theoretical effort and various experiments performed during the last decades.

One of the analytical models used to predict the VIV is a wake oscillator model, this thesis is focused upon. For this type of modelling the following questions have no clear answers as yet. For example, it is not fully clear what the effect of a low mass damping ratio on the amplitude of vibration in the cross-flow direction. Is it justified to use only the mean drag coefficient in the modeling?

The aim of this thesis is to improve the understanding of VIV by means of focusing on the motion in the streamwise direction of an elastically mounted rigid cylinder and on its effect on the cross-flow vibrations.

In this chapter, the problem statement, the research objective, the methodology, and the thesis outline are given.

1.1. Problem Statement

VIV occurs in many engineering fields. In the offshore industry, it is of importance for risers that extract oil from the subsoil, and tethered anchors for floating units, just mentioning some applications.

An impressive number of experimental investigations have been performed in the past. Most of those investigations, however, were focused on the crossflow vibrations as in Blevins&Coughran (2009). Much less attention has been paid to the motion in the streamwise direction and its coupling with the cross-flow motion.

Some models have been used for modeling the coupled in-line and cross-flow VIV. This has also been done with the help of the wake oscillator model. However, the underlying assumption in the earlier applied modelling is that the drag coefficient is assumed to keep to its static value, something that is not in agreement with the experiments.

In this thesis, the focus is placed on investigation the advantages and limitations of the recently proposed modified wake oscillator model by Yang Qu (2019).

1.2. Research Objective

In the recently proposed by Yang Qu wake oscillator model, a new coupling term is introduced in the wake equation of motion. The objective of this thesis is to investigate the performance of the new wake oscillator and compare its predictive capabilities with those of the wake oscillator model by Ogink and Metrikine (2010) which has a more simplistic description of the wake coupling.

In order to achieve the above-formulated objective, the following questions need to be answered:

- Do the new model results match the experimental results in terms of amplitude and lock-in range of reduced velocities?
- Does this model bring more advantages than drawbacks in comparison with the wake oscillator model by Ogink and Metrikine, 2010?
- Does this model capture any new physics?
- What is the sensitivity to the tuning parameters in the new model?

1.3. Research Steps

With the goal of obtaining a solid base to understand the VIV phenomena and being able to study it and perform a sound modelling, the following steps are taken:

1. Literature research on experimental research on a supported rigid cylinder forced and free oscillating experiments with and without constraints in the cross-flow direction.
2. A literature review of articles that report on the experimatal findings relevant for this thisis, such as, for example, Williamson and Govardhan (2004).
3. Implementation of Forced van der Pol oscillator model, to have a deeper understanding of the basis on how VIV models work.
4. Implementation of wake oscillator model by Ogink and Metrikine for free oscillating experiments.
5. Implementation of the modified wake oscillator model (Y. Qu, 2019) for free oscillation test.
6. Implementation of the modified wake oscillator model (Y. Qu, 2019) for forced experiments.
7. Execution of a sensitivity analysis with respect to the tuning parameters.
8. Investigation of how the external variables influence predictions of the model.
9. Making final conclusions.

1.4. Thesis Outline

The structure of the thesis is as follows.

Chapter 1: General outline

Chapter 2: Literature Review.

In this section, different kinds of tests performed in the past are described. Also, some engineering problems caused by VIV are elucidated. Finally, a brief summary of the major observations available in the literature is given.

Chapter 3: Implementation of the van der Pol oscillator model.

The van der Pol oscillator model is explained. In this section, models of a cylinder in free oscillation as well as in forced vibration are described.

Chapter 4: Wake oscillator model.

The equations of motion for cross-flow, in-line and wake variable are explained. In this section, some comparisons with experimental data are performed.

Chapter 5: Wake oscillator model with coupling term for in-line motion.

In this chapter, a coupling term is added to the wake oscillator model. The implementation and equations of this new model proposed by Qu (2019) are explained. In this section, the model is implemented for forced oscillation experiment as well as for free oscillation experiments.

Chapter 6: Sensitivity Analysis.

In this part, the model sensitivity to its parameters is checked. And how experimental data influenced in the model.

Chapter 7: Conclusions and Recommendations

Chapter 2

Background

In this chapter, the physics of the Vortex-induced vibration phenomenon is discussed. Also, the most frequently experiments are described: Forced vibration experiments, free oscillation experiments.

Moreover, in this chapter, some auxiliary equations, and basic concepts to understand and model the VIV phenomenon are explained. Furthermore, some examples of VIV phenomenon in daily life are mentioned.

The aim of this chapter is getting familiarized with the VIV phenomenon in order to continue with the implementation of some model in future chapters.

2.1. Physics of the Vortex Induced Vibrations phenomenon

Imagine you have a fluid with certain current velocity; it could be water, air, any fluid. Then, there is a rigid cylinder elastically supported in the current.

Figure 2. 1 Rigid cylinder elastically supported in the current

Taking a 2-dimension plane x'-y'. As the constant flow velocity increases, the cylinder will vibrate in both directions x' and y'. The force in the stream-wise direction (in this case the x'-direction or in-line direction) is known as drag force. The force in the cross-flow direction (in this case y'-direction) is known as lift force.

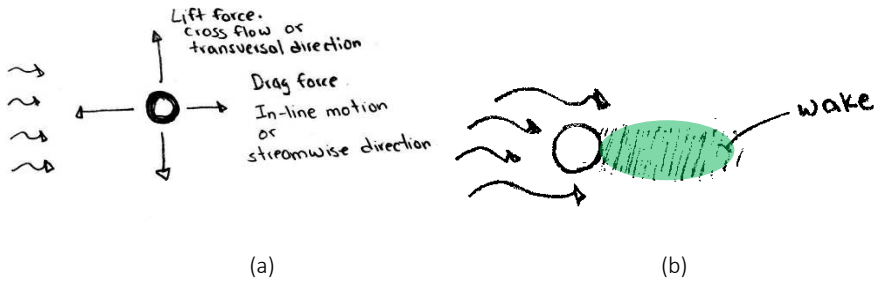

(a) (b)

Figure 2. 2

Now, some definitions:

Drag force. The viscosity and the fluid velocity will cause fluid separation on the part behind the cylinder (green shadow part) Fig. 2.2b. The latter will cause vortices, and those will cause a vacuum that will pull the cylinder in the streamwise direction. This force is called the drag force.

Lift force. In the lateral sides (marked blue points), the higher velocities in the wall of the cylinder are reached. Fig. 2.3a. According to the Bernoulli equation, the pressure on those points will descent to its minimum. And this will cause movement in the cross-flow direction. This force is known as lift force.

(a) (b)

Figure 2. 3

As mentioned before, it will be a fluid separation in the green shadow part (wake). In this part vortices will be created, the alternated frequency of the creation of these vortices is also known as shedding frequency (f_s). The pressure distribution in the cylinder changes with the creation of the vortices. Thus, a vortex force is created as the result of the pressure distribution on the surface of the cylinder. See Fig. 2.4

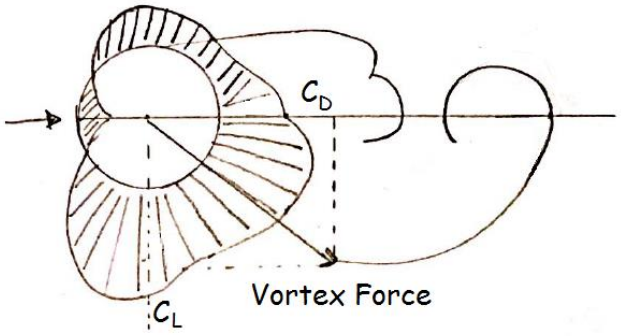

Figure 2. 4 Pressure distribution based on a figure by Ogink & Metrikine,2010. It shows the drag and lift components of the vortex force. The vortex force has resulted from the fluctuating pressure distribution on the surface of the cylinder.

In Fig. 2.5 we can see the parts of the wake.

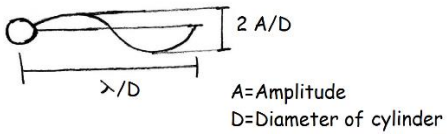

Figure 2. 5

Vortex Induced Vibration. Normally, the vortex shedding follows the Strouhal relation. When the shedding frequency reaches the natural frequency of the system (f_n), resonance happens, thus $f^* \approx f_s/f_n \approx 1$. Thus, energy is transferred to the structure from the wake. Leading to large amplitudes of vibrations. The shedding frequency remains the same, this is known as "lock-in". Furthermore, the shedding frequency no longer follows the Strouhal relation, also this will happen over a wide range of flow velocities. This regime is called Vortex Induced Vibration (VIV).

2.2. Auxiliary equations for modeling the VIV phenomenon

Some of the following concepts will look redundant to the reader; however, the author considers them important to get a better understanding of this thesis.

Radial frequency or angular frequency is the frequency that is measured in angles, and in terms of Pi.

The equations 2.1 show definitions converted to its dimensionless form using the shedding frequency.

(a) $\omega = \frac{2\pi}{T} \quad f = \frac{1}{T}$

$\omega = 2\pi f$

(b) $V_n = \frac{V}{D \cdot f_n} \rightarrow f_n = \frac{V}{V_n \cdot D}$

(c) $st = \frac{f_s \cdot D}{V} \rightarrow f_s = \frac{st \cdot V}{D}$

(d) $\Omega_n = \frac{\omega_n}{\omega_s} = \frac{2\pi f_n}{2\pi f_s} = \frac{\frac{V}{V_n \cdot D}}{\frac{st \cdot V}{D}} = \frac{1}{V_n \cdot st}$

(e) $\Omega_n = \frac{1}{V_n \cdot st}$

(f) $m^* = \frac{m}{\pi \rho D^2 L/4}$

Eq. 2. 1

ω: Radial frequency (rad/s)

T: Period [s]

st: Strouhal number

V_n: Reduced velocity [dimensionless]

f_i: Frequency of i, "i" can be referred to any term. [Hz]

V: Flow velocity [m/s]

f_n: Body oscillation frequency or natural frequency

D: Diameter of cylinder [m]

f_s: Shedding frequency [Hz]

Ω_n: Dimensionless natural frequency

ω_n: Radial frequency of the system

ω_s: Radial shedding frequency

m^*: Dimensionless structural mass

m: Structural mass

ρ= Density of fluid [kg/m^3]

L= Length of the cylinder [m]

2.3. Previous Experimental Research

We can see in our daily life this phenomenon. But how does it work?

Some experiments have been conducted by researchers, one of the first ones was Feng (1968), that conducted experiments for an elastically mounted cylinder. Where the relative density ($m^* \sim 250$) was

very large because the experiments were conducted in air. In this thesis, the focus will be in modeling for lower mass and damping ratios as it happens in fluids like water.

In order to analyze VIV engineer trust in semi-empirical models. These models are based on phenomenological modeling. Mainly two kinds of experiments are usually performed: forced vibration experiments and free oscillation experiments.

2.3.1. Forced vibration experiments

In the forced vibration experiments, a rigid cylinder inside of a fluid with constant velocity is forced to vibrate harmonically with a certain amplitude and within a range of frequencies. Then, the forces are measured and decomposed in two parts: the part in phase with the cylinder acceleration and the part in-phase with the cylinder velocity. This is done in chapter 5 of this document. For more information about forced oscillation experiments read Nishihara (2005).

An equation of motion of a system with damping, stiffness. It is as follows:

$$M\ddot{s} + c\dot{s} + ks = F \qquad \text{Eq. 2. 2}$$

Where M is the structural mass, d is the structural damping, k is the stiffness and F the fluid force. In a forced vibration experiment, the displacement s and its derivatives with respect to time are known. For this document, s can be in the cross-fluid direction or in the in-line direction.

$$s = s_0 \sin(\omega t) \qquad \text{Eq. 2. 3}$$

$$\dot{s} = s_0 \cos(\omega t)\omega \qquad \text{Eq. 2. 4}$$

$$\ddot{s} = -s_0 \sin(\omega t)\omega^2 \qquad \text{Eq. 2. 5}$$

where ω is the radial body oscillation frequency, and s_o is the amplitude of oscillation.

While the rigid cylinder is forced to vibrate in one of the directions, cross-flow or in-line, the other direction is restricted.

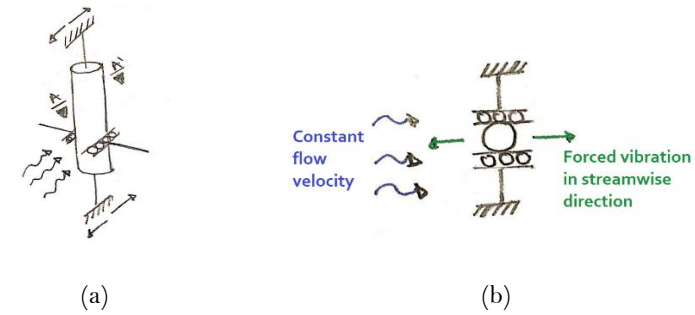

(a) (b)

Figure 2. 6 (a) Model analyzed on a forced oscillation test with forced vibration in the streamwise direction. (b) View A-A'. Model analyzed on a forced oscillation test.

A regular setting is as follows: the fluid is pumped from an underground reservoir to an upper reservoir. The valve is open, the fluid falls with controlled velocity, thanks to the valve and gravity. And a rigid cylinder is forced to move (vibrate) with certain amplitude and frequency, the latter thanks to a crank.

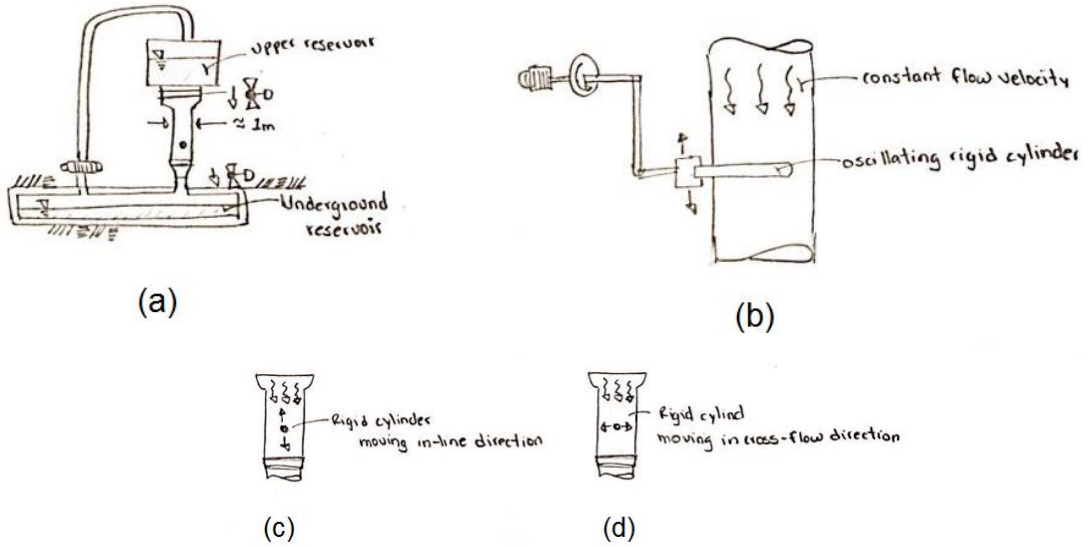

Figure 2. 7 Setting of a typical forced oscillation test.

2.3.2. Free Vibration Experiments

In the free vibration experiments, there is a rigid cylinder elastically mounted inside of a fluid with constant velocity. And one dof of the cylinder is restricted. Then, the displacement of the other dof is measure. From this data, the oscillation frequency can be calculated. This experiment is repeated for a range of different velocities. At the end of the experiment, a graph with a vertical axis with dimensionless amplitude (Y_o/D or X_o/D and in horizontal axis with Vn (relative velocity) is obtained.

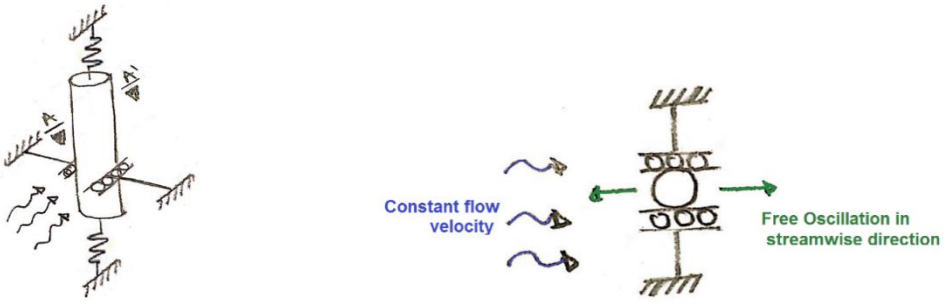

Figure 2. 8 (a) Model analyzed on a free oscillation test. The rigid cylinder is mounted on elastic supports. In this example, only cross-flow vibration is restricted. (b) View A-A'. Model analyzed on a forced oscillation test.

2.3.3. Preliminary Test for Stationary Cylinder

In order to match forced vibration experiments and corroborate results from models, it is important to know how the dynamic system behaves as a stationary cylinder.

So, when the model for forced vibrations in settled, it will be possible to corroborate the results not just with forced vibration experiments, but also with the stationary cylinder.

2.3.4. Other Experiments

Certain wake patterns can be induced by body motion. Brika & Laneville's smoked visualizations show the modes 2S and 2P.

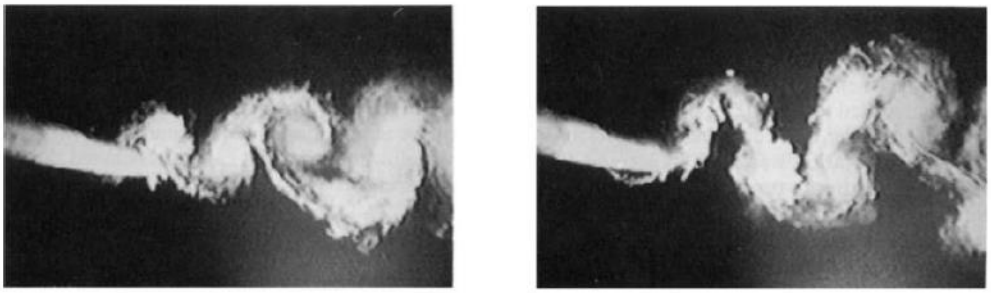

(a) (b)

Figure 2. 9 First smoke mode visualizations by Brika & Laneville's (1995). (a) Mode 2S. (b) Mode 2P.

A pattern can be seen in the creation of this wakes. In figure 2.13 the narrows show the side of the 'creation' of the wake. In mode 2S (s from single), the creation of the vortices is alternated: A, B, A, B…etc. On the other hand, in mode 2P, the vortices creation is in pairs: B, A, A, B, B…etc. See fig. 2.14.

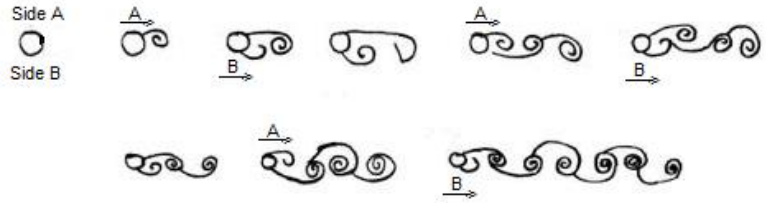

Figure 2. 10 Mode 2S.

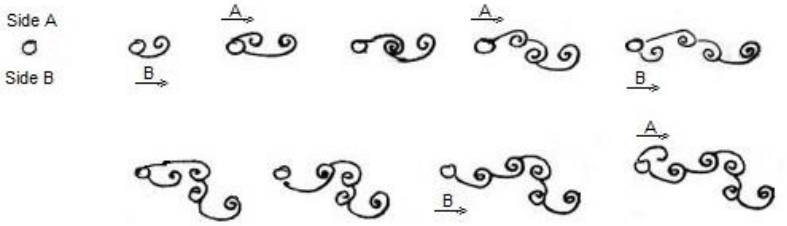

Figure 2. 11 Mode 2P.

During free oscillation experiments by Jauvtis & Williamson (2004). Two amplitude branches were detected. The experiments were conducted for different relative velocities, and they found a jump of behavior. Meaning that in the graph, A (cross flow dimensional amplitude) Vs Vn (Relative velocity). There are two curves. In their terms, they were called the lower branch and the upper branch. In chapter 4 there is more information about this graph. Apart from finding these two branches (Williamson and Roshko, 1988), they found that the mode regimes are relevant to the synchronization regime. See fig 2.15

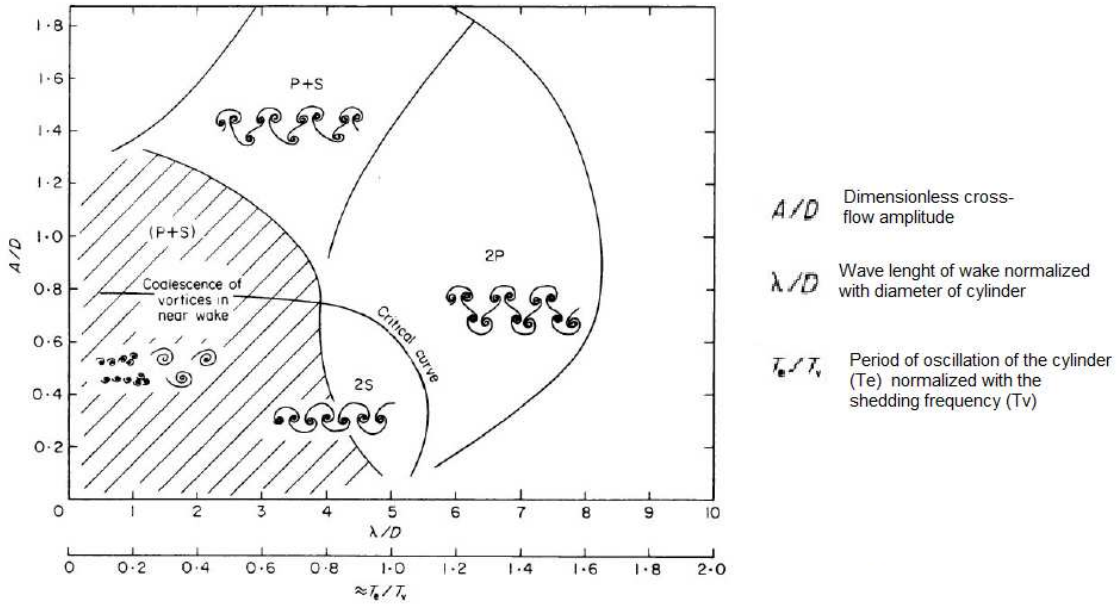

Figure 2. 12 Map for vortex wake modes (Williamson & Rosko, 1988)

Furthermore, Govardhan and Williamson (2000) found that, when there is a jump between the branches, there is also a jump between the modes and in the vortex phase. In chapter 4, some graphs comparing the results from wake oscillator model and the phases are presented.

It has been found that not only the form of the phase changes, also it is interesting to see how the synchronization in terms of frequencies occurs during the lower branch.

2.4. Examples in Engineering

VIV can cause severe consequences in a wide range of structures. Those are from elastically supported systems to pivoted systems or even tethered systems. Fig. 2.6

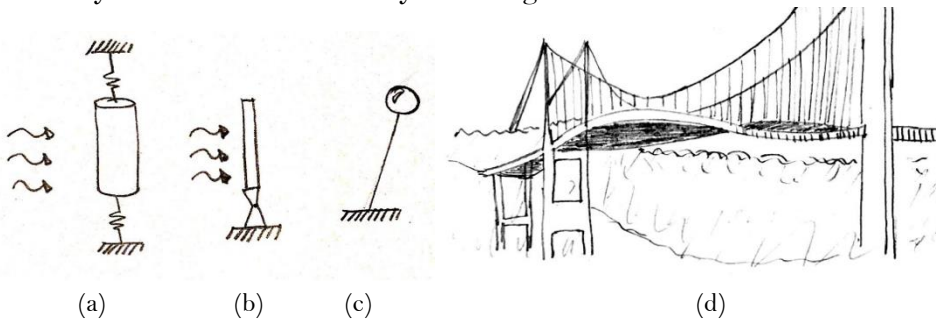

Figure 2. 13 (a) Elastically supported systems. (b) Pivoted systems. (c) Tethered systems. (d) Sketch of the twisted shape of Bridge Tacoma Narrows due to VIV.

One example to remember was the famously known case of the bridge Tacoma Narrows in The USA. That had a dramatic collapse due to VIV induced by the wind. Indeed, in the 1940s there were not many studies of VIV, but from that experience more and more engineers were interested in the phenomenon.

(a) (b)

Figure 2. 14 (a) VIV on a section of the bridge Tacoma Narrows. (b) VIV on a cross-section of the bridge Tacoma Narrows.

VIV is found in common manmade structures, i.e. a simple flag pole, chimneys, tall and thin buildings, wind turbine supports or even risers for marine structures. Or not so common as the prototype breed factor Monjji in Japan, that was damaged due to vibrations on the in-line direction.

In fact, we can see often VIV in our daily life, as in poles for lamps, or even flagpoles in our university.

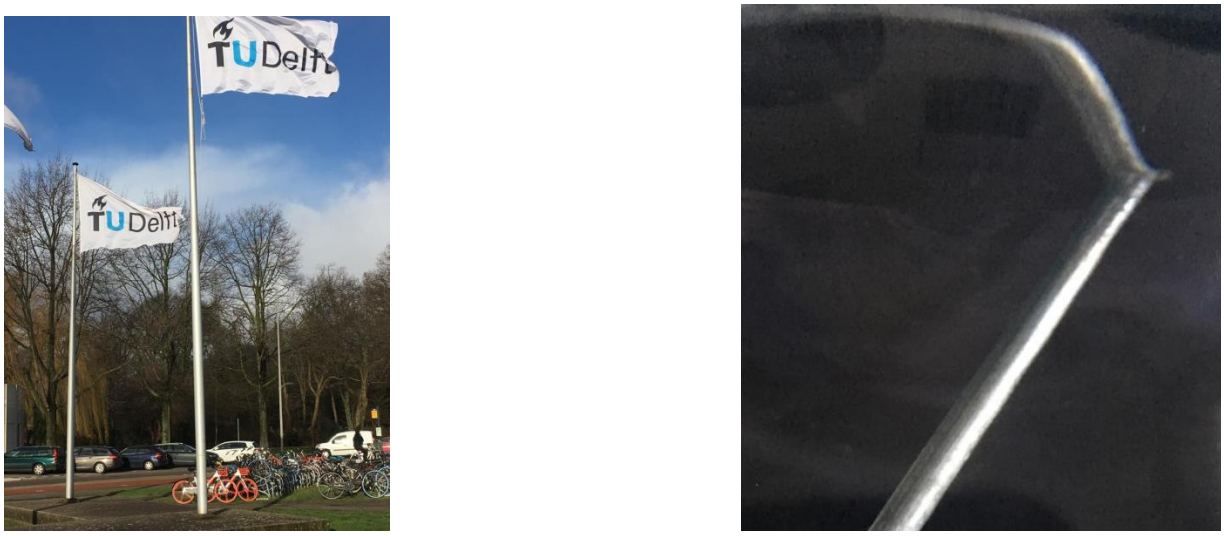

(a) (b)

Figure 2. 15 Examples of VIV in our daily life. (a). A flag pole in TU Delft campus. The flagpole is under different wind velocities. (b) Submerged part of an inclined cylinder in water with constant velocity. In both examples, there are vibrations in both directions x'-y'. Under certain flow velocities, both can get into lock-in regime.

2.5. Comments

The VIV phenomenon is interesting for many engineers who are worried about the fatigue in their structures. It is a phenomenon that has been investigated for many researchers mainly since the last three decades.

In order to explore the phenomenon, some assumptions and simplifications need to be made. Moreover, many types of research have been performed with the goal of understanding not only the amplification of vibration but also the frequency ranges of oscillation and the visualization of the wake behind the cylinder.

Now that we have a basic understanding of the phenomenon, and of the investigation that has been made before, it will be easy to follow the next chapters. In future chapters, the implementation of certain models to investigate the VIV phenomenon is done.

Chapter 3

The van der Pol Oscillator

With the intention of achieving the goal of modeling the VIV phenomenon some steps need to be taken. First, the basic model to describe the VIV phenomenon is explored in this chapter. The complexity of modeling will be increased chapter by chapter.

In order to get familiar with the modeling of the VIV phenomenon in this chapter The van der Pol oscillator is used to investigate two cases:

- The van der Pol oscillator with a forcing term equal to zero.
- The van der Pol oscillator with a forcing term.

Each of the mentioned models describe the equations used, the implementation of the model with the function ODE45 in MATLAB, and comments on the results.

3.1. Model description and equation of the van der Pol oscillator model

Several attempts have been made in the past in order to improve the phenomenological modeling for VIV. One of these is using the van der Pol oscillator model.

A harmonic oscillator is an oscillator that consists of a mass, stiffness, and could have or not damped. The solution of the equation gives an amplitude and an oscillating part, i.e. Â sin(ωt).

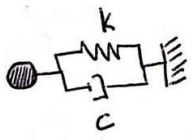

Figure 3. 1 A harmonic oscillator

The equation of the van der Pol oscillator is:

$$\ddot{q} + \varepsilon\omega_s(q^2 - 1)\dot{q} + \omega_s{}^2 q = f(t) \qquad \text{Eq. 3. 1}$$

Where q is the wake variable, ω_s is the shedding frequency and f(t) is the forcing term. The term $-\varepsilon\omega_s q^2\dot{q}$ is the damping of the equation.

$$\ddot{q} + \omega_s{}^2 q = f(t) + \varepsilon\omega_s\dot{q} - \varepsilon\omega_s q^2\dot{q} \qquad \text{Eq. 3. 2}$$

Rearranging the equation (eq. 3.2) it is easier to see that the term $\varepsilon\omega_s\dot{q}$ uses the increase of q, and the term $-\varepsilon\omega_s q^2\dot{q}$ trols the growing.

3.2. The van der Pol oscillator with a forcing term equal to zero

Two issues are explored in this section: the influence of a forcing term equal to zero in the equation of the van der Pol oscillator and how this model can be used to model a fixed rigid cylinder in the current.

This section includes a description and assumptions made for the model, the algorithm and comments on the results.

3.2.1. Model description and equations

In this model the external force is considered equal to zero, f(t)=0. Thus, the van der Pol equation is used as follows:

$$\ddot{q} + \varepsilon\omega_s(q^2 - 1)\dot{q} + \omega_s{}^2 q = 0 \qquad \text{Eq. 3. 3}$$

$$\ddot{q} + \mu_1(q^2 - 1)\dot{q} + \mu_2 q = 0 \qquad \text{Eq. 3. 4}$$

$$\mu_1 = \varepsilon\omega_s \quad \mu_2 = \omega_s{}^2 \qquad \text{Eq. 3. 5}$$

3.2.2. Algorithm

The diagram 3.1 shows the programming algorithm. It works with the codes: 'core.m', 'initial2.m' and 'vdp2.m'. The code of vdp2.m can be found in appendix d.

The main code is core.m, inside this code the code initial2.m is called. In initial2.m the parameters are defined and storage in the arrangement p. After calling the parameters in initial2.m, the equation is called to be solved with the function ode45 with the line [t,y]=ode45(@vdp2,tspan,ini,[],p); . In the code vdp2.m the equation is defined and adjusted to be solved. The equation to be solved in vdp2.m is the following:

```
dydt = [y(2); p.miu1*(1-y(1)^2)*y(2)-p.miu2*y(1)];
```

With the help of the function ode45 the equation in vdp2.m is solved. The function returns a matrix with the solution for q and dq/dt. This matrix is [tn x 2], where tn is the length of the time span.

The code core.m finishes plotting the results.

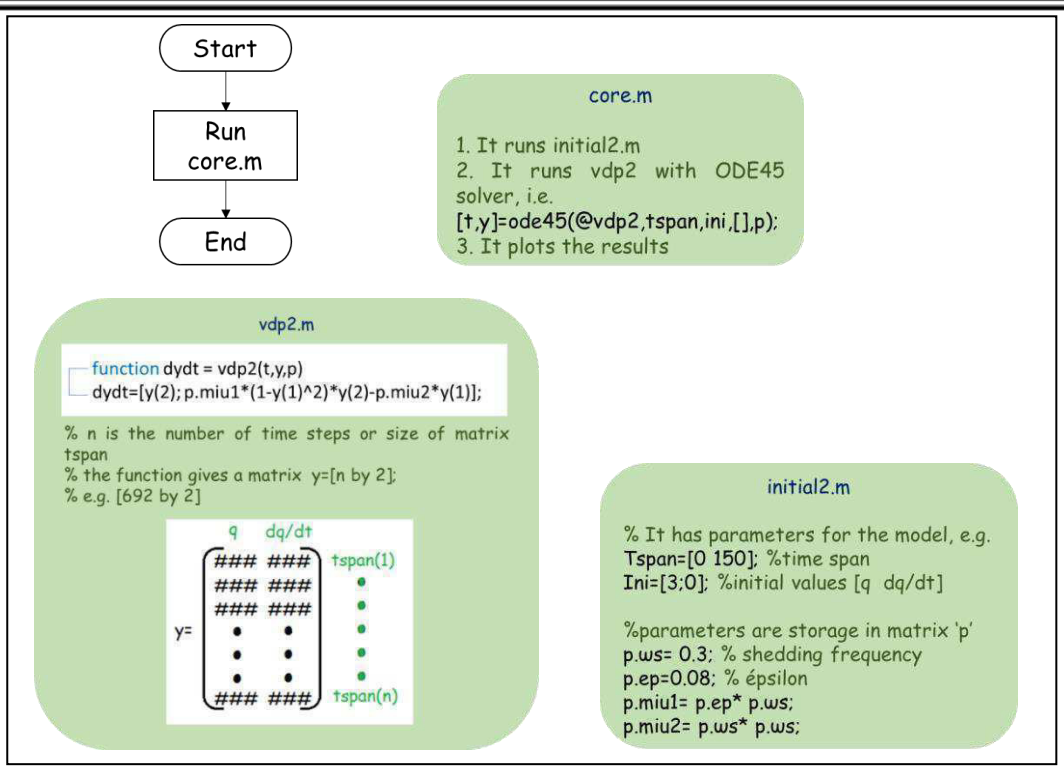

Diagram 3. 1 Algorith for the implementation of The van der Pol oscillator model in MATLAB

3.2.3. Results for the van der Pol oscillator with a forcing term equal to zero

In order to accomplish the goal of a better understanding, this section investigate two cases: one a standard case where we can see the influence of the initial conditions on the response, and other where the influence of epsilon on the response is investigated.

Performance of a standard case

For this case, the equation 3.4 was used. The model used the following parameters: ω_s =0.5; ε = 0.08, initial conditions= [1 0]; time span = (0:0.1:300).

In the figure 3.2a the evolution of q and dq/dt are shown against time. For displacement, the initial value of q is 1, as stated in the initial conditions, also the response looks very harmonic. A steady state is reached after some cycles, at around 170 s with an amplitude of 2. In the case of the velocity, there are similar results, the velocity starts with a value of zero, and it starts increasing until an amplitude of 1 is reached at around 120s.

In the figure 3.2b the phase plane is shown. It can be seen some inner circles, those are formed in the first part of the time series, where the amplitude of q and dq/dt are still increasing and they have not yet reached a steady state. A limit circle shows the oscillating amplitude in a steady-state regime, with q between 2 and -2 and dq/dt between 1 and -1. The phase plane plot is in accordance with the results obtained in figure 3.2a.

The figure 3.2c shows the spectrum normalized with the shedding frequency ω_s. The figure shows that the response is mainly at the shedding frequency.

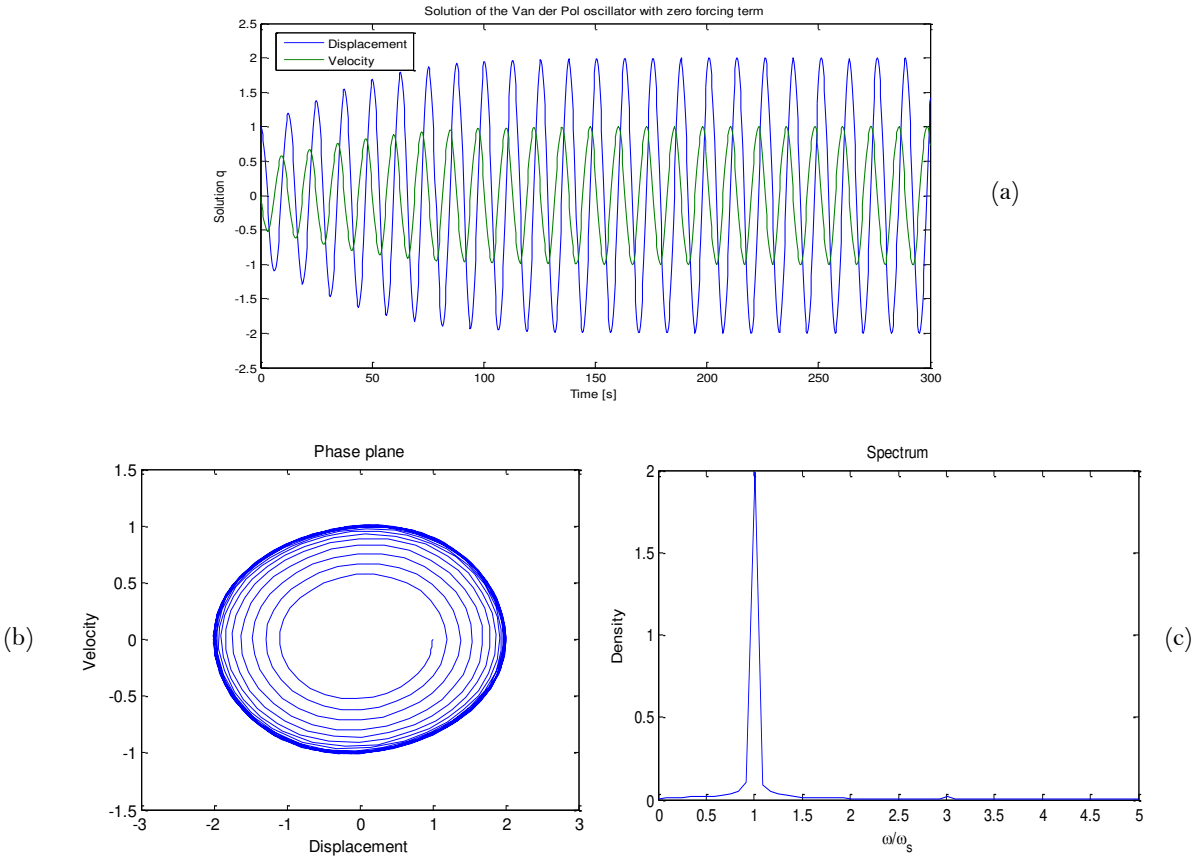

Figure 3. 2 Results for the van der Pol oscillator with a forcing term equal to zero: (a) Graph of q vs Time (b) Phase plane (c) Frequency spectrum

Performance with different ε

In this section the influence of ε in the response is investigated. The, two cases are explored:

- Case 1. Where ε=0.5
- Case 2. Where ε=1

Case 1. In this case the following parameters were used: ω_s =0.5; ε = 0.5, initial conditions= [1 0]; time span = (0:0.1:300).

In the figure 3.3a the evolution of q and dq/dt are shown against time. For displacement, the initial value of q is 1, as stated in the initial conditions. A steady state is reached after some cycles, at around 50 s with an amplitude of 2. In the case of the velocity, there are similar results, the velocity starts with a value of zero, and it starts increasing up to an amplitude of 1, that is reached at around 50s.

In the figure 3.3b the phase plane is shown. The boundary shape shows the oscillating amplitude in a steady-state regime, with q between 2 and -2 and dq/dt between 1.2 and -1.2. The phase plane plot is in accordance with the results obtained in figure 3.3a.

The figure 3.3c shows the frequency spectrum, where frequencies are normalized with the shedding frequency ω_s. In the figure, we can see that there are two peaks one at 1 and other at 3.

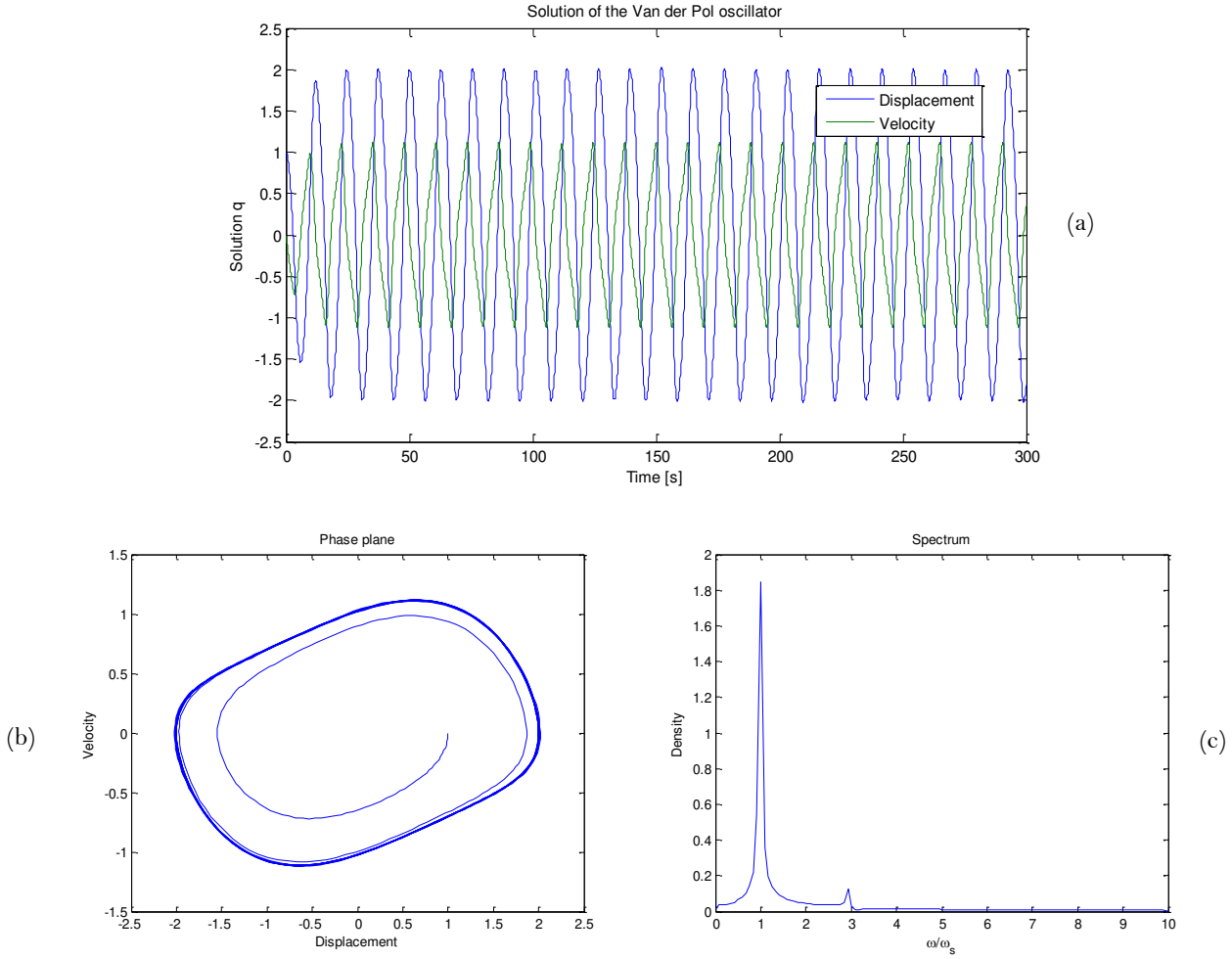

Figure 3. 3 Results for the van der Pol oscillator with a forcing term equal to zero: ε=0.5 (a) Graph of q vs Time (b) Phase plane (c) Frequency spectrum

Case 2. In this case the following parameters were used: ω_s =0.5; ε = 1, initial conditions= [1 0]; time span = (0:0.1:300).

In the figure 3.4a the evolution of q and dq/dt are shown against time. For displacement, the initial value of q is 1, as stated in the initial conditions. A steady state is reached after some cycles, at around 50 s with an amplitude of 2. In the case of the velocity, there are similar results, the velocity starts with a value of zero, and it starts increasing up to an amplitude of 1, that is reached at around 50s.

In the figure 3.4b the phase plane is shown. The boundary shape shows the oscillating amplitude in a steady state regime, with q between 2 and -2 and dq/dt between 1.3 and -1.3. The phase plane plot is in accordance with the results obtained in the figure 3.4a.

In figure 3.4c the frequency spectrum is shown. In the figure, we can see that there are four peaks: one at 1, other at 2.84 another at 4.68 and one at 6.60.

In conclusion, there is possible to say that the epsilon influences in the number of peaks present in the frequency spectrum of the response. Then, with higher values of epsilon, higher the variety of frequencies that contain the response. Or in other words, the response shows different frequency responses.

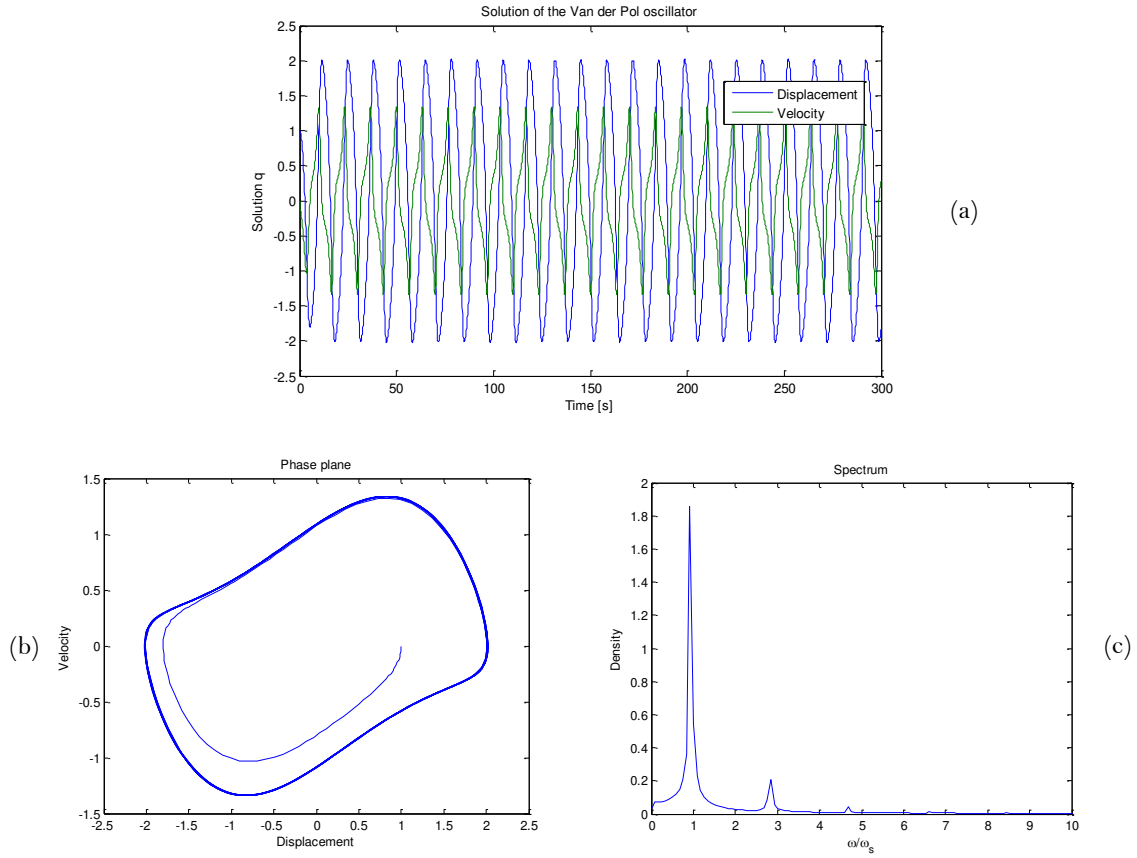

Figure 3. 4 Results for the van der Pol oscillator with a forcing term equal to zero: ε=1 (a) Graph of q vs Time (b) Phase plane (c) Frequency spectrum

3.2.4. Using the van der Pol oscillator to model a fixed cylinder in current

As explained in chapter two, a fixed cylinder in the current is one of the main experiments performed by researchers to analyze the VIV. The equation of the van der Pol oscillator with a zero forcing term can also be used to model a fixed cylinder in the current.

In this section, the modeling of a fixed cylinder in the current using the van der Pol oscillator is explored. First, the model is introduced and the assumptions that allow to use the van der Pol equation for this model are stated.

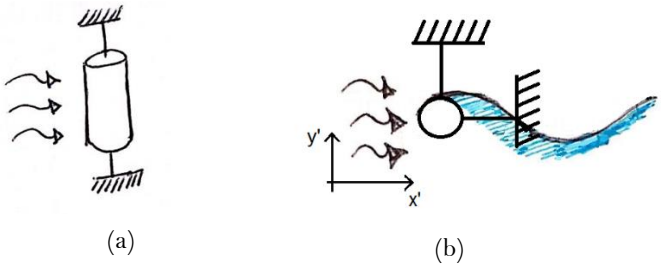

Figure 3. 5 Sketch of a fixed cylinder in the current. (a) Vertical view (b) Plane x'-y'

The model of a fixed rigid cylinder in the current can be seen in three dimensions. In this case as we use a rigid cylinder two dimensions are considered. The model will be based on a plane x'-y'. In this model the undisturbed current comes parallel to the x' axis.

Basically, three assumptions in the van der Pol oscillator model need to be considered in order to model a fixed cylinder in the current:

1. There is a constant flow velocity.

2. Normally, three equations of motion, should be used: for vibration in x' direction, for vibration in y' direction and for the wake variable. The cylinder is restricted in cross-flow direction (y) and in streamwise direction (x). Then the displacements x=0, and y=0. Thus, there is no equation of motion in those two directions.

3. The wake is modelled by the van der Pol equation. The amplitude of the wake and the lift force is influenced by the motion of the cylinder. However, in this case there is no movement of the cylinder, then the external force can be considered zero, f(t)=0.

$$\ddot{q} + \varepsilon\omega_s(q^2 - 1)\dot{q} + \omega_s{}^2 q = 0 \qquad \text{Eq. 3. 1}$$

As seen above, after these three assumptions the equation of the van der Pol oscillator with a zero forcing term can be used also to model a rigid fixed cylinder in the current.

3.3. The van der Pol oscillator with a forcing term

In the last section the model with a zero forcing term was investigated, In this section, the performance of the van der Pol oscillator with a forcing term is explored.

This section includes a model description and the terms used in the van der Pol equation, the implementation to solve the equation with the help of the function ODE45 in MATLAB, and some comments on the results.

3.3.1. Model description and equations

The van der Pol oscillator equation is:

$$\ddot{q} + \varepsilon\omega_s(q^2 - 1)\dot{q} + \omega_s{}^2 q = f(t) \qquad \text{Eq. 3. 6}$$

Where:

$$\mu_1 = \varepsilon\omega_s \quad \mu_2 = \omega_s{}^2 \qquad \text{Eq. 3. 7}$$

The forcing term f(t) could be have any signal, however all the signals can be represented by a sum of sine signals. Therefore the term f(t) will be equal to $\hat{c}\sin(\omega_f t)$, where $\hat{c}$ is the amplitude of the force and $\sin(\omega_f t)$ is the oscillating part with ω_f as the radian frequency of the force oscillation.

3.3.2. Algorithm

The algorithm used is the same as the one used in Diagram 3.1. But the equation to be solved in vdp2.m is the following:

```
dydt = [y(2); p.miu1*(1-y(1)^2)*y(2)-p.miu2*y(1)+p.A*sin(p.omega*t)];
```

In this equation p.A is the amplitude of the force, p.omega is the radian frequency of the force oscillation, and t the time. In the appendix D the code vdp2.m is found with the code line above.

3.3.3. Results of the van der Pol oscillator with a forcing term

In this section, some tests have been performed on the van der Pol oscillator with a forcing term. Two main cases are investigated in this section:

-The influence of the ratio ω_f / ω_s on the frequency response.

-The influence of the force amplitude $\hat{c}$ on the response.

Influence of the ratio ω_f / ω_s

In this section, the influence of the ratio of ω_f / ω_s on the results is checked. Therefore, three cases are checked. Those cases are:

- Model with ω_f=0.5; ω_s =0.5, ω_f / ω_s= 1.

-Model with ω_f=0.7; ω_s =0.5, ω_f / ω_s= 1.4.

-Model with ω_f=5; ω_s =0.5, ω_f / ω_s= 10.

The first case has the parameters: f(t)= $\hat{c}$ sin(ω_f t), $\hat{c}$=3; ω_f=0.5; ω_s =0.5; ε = 0.08, initial conditions = [1 0]; time span = (0:0.1:300).

In the figure 3.6 shows the evolution of q vs the time series. As the initial conditions stated, it starts with 1, and after a few cycles, it reaches faster a steady state regime with an amplitude of 8.16 at 10s. The figure 3.7a shows the phase plane and how the values of q varies between 8.27 and -8.27. On the other hand, the values of dq/dt varies between 6.65 and -6.65. The figure 3.7a shows a remarked shape without inner shapes as in the phase plane on figure 3.3b, this means that the steady state is reached in two or three cycles.

The figure 3.7b shows the frequency spectrum, where frequencies are normalized with the force-frequency ω_f. The figure shows 3 peaks, one main peak at 1, other at 3 and another at 5. The highest peak is at 1. Meaning that most common frequency in the response is at the forcing frequency.

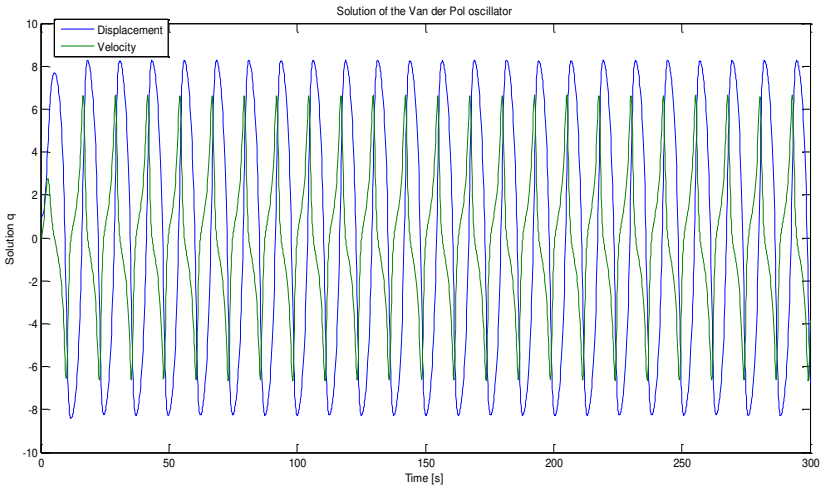

Figure 3. 6 Results for the van der Pol oscillator with a forcing term and ωf /ωs= 1. Graph of q vs Time

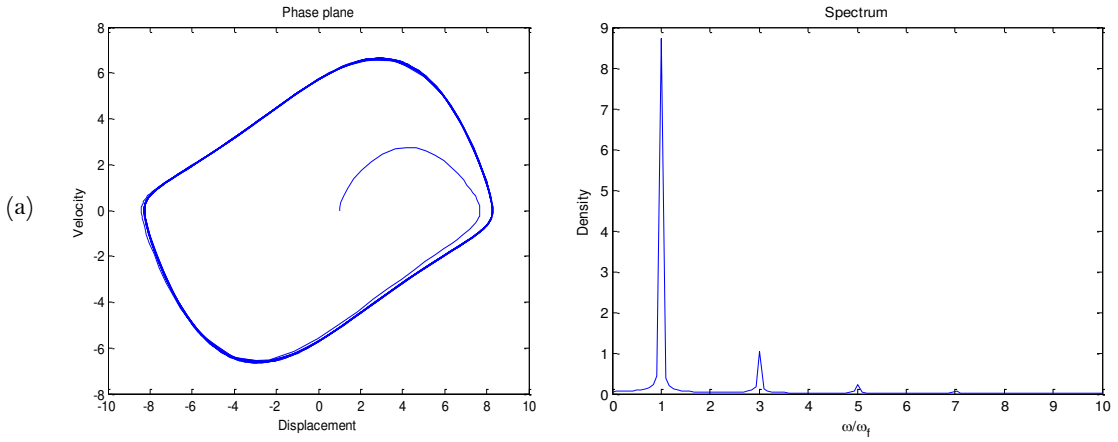

Figure 3. 7 Results for the van der Pol oscillator with a forcing term and ωf /ωs= 1. (a)Phase plane: q vs dq/dt (b) Frequency spectrum [ω/ωf]

The second case has the parameters: f(t)= $\hat{c}$ sin(ω_ft), $\hat{c}$=3; ω_f=1; ω_s =0.7; ε = 0.08, initial conditions= [1 0]; time span = (0:0.1:300).

In figure 3.8 the q started with a value of 1 and in less than a cycle, it reached an amplitude of 7. The steady-state regime starts at 18s with an amplitude of around 6.9.

Figure 3.9a shows a semicircular shape. It also shows different shapes inside the more remarked shape. However, a steady-state regime is reached, where the values of q vary between values of 7 and -7 and the values of dq/dt vary between 6 and -6.

The figure 3.9b shows the frequency spectrum, where frequencies are normalized with the force-frequency ω_f. The figure shows 3 peaks, one main peak at 1, other at 3 and another at 5. The highest peak is at 1. Meaning that most common frequency in the response is at the forcing frequency.

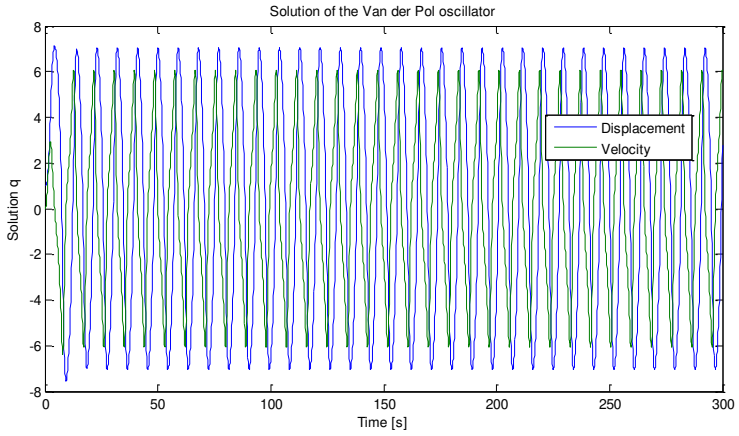

Figure 3. 8 Results for the van der Pol oscillator with a forcing term and ωf /ωs= 1.4: Graph of q vs Time

(a)

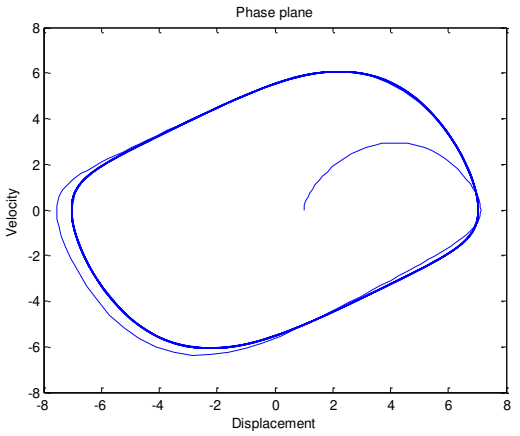

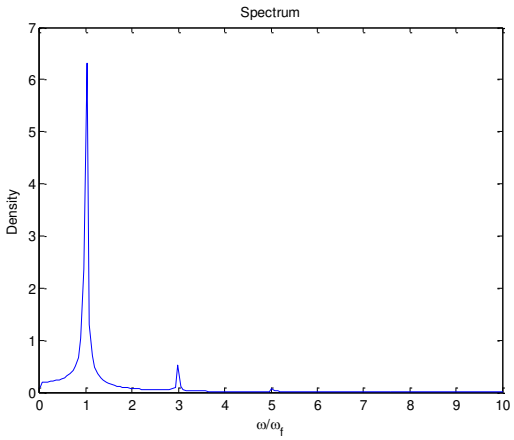

(b)

Figure 3. 9 Results for the van der Pol oscillator with a forcing term and ωf /ωs= 1.4: (a)Phase plane: q vs dq/dt (b) Frequency spectrum [ω/ωf]

The third case has the parameters: f(t)= $\hat{c}$ sin ($\omega_f t$), $\hat{c}$=3; ω_f=1.5; ω_s =0.5; ε = 0.08, initial conditions= [1 0]; time span = [0 300].

Figure 3.10 shows the evolution of q during the time. The amplitude started with 1 as stated in the initial conditions. The response increases until it reaches a steady state regime with an amplitude of 2, this happens at 110s.

Figure 3.11a shows a shape in the form of a cloud. The value of q fluctuates in a range between 2 and -2, and dq/dt within the range between 1.6 and -1.6.

In figure 3.11b the normalized frequency spectrum is shown. In the figure, two peaks are shown, the biggest at 0.10 and other at 1. This means that most of the frequency response is at the shedding frequency.

In conclusion, after checking the responses in each case. It can be noticed that when the forcing frequency is close to the shedding frequency (as ω_f=0.5, and ω_f=0.7) the response is given mainly in the force-frequency. On the other hand, when the forcing frequency is far from the shedding frequency, the system responses mainly with a frequency equal to the shedding frequency.

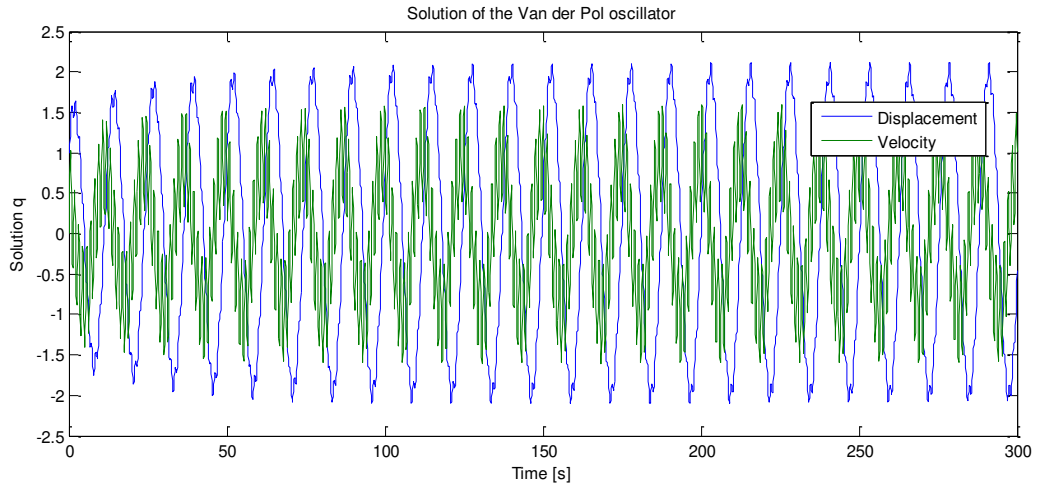

Figure 3. 10 Results for the van der Pol oscillator with a forcing term and ωf /ωs= 3: (a) Graph of q vs Time (b)Phase plane: q vs dq/dt (c) Frequency spectrum

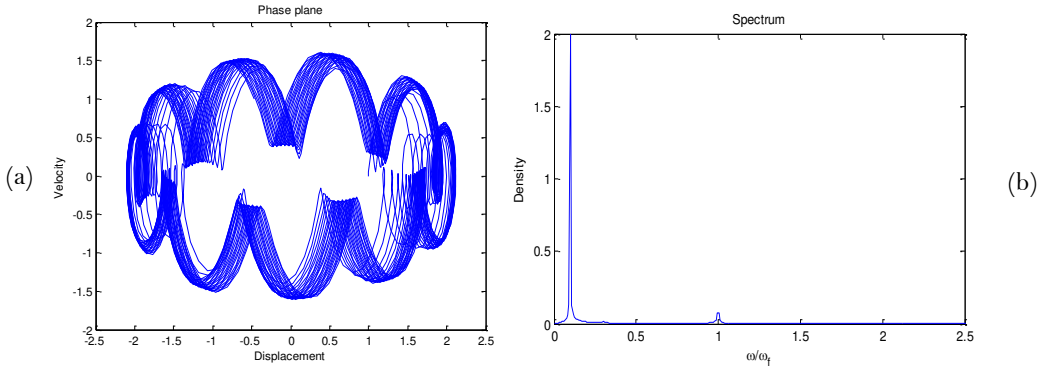

Figure 3. 11 Results for the van der Pol oscillator with a forcing term and ωf /ωs= 3: (a)Phase plane: q vs dq/dt (b) Frequency spectrum

Influence of the force amplitude $\hat{c}$ on the response

In this section, the influence of the force amplitude $\hat{c}$ on the results is checked. Thus, two cases are explored:

- Model with $\hat{c}$=2.
- Model with $\hat{c}$=10.
- Model with $\hat{c}$=15.

The first case has the parameters: f(t)= $\hat{c}$ sin(ω_f t), $\hat{c}$=2; ω_f=2.7; ω_s =0.5; ε = 0.08, initial conditions = [1 0]; time span = (0:0.1:700).

Figure 3.12 shows the evolution of q during the time. The amplitude started with 1 as stated in the initial conditions. The response increases until it reaches a steady state regime with an amplitude of 2.14, at 100s.

Figure 3.13a shows a shape in form of a ring in 3d. The value of q fluctuates in a range between 2.25 and -2.25, and dq/dt within the range between 1. and -1.7.

In figure 3.13b, the normalized frequency spectrum is shown. In the figure, two main peaks are shown, the biggest at 0.18 with a density of 1.7 and other at 1 with a density of 0.2. This means that most of the frequency response is at the shedding frequency.

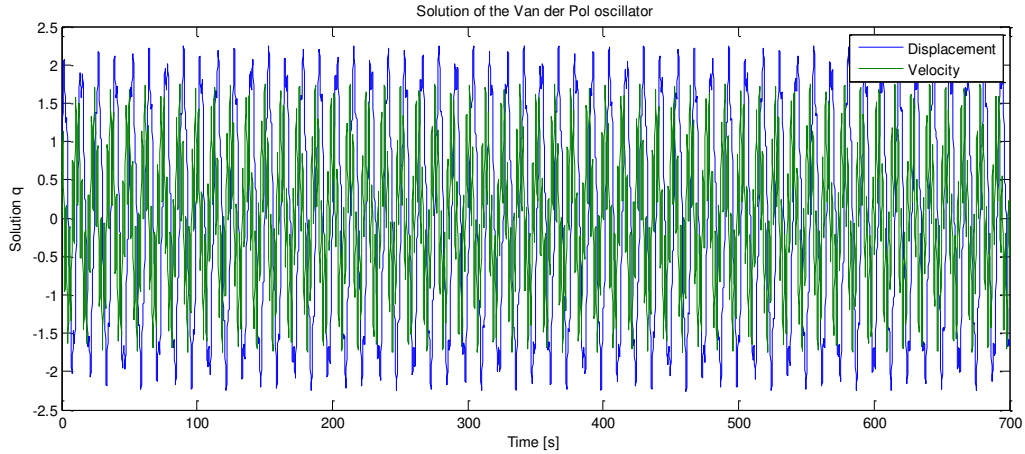

Figure 3. 12 Results for the van der Pol oscillator with a forcing term $\hat{c}$= 2: Graph of q vs Time

(a)

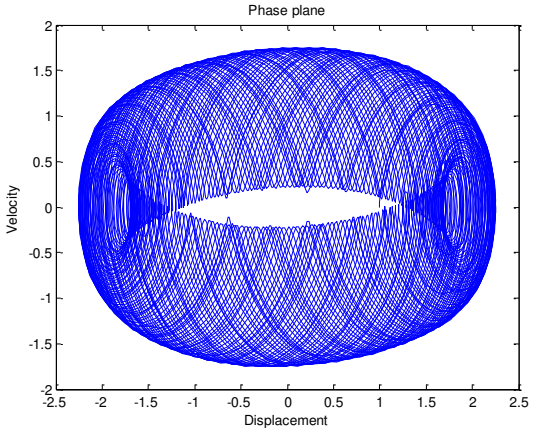

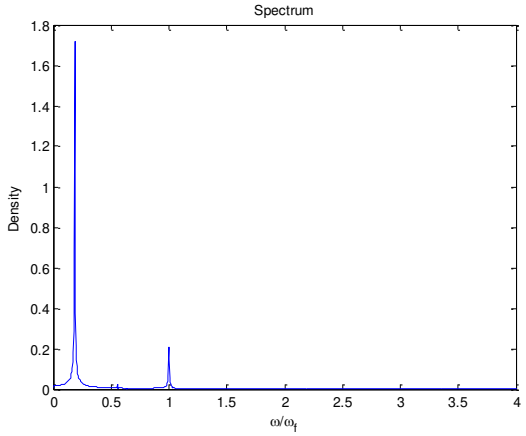

(b)

Figure 3. 13 Results for the van der Pol oscillator with a forcing term $\hat{c}$= 2: (a) Graph of q vs Time (b)Phase plane: q vs dq/dt (c) Frequency spectrum [ω/ω_f]

The second case has the parameters: f(t)= $\hat{c}$ sin (ω_f t), $\hat{c}$=10; ω_f=2.7; ω_s =0.5; ε = 0.08, initial conditions = [1 0]; time span = (0:0.1:300).

Figure 3.14 shows the evolution of q during the time. The amplitude started with 1 as stated in the initial conditions. The response increases until it reaches a steady state regime with a maximum amplitude of 4.326, at 69s.

Figure 3.15a shows a shape in form of a semi-circle. The value of q fluctuates in a range between 2.6 and -2.6, and dq/dt within the range between 4.35 and -4.35.

In figure 3.15b, the normalized frequency spectrum is shown. In the figure, two main peaks are shown, the first one at 0.18 with a density of 0.75 and other at 1 with a density of 0.97. This means that most of the frequency response is at the force-frequency.

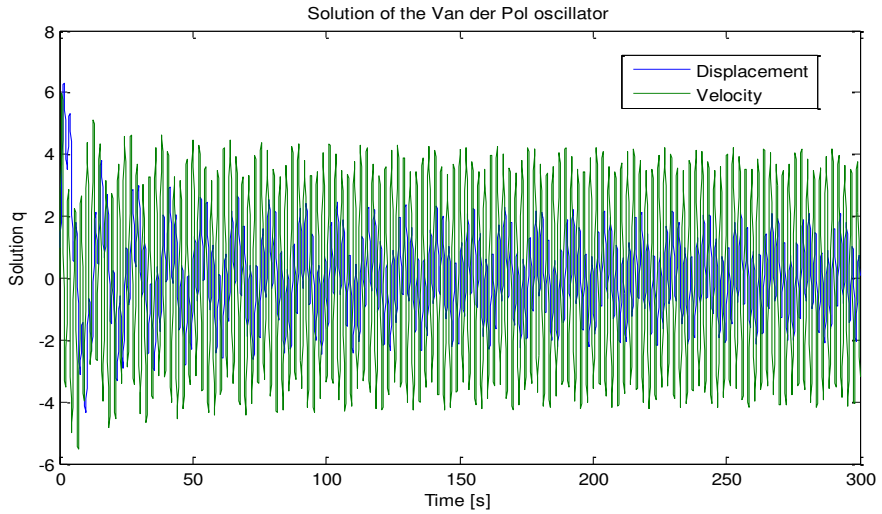

Figure 3. 14 Results for the van der Pol oscillator with a forcing term $\hat{c}$= 10: Graph of q vs Time

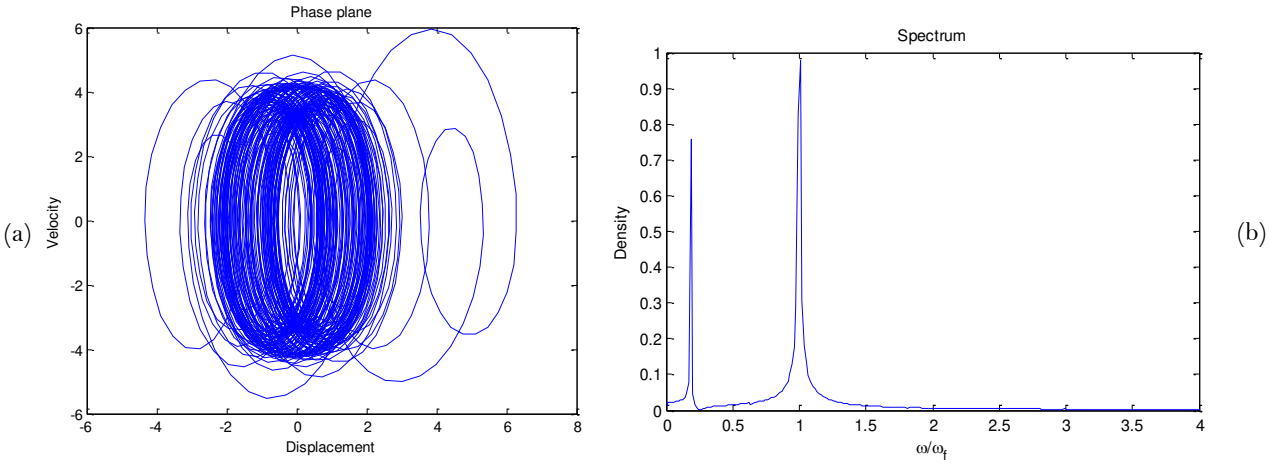

Figure 3. 15 Results for the van der Pol oscillator with a forcing term $\hat{c}$= 10: (a)Phase plane: q vs dq/dt (b) Frequency spectrum [ω/ω_f]

The third case has the parameters: f(t)= $\hat{c}$ sin ($\omega_f t$), $\hat{c}$=15; ω_f=2.7; ω_s =0.5; ε = 0.08, initial conditions = [1 0]; time span = (0:0.1:300).

Figure 3.16 shows the evolution of q during the time. The amplitude started with 1 as stated in the initial conditions. The response increases until it reaches a steady state regime with a maximum amplitude of 5.7, at 98s.

Figure 3.17a shows an oval shape. The value of q fluctuates in a range between 2.38 and -2.38, and dq/dt within the range between 5.9 and -5.9.

In figure 3.17b the normalized frequency spectrum is shown. In the figure, two main peaks are shown, one at 0.13 with a density of 0.06 and the biggest at 1 with a density of 0.97. This means that most of the frequency response is at the forcing frequency.

After analyzed the three cases with different force amplitude $\hat{c}$, it was possible to notice the following:

1. The force amplitude influences the amplitude of the response.
2. With a higher force amplitude, there is more energy in the spectrum, therefore more density in the peaks is reached.
3. Independent of the ratio ω_f / ω_s, if the force amplitude is high enough, it can cause that the response is mainly given in a frequency equal to the force-frequency (see figures 3.15b and 3.17b).

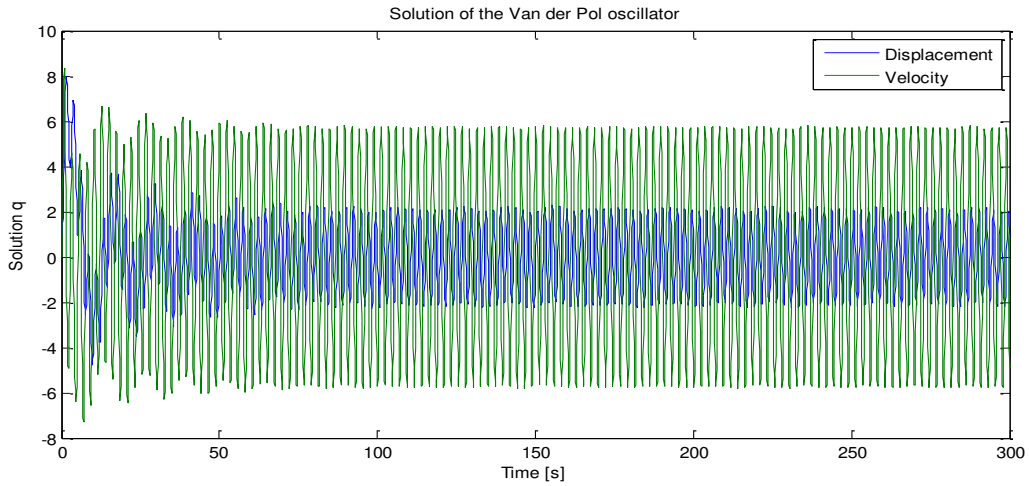

Figure 3. 16 Results for the van der Pol oscillator with a forcing term $\hat{c}$= 15: Graph of q vs Time

(a)

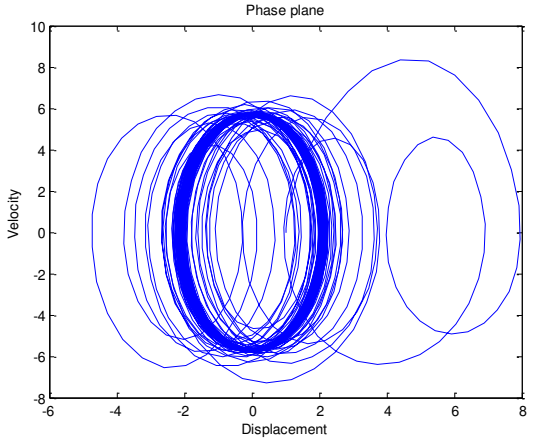

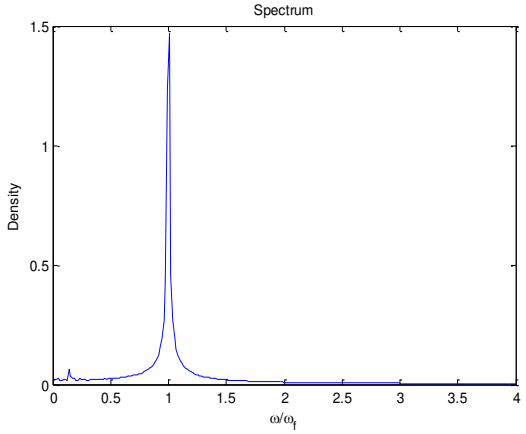

(b)

Figure 3. 17 Results for the van der Pol oscillator with a forcing term $\hat{c}$= 15: (a)Phase plane: q vs dq/dt (b) Frequency spectrum [ω/ω_f]

4.4. Conclusions on the van der Pol oscillator model

In this chapter, the model description, the governing equations and the implementation of the van der Pol oscillator model were explained. Furthermore, in order to have a deeper understanding some investigations have been made to the model.

First, the van der Pol oscillator model with a zero-forcing term was checked. As sensitivity analysis of ε was performed for this model.

Second, the van der Pol oscillator model was tested with a forcing term. In this part, two tests were conducted. One, the influence of the ω_f / ω_s on the response. Two, the impact of the force amplitude $\hat{c}$ on the response.

Some interesting results were found in this chapter, and the aim of it has been reached. Now, that there is familiarity with the van der Pol oscillator equation, the following chapters should be easier to follow, however, in case of doubts, this chapter can be read again.

Chapter 4

Wake Oscillator Model by Ogink and Metrikine

In chapter 3 the van der Pol oscillator was explored. And the van der Pol equation with a zero-forcing term was used to model a fixed rigid cylinder in the current. In this chapter the wake oscillator model by Ogink & Metrikine, 2010 is used to model the VIV of a rigid cylinder elastically supported in the current. The model is focused on free oscillation experiments and their results are compared with experimental results by Jauvtis & Williamson, 2004. for the low mass-damping ratios: $m^*=2.6$ and $m^*=7$.

The chapter includes the description of the wake oscillator model, its governing equations for a rigid cylinder elastically supported in the current in free oscillation experiments. And finally, results and comments.

The aim of this chapter is to get familiar with the wake oscillator model, its governing equations and the implementation to be solved with the function ode45 of Matlab. The understanding of this chapter will allow the reader to have an easier comprehension of chapter 5 where the wake oscillator with a new in-line coupling term is introduced. Furthermore, it will be possible to check which drawbacks of the coupled wake oscillator model will be improved by the new model introduced in chapter 5.

4.1. Model description

For modeling the wake, we need to consider some facts.

1. We can make the modeling in a 2-dimensional plane x'-y'.
2. There are two dof for the displacement of the cylinder and one for the wake variable. This makes three equations of motion.
3. They work all together as a system, then, they need certain terms that couple their equations.
4. It is necessary to use the relative flow velocity. As we have a velocity flow and the instantaneous velocity of the cylinder.
5. The flow has an angle of attack β.
6. The shear stresses are very small therefore they can be neglected.

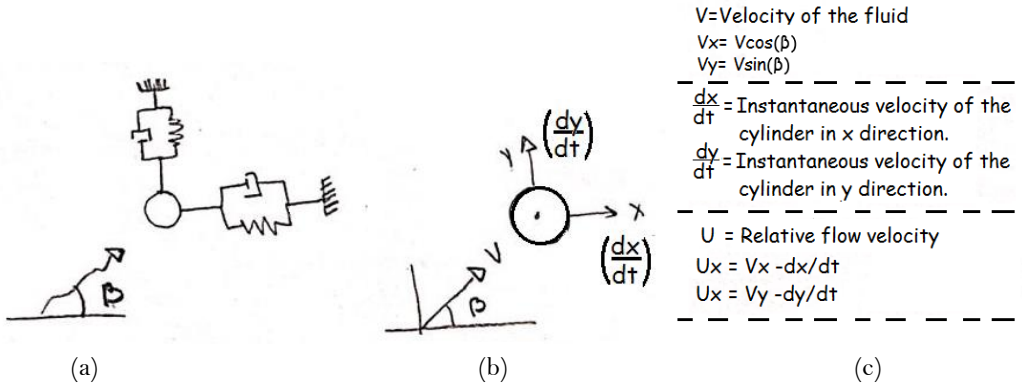

Figure 4. 1 (a) It shows the system for the two dof of the cylinder. (b) Instantaneous velocity of the cylinder and the fluid velocity. (c) Relations for the relative flow velocity.

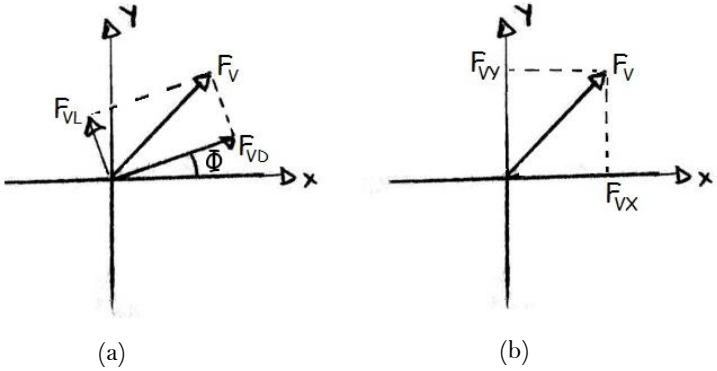

Figure 4. 2 Decomposition of vortex force (Fv) in drag and lift force

As explained in chapter 2, the fluctuating pressure on the cylinder due to the vortices creates a vortex force. The vortex force has a drag component and a lift component (Figure 4.2a).

$$\overrightarrow{F_{VD}} = (F_{VD}\cos(\Phi), F_{VD}\sin(\Phi)) \qquad \text{Eq. 4. 1}$$

$$\overrightarrow{F_{VL}} = (-F_{VL}\sin(\Phi), F_{VL}\cos(\Phi)) \qquad \text{Eq. 4. 2}$$

The vortex force also can be split into x and y components (Figure 4.2b).

$$F_{VX} = (F_{VD}\cos(\Phi) - F_{VL}\sin(\Phi)) \qquad \text{Eq. 4. 3}$$

$$F_{VY} = (F_{VD}\sin(\Phi) + F_{VL}\cos(\Phi)) \qquad \text{Eq. 4. 4}$$

The vortex force can be decomposed as a function of drag and lift coefficients: CVL, CVD. See Appendix D.

$$C_{VY} = \frac{U^2}{V^2}(C_{VD}\sin(\Phi) + C_{VL}\cos(\Phi)) \qquad \text{Eq. 4. 5}$$

$$C_{VX} = \frac{U^2}{V^2}(C_{VD}\cos(\Phi) - C_{VL}\sin(\Phi)) \qquad \text{Eq. 4. 6}$$

where:

$$\sin(\Phi)=\frac{U_y}{V} \qquad \cos(\Phi)=\frac{U_x}{V} \qquad \text{Eq. 4. 7}$$

The equations of motion in x and y direction of a cylinder elastically supported are:

$$(m+m_a)\frac{d^2x}{dt^2}+c\frac{dx}{dt}+kx=\frac{1}{2}\rho DV^2C_{VX} \qquad \text{Eq. 4. 8}$$

$$(m+m_a)\frac{d^2y}{dt^2}+c\frac{dy}{dt}+ky=\frac{1}{2}\rho DV^2C_{VY} \qquad \text{Eq. 4. 9}$$

Where x and y are in function of t, c is the damping, k is the stiffness and $(m + m_a)$ is the mass and the added mass.

Using $\tau = \omega_s t$. And $d\tau/dt = \omega_s$. The dimensionless equations of motion are:

$$\frac{d^2y}{d\tau^2}+2\Omega_n\zeta\frac{dy}{d\tau}+\Omega_n^2y=\frac{1}{m^*+C_a}\bullet\frac{1}{2\pi^3St^2}C_{VY} \qquad \text{Eq. 4. 10}$$

$$\frac{d^2x}{d\tau^2}+2\Omega_n\zeta\frac{dx}{d\tau}+\Omega_n^2x=\frac{1}{m^*+C_a}\bullet\frac{1}{2\pi^3St^2}C_{VX} \qquad \text{Eq. 4. 11}$$

Where:

$$C_{VX}=\left[C_{VD}\left(\cos(\beta)-2\pi St\frac{dx}{d\tau}\right)-C_{VL}\left(\sin(\beta)-2\pi St\frac{dy}{d\tau}\right)\right]\left[\left(\cos(\beta)-2\pi St\frac{dx}{d\tau}\right)^2+\left(\sin(\beta)-2\pi St\frac{dy}{d\tau}\right)^2\right]^{0.5} \qquad \text{Eq. 4. 12}$$

$$C_{VY}=\left[C_{VD}\left(\sin(\beta)-2\pi St\frac{dy}{d\tau}\right)+C_{VL}\left(\cos(\beta)-2\pi St\frac{dx}{d\tau}\right)\right]\left[\left(\cos(\beta)-2\pi St\frac{dx}{d\tau}\right)^2+\left(\sin(\beta)-2\pi St\frac{dy}{d\tau}\right)^2\right]^{0.5} \qquad \text{Eq. 4. 13}$$

The algebraic calculation can be founded in Mina,2013. According to Faccinetti, Langre & Biolley, 2004; the lift part is related to the amplitude of the lift coefficient for a stationary cylinder $\hat{C}_{L0}$.

Some important notes are:

1. $C_{VL} = q\,\hat{C}_{L0}/2$. Relation according to Faccinetti, Langre & Biolley, 2004.
2. $\hat{C}_{L0}$ depends on Reynolds number. But for VIV usually is studied in the subcritical regime where $\hat{C}_{L0}$ is almost constant.
3. $\hat{C}_{L0}$ can be determined through the experiments of a fixed cylinder in the current. This will be used in chapter 5.
4. In this analysis, C_{VD} is taken equal to the mean drag coefficient of a fixed cylinder. $C_{VD} = \hat{C}_{D0}$.

Coming back to the equation of the wake oscillator. The following systems was proposed by Ogink & Metrikine, 2010 as a modified version of Fachinetti's model.

In the forcing term of the equation for the wake oscillator, a linear acceleration coupling has been applied.

$$\ddot{q}+\varepsilon\omega_s(q^2-1)\dot{q}+\omega_s^2q=\frac{A}{D}(\ddot{y}\cos\beta-\ddot{x}\sin\beta) \qquad \text{Eq. 4. 14}$$

The dimensionless equation is as follows:

$$\frac{d^2q}{d\tau^2}+\varepsilon(q^2-1)\frac{dq}{d\tau}+q=A\left(\frac{d^2y}{d\tau^2}\cos\beta-\frac{d^2x}{d\tau^2}\sin\beta\right) \qquad \text{Eq. 4. 15}$$

Where A and ε are tuning parameters.

4.2. The system of Equations for Free Oscillation Model using the wake oscillator model

In this analysis, the following dimensionless equations are used.

$$\frac{d^2q}{d\tau^2}+\varepsilon(q^2-1)\frac{dq}{d\tau}+q=A\left(\frac{d^2y}{d\tau^2}\cos\beta-\frac{d^2x}{d\tau^2}\sin\beta\right)$$ <-Equation for wake oscillator Eq. 4. 16

$$\frac{d^2y}{d\tau^2}+2\Omega_n\zeta\frac{dy}{d\tau}+\Omega_n^2 y=\frac{1}{m^*+C_a}\bullet\frac{1}{2\pi^3 St^2}C_{vy}$$ Eq. 4. 17

$$\frac{d^2x}{d\tau^2}+2\Omega_n\zeta\frac{dx}{d\tau}+\Omega_n^2 x=\frac{1}{m^*+C_a}\bullet\frac{1}{2\pi^3 St^2}C_{vx}$$ Eq. 4. 18

<-Equations for cross-flow and in-line vibration

Where:

$$C_{VX}=\left[\hat{C}_{DO}\left(\cos(\beta)-2\pi St\frac{dx}{d\tau}\right)-\frac{\hat{C}_{LO}q}{2}\left(\sin(\beta)-2\pi St\frac{dy}{d\tau}\right)\right]\left[\left(\cos(\beta)-2\pi St\frac{dx}{d\tau}\right)^2+\left(\sin(\beta)-2\pi St\frac{dy}{d\tau}\right)^2\right]^{0.5}$$ Eq. 4. 19

$$C_{VY}=\left[\hat{C}_{DO}\left(\sin(\beta)-2\pi St\frac{dy}{d\tau}\right)+\frac{\hat{C}_{LO}q}{2}\left(\cos(\beta)-2\pi St\frac{dx}{d\tau}\right)\right]\left[\left(\cos(\beta)-2\pi St\frac{dx}{d\tau}\right)^2+\left(\sin(\beta)-2\pi St\frac{dy}{d\tau}\right)^2\right]^{0.5}$$ Eq. 4. 20

As it was mentioned before, two branches were found by many other researchers. In this regard, just one model is preferred to fit results with both amplitude branches. However, this has not been possible yet. Then, Ogink & Metrikine proposed two sets of parameters to match each branch. These parameters are set to fit with the experimental results for low mass-damping ratio by Jauvtis & Williamson, 2004.

	$\hat{C}_{L0}$	$\hat{C}_{D0}$	St	A	ε
Upper branch	0.3842	1.1856	0.1932	4.0	0.05
Lower branch	0.3842	1.1856	0.1932	12	0.7

Table 4. 1

4.3. Implementation of Free Oscillation Model

Some important assumptions for the implementation are:

1. In this model, y/D is the dimensionless amplitude in the cross-flow direction. And x/D is the dimensionless amplitude in stream-wise direction.
2. The amplitudes Â (that could be y/D or x/D, for sake of simplicity) are unknown.
3. The amplitude Â reaches a steady state just after a few periods of oscillation, but to be sure this analysis analyzes the response only after the first 50 periods.
4. Â is determined by finding the recurrent maximum displacement.
5. Ωc is determined from the biggest peak in the frequency spectrum after using Fourier ($f_{fourier}$). Thus, $\Omega c= 2\pi f_{fourier}$. Then, Ωcx is the in-line radian frequency and Ω_{cy} is the cross-flow radian frequency.
6. The dimensionless natural radian frequency is calculated for each Vn, $\Omega n=1/(st*Vn)$.
7. The system of equations is solved with the MATLAB function ODE45.
8. The model works with a range of reduced velocities Vn=2 to 12, with stepsize= dVn=0.1.
9. Initial conditions for the first Vn is storage in the matrix ini= [y dy/dt x dx/dt q dq/dt]= [0 0 0 0 0.1 0].
10. For each new cycle with a different Vn the last results of [y dy/dt x dx/dt q dq/dt] are taken.

4.4. Algorithm

Diagram 4.1 shows the programming algorithm and the diagram of the code mainmoni.m and anita.m. It works with the codes: 'mainmoni.m', 'initialanitaupper.m', 'initialanita.m', 'anita.m' and 'spectrum_dos.m'. Furthermore, the code anita.m can be found in appendix d.

The main code is mainmoni.m. Inside mainmoni.m are four main parts. First, the initial data is set. Second, other parameters are called and storage in the arrangement p: the code initialanitaupper.m is used for parameters for modeling the upper branch and the code initialanita.m is used for modeling lower branch results. Third, cycles, where the equation is solved with the help of the function ode45, are run for each reduced velocity (Vn) and storage in a matrix. The cycles part is described in the part c of the diagram 4.1. Fourth, the results are plottedted.

The code anita.m is described in the section 4.5

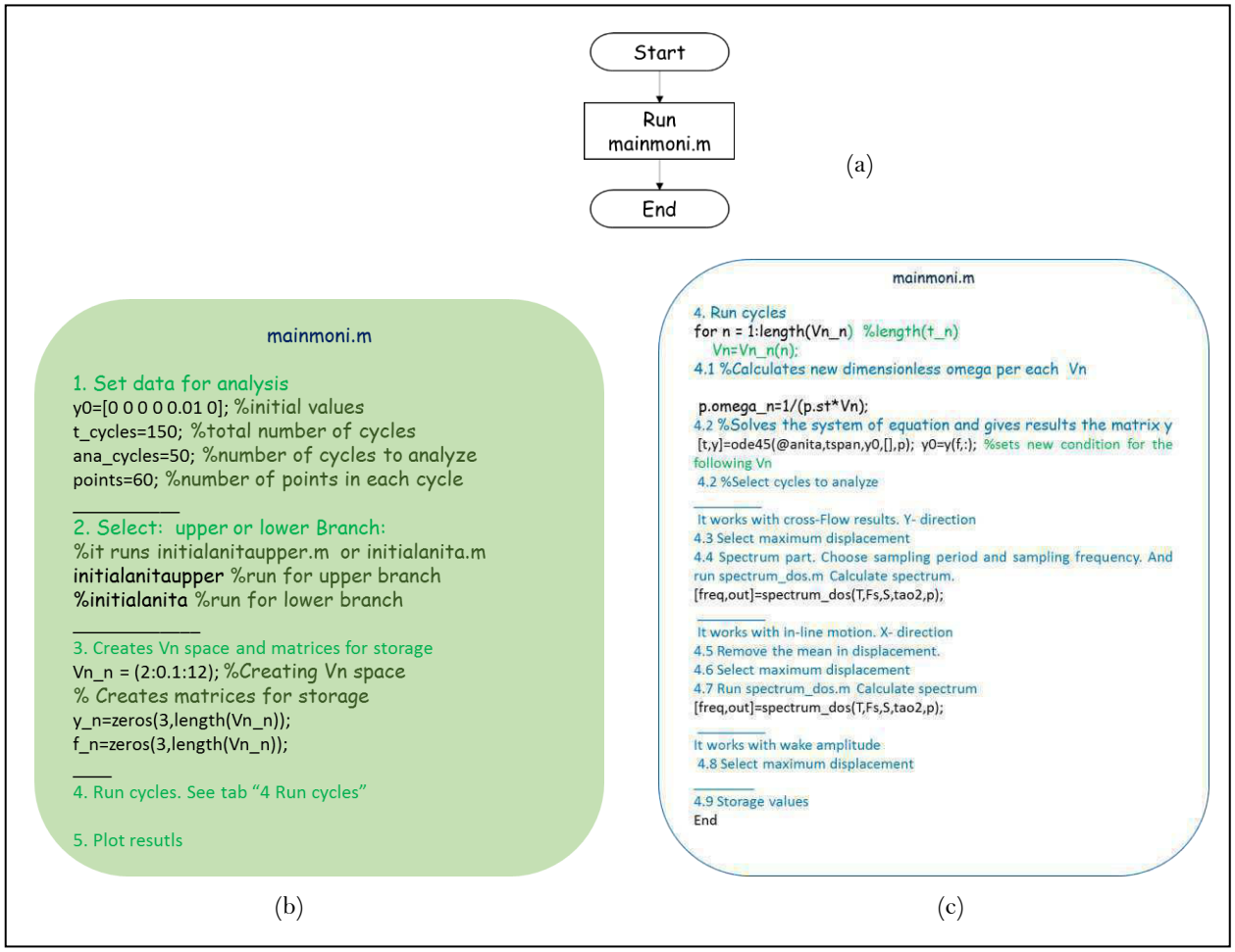

Diagram 4. 1

4.5. Solving Equations with Function ODE45

In order to solve the differential equations, they need to be rewritten. The equation 4.21 shows how the equation is rewritten, and the equation 4.24 shows how is implemented in the code. Similar happens with equation 4.22 and equation 4.25, and equation 4.23 and equation 4.26.

$$\frac{d^2y}{d\tau^2} = -2\Omega_n\zeta\frac{dy}{d\tau} - \Omega_n^2 y + \frac{1}{m^* + C_a}\bullet\frac{1}{2\pi^3 St^2}C_{vy} \qquad \text{Eq. 4. 21}$$

$$\frac{d^2x}{d\tau^2} = -2\Omega_n\zeta\frac{dx}{d\tau} - \Omega_n^2 x + \frac{1}{m^* + C_a}\bullet\frac{1}{2\pi^3 St^2}C_{vx} \qquad \text{Eq. 4. 22}$$

$$\frac{d^2q}{d\tau^2} = -\varepsilon(q^2-1)\frac{dq}{d\tau} - q + A\left(\frac{d^2y}{d\tau^2}\cos\beta - \frac{d^2x}{d\tau^2}\sin\beta\right) \qquad \text{Eq. 4. 23}$$

$$y(2); -2\Omega_n\zeta\frac{dy}{d\tau} - \Omega_n^2 y + \frac{1}{m^* + C_a}\bullet\frac{1}{2\pi^3 St^2}C_{vy}; \qquad \text{Eq. 4. 24}$$

$$y(4); -2\Omega_n\zeta\frac{dx}{d\tau} - \Omega_n^2 x + \frac{1}{m^* + C_a}\bullet\frac{1}{2\pi^3 St^2}C_{vx}; \qquad \text{Eq. 4. 25}$$

$$y(6); -\varepsilon(q^2-1)\frac{dq}{d\tau} - q + A\left(\frac{d^2y}{d\tau^2}\cos\beta - \frac{d^2x}{d\tau^2}\sin\beta\right); \qquad \text{Eq. 4. 26}$$

Inside mainmoni.m the equation is called to be solved with the function ode45 with the line [t,y]=ode45(@anita,tspan,y0,[],p); .In the code anita.m the equation is defined and adjusted to be solved. The equation to be solved in anita.m is the following:

```
dydt = [y(2); -2*p.zi*p.omega_n*y(2)-p.omega_n*p.omega_n*y(1)+p.b*cvy;

y(4); -2*p.zi*p.omega_n*y(4)-p.omega_n^2*y(3)+p.b*cvx; y(6);

-p.ep*(y(5)^2-1)*y(6)-y(5)+p.A*(p.cosa*(-2*p.zi*p.omega_n*y(2)...

-p.omega_n^2*y(1)+p.b*cvy)-p.sina*(-2*p.zi*p.omega_n*y(4)...

-p.omega_n^2*y(3)+p.b*cvx))];
```

The function returns a matrix with the solution for y, dy/dt, x, dx/dt, q, dq/dt. This matrix is [tn x 6], where tn is the length of the time span. The complete code anita.m is in Appendix D. Diagram 4.2 with the function is shown below.

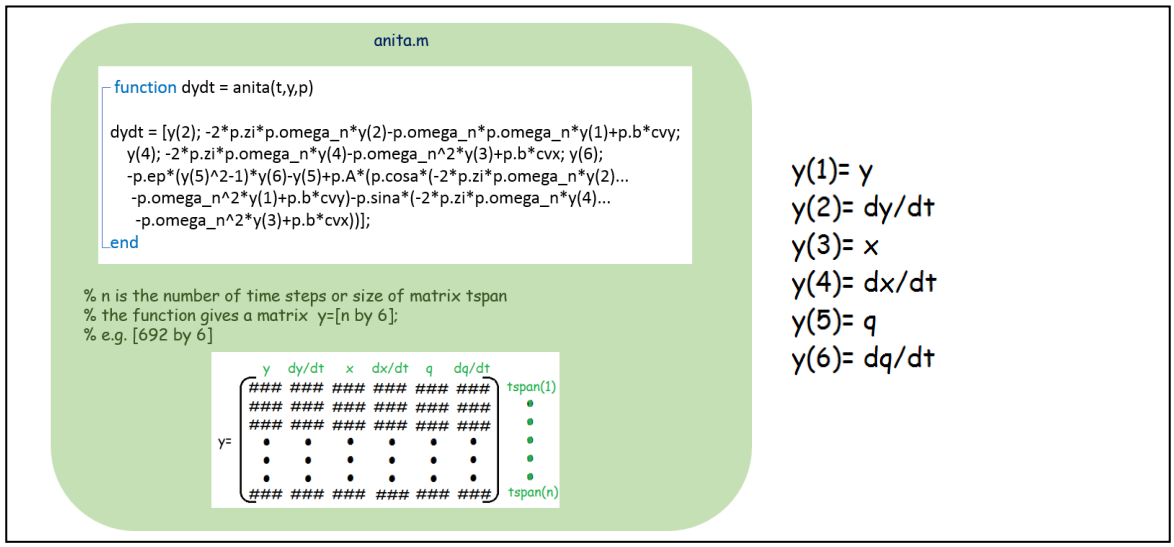

Diagram 4. 2

4.6. Results of Free oscillation model

The model was run for each Vn in the range 2-12 with a step size dVn=0.1. As mentioned at the beginning of the chapter, two low mass-damping ratios are compared with the experiments by Jauvtis & Williamson, 2004. First, the results for m*=7 are described and then for m*=2.6. The 8 graphs together can be found in Appendix E.

4.6.1. Results of Free oscillation model for m*=7

The parameters used for m*=7 are shown in table 4.2

	m*	Ca	ζ	(m*+Ca)ζ
General parameters	7.0	1.0	0.0015	0.0117

Table 4. 2 Parameters for m*=7

The figures 4.3a and 4.3b show the results for cross-flow direction. In both figures we can see that the model results have the van derthat in the results found by Jauvtis & Williamson, 2004.

In the figure 4.3a the cross-flow amplitude is shown. The model results have two main elevations, one at around Vn=4.5 and another at Vn=6. Both congruent with the results. Other issue is that the maximum amplitude of the upper branch for the model results is around 0.91 at Vn=5.5, meanwhile in the experiments is around 1 at Vn=5.98, so the curve of the experiment results looks moved to the right (towards higher reduced velocities). For the lower branch results the maximum amplitudes are similar, however, the curve of experiments also looks moved to the right. Lastly, in the experiments at Vn=3 there is a small hill that the model does not represent at all.

The figure 4.3b shows the radian frequency ratio Ωcy/Ωn. In the figure a lock-in range is seen in the range between Vn=4 to 9 in the model results, in the experiment results some apparent 4 lock-in ranges are found. The first one between Vn=1.9 and 3.8, the second between Vn=4.3 and 5.3, the third one between Vn=5.3 and 6.3, and the fourth one between Vn=6.3 and 11. These four are congruent with the results on figure 4.3a, the first one shows an small hill of maximum amplitude equal to 0.1, the second shows an inverted curve of amplitude around 0.25, the third one coincides with the peak of the upper branch and the fourth coincides with the range of the lower branch.

(a)

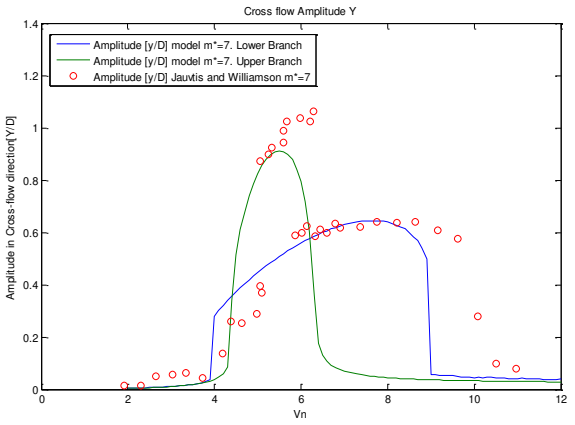

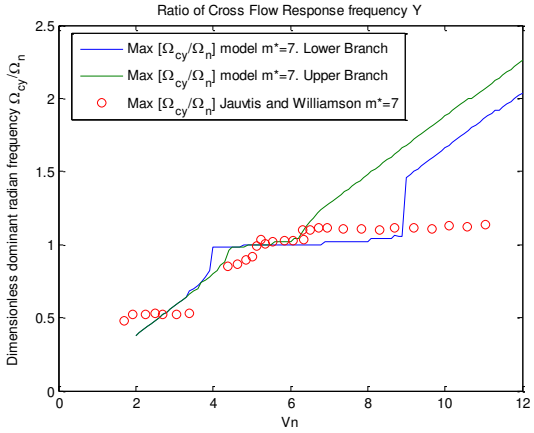

(b)

Figure 4. 3 m*=7. (a) Dimensionless Cross flow amplitude (b) Ratio of Cross-flow response frequency Ωcy/Ωn.

The figures 4.4a and 4.4b show the results for in-line direction. In both figures, we can see that the model results have the van derthat the results found by Jauvtis & Williamson, 2004.

In figure 4.4a, the in-line amplitude is shown. The model results represent both branches, the upper branch and the lower branch. The maximum amplitude of the upper branch for the model results is around 0.02 at Vn=5.5, meanwhile in the experiments is around 0.031 at Vn=5.4, s. Thus, both curves, the model and the experimental results have a similar shape, but they differ on amplitude. Lastly, in the experiments at Vn=3, there is a hill that the model does not represent.

The figure 4.4b shows the radian frequency ratio Ωcx/Ωn. In this figure, there are no experimental results to compare with. However, the range of frequencies with lock-in coincides with the upper and lower branches in figure 4.4a. But there is no representation of the hill in the range between Vn=2 to 3.4 that is present on figure 4.4a.

(a)

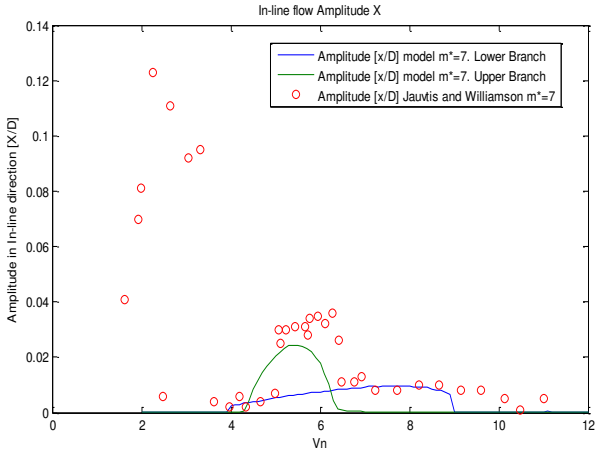

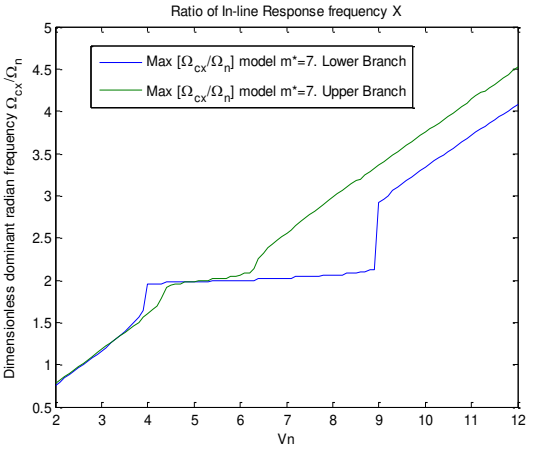

(b)

Figure 4. 4 m*=7. (a) Dimensionless In-line amplitude (b) Ratio of In-line response frequency Ωcx/Ωn.

4.6.2. Results Free oscillation model for m*=2.6

The parameters used for m*=2.6 are shown in the table 4.3

	m*	Ca	ζ	(m*+Ca)ζ
General parameters	2.6	1.0	0.0036	0.013

Table 4. 3 Parameters for m*=2.6

The figures 4.5a and 4.5b show the results for cross-flow direction. In both figures, we can see that the model results have the same order of magnitude that the results found by Jauvtis & Williamson, 2004.

In figure 4.5a, the cross-flow amplitude is shown. The model results have two main elevations, one at around Vn=5.5 with 0.89D and at Vn=7.9 with 0.64D. Although in the experimental results the highest amplitude of the upper branch is 1.5D at Vn=2.7 and in the lower branch is about .76D at Vn=8.19. The ranges of lock-in of the lower and upper branches coincide, in the experimental results the range of the upper branch is between Vn=4 to 8.27. However, in the experimental results other two hills in the curve can be seen, one in the range between Vn=2.17 to 4 and other in the range between Vn=12.5 to 13.5, but the model does not represent these curves.

The figure 4.5b shows the radian frequency ratio Ωcy/Ωn. In the figure, a lock-in range is seen in the range between Vn=3.6 to 9.1 in the model results for the lower branch, in the experiment results five lock-in ranges are found.

The first one between Vn=1.9 and 3.86 the second between Vn=3.8 and 4.7, the third one between Vn=4.7 and 8.4, the fourth one between Vn=7.9 and 13 and the fifth between Vn=13 and 13.5. These five ranges are congruent with the results on figure 4.5a. On the other hand, the model represents the lower and upper branch (the third and fourth lock-in ranges), but the others are not represented.

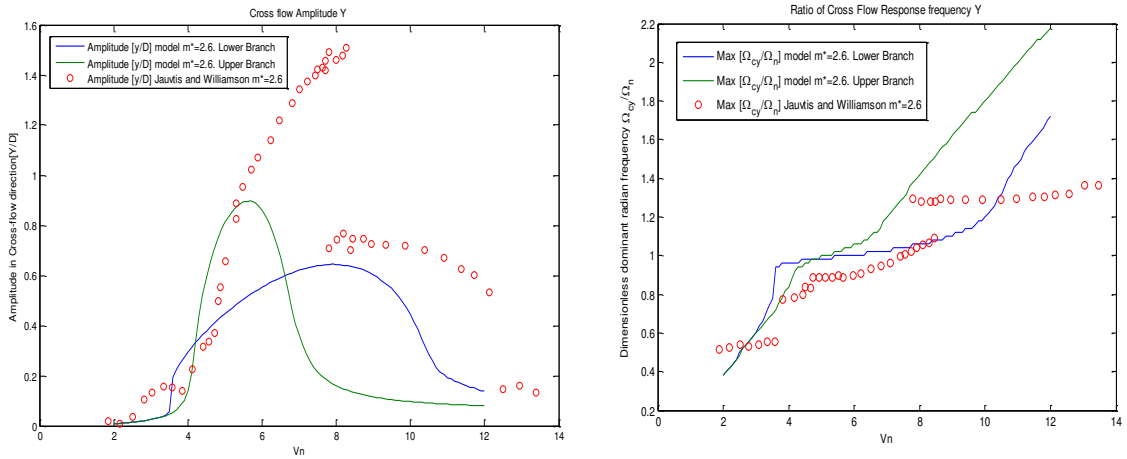

(a) (b)

Figure 4. 5 m*=2.6. (a) Dimensionless Cross flow amplitude (b) Ratio of Cross-flow response frequency Ωcy/Ωn.

The figures 4.6a and 4.6b show the results for the in-line direction. In both figures, we can see that the model results have the same order of magnitude that the experimental results.

In figure 4.6a, the in-line amplitude is shown. In this graph, it is possible to see that the amplitudes are much smaller than the amplitudes in the cross-flow direction. The model results represent the two curves for the lower and the upper branch. For the upper branch curve, the model gives results smaller

in amplitudes than the experiment results by 0.26D, the experiment results give six times the amplitude of the model results. And the range of Vn where the upper branch is positioned coincides.

For the case of the lower branch, the lock-in range only coincides between Vn=8 to 12, but in the experimental results, the curve is moved to higher reduced velocities. And the amplitude of the experimental results is much higher with 0.079D than the model results with 0.01D. Also, in the experimental results, there are other two hills apart from the upper and the lower branch. One in the range between Vn=2 to 3.8, and the other in the range between Vn=12 to 14. The last two are not represented by the model results. However, probably the hill in the range between Vn=12 to 14 is due to the calibration of the experiment.

The figure 4.6b shows the radian frequency ratio Ωcx/Ωn. In this figure, there are no experimental results to compare with. However, the range of frequencies with lock-in coincides with the upper and lower branches in figure 4.4a. But there is no representation of the two small ranges of lock-in between Vn=2 to 4 and Vn=12 to 14.

(a)

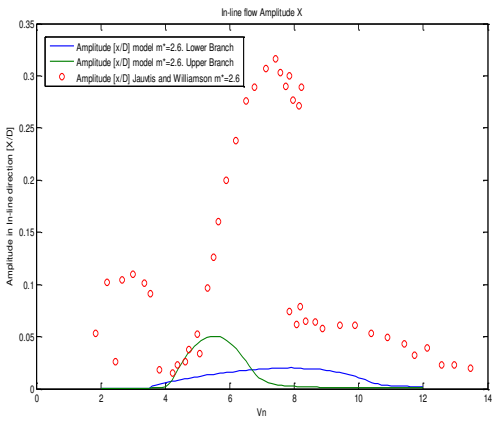

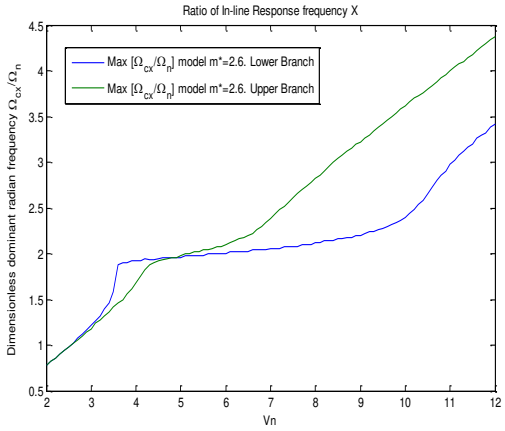

(b)

Figure 4. 6 m*=2.6. (a) Dimensionless In-line amplitude (b) Ratio of In-line response frequency Ωcx/Ωn.

4.7. Conclusions on free oscillation model with wake oscillator

In this chapter the performance of the wake oscillator model by Ogink and Metrikine,2010 has been investigated. The model and the governing equations have been explored. The model was focused on the free oscillation experiments by Jauvtis & Williamson, 2004. for the low mass-damping ratios: m*=2.6 and m*=7.

Considering the results for m*=7, it was interesting to see how good the two curves for lower and upper branches fit in amplitude and in the lock-in range for cross floss direction, the same for the results in radian frequency. And the same happens in the in-line direction, good match in amplitude and in the range of lock-in frequencies. Then, we can say that there is a good match in both directions with the lower and upper branches. However, the experimental results show two other hills in the curve apart from the lower and upper branches, going from low to high reduced velocities, one before the upper branch and other after the lower branch, those two hills are not represented by the model, neither in the amplitude plots or in the radian frequency ratio plots.

On the other hand, observing the results for m*=2.6, it seen that there is not that good match as in for m*=7, for both directions, the amplitudes are in the same order of magnitude, and the lock-in ranges in the model results coincide almost in the same range as the experiment results, but the experimental results are moved toward high reduced velocities. However, the amplitude represented by the model is almost a half of the amplitude obtained in the experiments in the cross-flow direction and a sixth in in-line direction. Also, the experiments show what looks like five lock-in ranges, in both cross-flow and

in-line direction. Going from low to high reduced velocities, a hill before the upper branch and other after the lower branch, those hills are not represented by the model either in the amplitude plots or in the radian frequency plots.

Another interesting fact is that, if we try to relate both graphs cross-flow and in-line direction amplitudes in the experiments they have similar lock-in ranges.

In this chapter, it was possible to detect goals and drawbacks from the model, giving room for improvement for the new model that is introduced in chapter 5.

Chapter 5

Wake oscillator model with a new coupling term in the wake equation of motion

In chapter 4 the Wake oscillator model by Ogink and Metrikine,2010 was used to model the VIV phenomenon on a rigid cylinder in the current. In this chapter, the main focus is the new wake oscillator model by Qu,2019.

The chapter includes the description and the governing equations of the new wake oscillator model by Qu,2019. Also, two main cases are performed:

- The new wake oscillator to model free oscillation experiments.
- The new wake oscillator to model forced in-line vibration experiments.

The aim of this chapter is to give an insight into the wake oscillator model modified by Qu, 2019, its governing equations and the implementation to be solved with the function ode45 of Matlab. At the end of the chapter, some comments on the results are made.

This chapter is the focus of this thesis as well as chapter 6, where a sensitivity analysis is made. The comprehension of this chapter will help to understand the content of chapter 6.

5.1. Model description and equations

In chapter 4, for modeling the wake, the wake oscillator model was used with the set of parameters proposed by Ogink & Metrikine to fit the lower and upper branch detected in the experiments of Jauvtis & Williamson, 2004. In this chapter other adaptations are made by Qu,2019 to the wake oscillator model.

We need to consider some facts.

1. We can make the modeling in a 2-dimensional plane x'-y'.

2. There are two dof for the displacement of the cylinder and one for the wake variable. Thus, three equations of motion are used.
3. They work all together as a system, then, they need certain terms that couple their equations.
4. It is necessary to use the relative flow velocity. As we have a velocity flow and the instantaneous velocity of the cylinder.
5. The flow has an angle of attack $\beta=0$, then the terms $\cos(\beta)=1$, $\sin(\beta)=0$. Similar as in chapter 4.
6. A new term that coupled the in-line motion is added in the wake equation of motion.
7. As explained in chapter 4, the shear stresses are neglected.

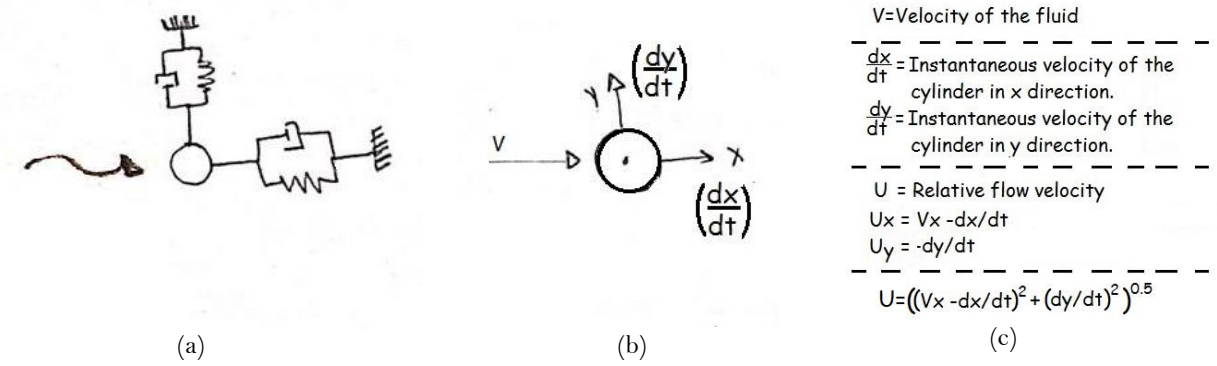

Figure 5. 1. (a) It shows the system for the two dof of the cylinder. (b) Instantaneous velocity of the cylinder and the fluid velocity. (c) Relations for the relative flow velocity.

Similar as in chapter 4, the vortex force can be decomposed in x and y components. According to Qu,2019 we have the following equations.

$$F_{VX}=\frac{1}{2}C_D\rho D U^2\cos(\Phi)+\frac{1}{2}C_L\rho D U^2\sin(\Phi) \qquad \text{Eq. 5. 1}$$

$$F_{VY}=\frac{1}{2}C_D\rho D U^2\sin(\Phi)+\frac{1}{2}C_L\rho D U^2\cos(\Phi) \qquad \text{Eq. 5. 2}$$

Where:

$$\sin(\Phi)=\frac{(-dy/dt)}{U} \qquad \cos(\Phi)=\frac{(Vx-dx/dt)}{U} \qquad \text{Eq. 5. 3}$$

C_D is the stable or constant part of the drag force in this model C_{DM} is taken as the same as C_D. Also, in this model, C_L is the hydrodynamic lift force on a stationary cylinder and $\alpha=2$ (to generate an oscillating drag coefficient of 0.1 on a stationary cylinder).

According to Qu,2019, a coupling term that relates the lift force with the fluctuating force in the in-line direction is added.

$$F_{VX}=\frac{1}{2}C_D\rho D U^2\cos(\beta)+\frac{1}{2}C_L\rho D U^2\sin(\beta)+\frac{1}{2}\alpha C_L^2\rho D U_x|U_x| \qquad \text{Eq. 5. 4}$$

After substitution, the equations are as follows:

$$\frac{d^2x}{dt^2}+2\zeta_x\omega_{xn}\frac{dx}{dt}+\omega_{xn}^2x=\frac{1}{2}\rho D V^2\frac{C_{VX}}{m+m_a} \qquad \text{Eq. 5. 5}$$

$$\frac{d^2y}{dt^2} + 2\zeta_y\omega_{yn}\frac{dy}{dt} + \omega_{yn}^2 y = \frac{1}{2}\rho DV^2\frac{C_{VY}}{m+m_a} \qquad \text{Eq. 5. 6}$$

Where:

$$C_{VX} = -C_L\frac{U}{V^2}\frac{dy}{dt} + C_{DM}\frac{U}{V^2}\left(V-\frac{dx}{dt}\right) + \alpha C_L^2\left(1-\frac{1}{V}\frac{dx}{dt}\right)\left|1-\frac{1}{V}\frac{dx}{dt}\right| \qquad \text{Eq. 5. 7}$$

$$C_{VY} = C_L\frac{U}{V^2}\left(V-\frac{dx}{dt}\right) - C_{DM}\frac{U}{V^2}\frac{dy}{dt} \qquad \text{Eq. 5. 8}$$

The dimensionless equations of motion before introducing the new coupling term in eq. 5.9 are as follows:

$$\frac{d^2q}{d\tau^2} + \varepsilon(q^2-1)\frac{dq}{d\tau} + q = A\left(\frac{d^2Y}{d\tau^2}\cos\beta - \frac{d^2X}{d\tau^2}\sin\beta\right) \qquad \text{Eq. 5. 9}$$

$$\frac{d^2y}{d\tau^2} + 2\Omega_n\zeta\frac{dy}{d\tau} + \Omega_n^2 y = \frac{1}{m^*+C_a}\bullet\frac{1}{2\pi^3 St^2}C_{VY} \qquad \text{Eq. 5. 10}$$

$$\frac{d^2x}{d\tau^2} + 2\Omega_n\zeta\frac{dx}{d\tau} + \Omega_n^2 x = \frac{1}{m^*+C_a}\bullet\frac{1}{2\pi^3 St^2}C_{VX} \qquad \text{Eq. 5. 11}$$

Where:

$$C_{VX} = \left[C_{DM}\left(1-2\pi St\frac{dx}{d\tau}\right) + 2\pi St\frac{dy}{d\tau}C_L\right]\left[\left(1-2\pi St\frac{dx}{d\tau}\right)^2 + \left(2\pi St\frac{dy}{d\tau}\right)^2\right]^{0.5} + \alpha C_L^2\left(1-2\pi St\frac{dx}{d\tau}\right)\left|1-2\pi St\frac{dx}{d\tau}\right|$$

Eq. 5. 12

$$C_{VY} = \left[-2\pi St\frac{dy}{d\tau}C_{DM} + C_L\left(1-2\pi St\frac{dx}{d\tau}\right)\right]\left[\left(1-2\pi St\frac{dx}{d\tau}\right)^2 + \left(2\pi St\frac{dy}{d\tau}\right)^2\right]^{0.5}$$

Eq. 5. 13

According to Qu,2019 there is a relation between the in-line motion and the wake amplitude, and this could be represented in the form of a parametric excitation introduced in equation 5.9

$$\frac{d^2q}{dt^2} + \varepsilon\omega_s(q^2-1)\frac{dq}{dt} + \omega_s^2 q - \frac{k}{D}\frac{d^2x}{dt^2}q = A\frac{d^2y}{dt^2} \qquad \text{Eq. 5. 14}$$

The dimensionless form is as follows:

$$\ddot{q} + \varepsilon(q^2-1)\dot{q} + q - K\ddot{x}q = A\ddot{y} \qquad \text{Eq. 5. 15}$$

5.2. Free oscillation model in the current

In this section, the new wake oscillator model by Qu,2019 is used to model the free oscillation experiments.

Two low-mass damping ratios (m*=2.7 and m*=7) are used to compare the model results with the experimental results found by Jauvtis & Williamson, 2004. Also, the implementation and comments on the results are made. At the end of this section, the cylinder trajectories are commented.

5.2.1. Implementation of Free Oscillation Model

Some important notes for the implementation are:

1. The dimensionless amplitudes Â (that could be y/D or x/D, for sake of simplicity) are unknown.
2. The dimensionless amplitude Â reach a steady state just after a few periods of oscillation, but to be sure this analysis will analyze the response only after the first 50 periods.
3. Â is determined by finding the recurrent maximum displacement.
4. Ωc is determined from the biggest peak in the frequency spectrum after using Fourier ($f_{fourier}$). Then, Ωc_x is the in-line frequency and Ωc_y is the cross-flow frequency. Thus, $\Omega c=(2\pi * f_{fourier})/\Omega_n$
5. The system of equations is solved with the MATLAB function ODE45.
6. The model works with the range of reduced velocity **Vn**=2 to 12, with stepsize= dVn=0.1.
7. The dimensionless frequency is calculated for each **Vn**, $\Omega_n=1/(st*Vn)$.
8. Initial conditions for the first **Vn** is ini= [y dy/dt x dx/dt q dq/dt]= [0 0 0 0 0.1 0].
9. It takes the last results of [y dy/dt x dx/dt q dq/dt] for the new **Vn**.

5.2.2. Equations for Free Oscillation Model

For this analysis, the dimensionless equations are used.

$$\ddot{q}+\varepsilon(q^2-1)\dot{q}+q-K\ddot{x}q=A\ddot{y}$$ <-Equation for wake oscillator Eq. 5. 16

$$\frac{d^2y}{d\tau^2}+2\Omega_n\zeta\frac{dy}{d\tau}+\Omega_n^2 y=\frac{1}{m^*+C_a}\bullet\frac{1}{2\pi^3 St^2}C_{vy}$$ Eq. 5. 17

$$\frac{d^2x}{d\tau^2}+2\Omega_n\zeta\frac{dx}{d\tau}+\Omega_n^2 x=\frac{1}{m^*+C_a}\bullet\frac{1}{2\pi^3 St^2}C_{vx}$$ Eq. 5. 18

<-Equations for cross-flow and in-line vibration

Where

$$C_{VX}=\left[C_{DM}\left(1-2\pi St\frac{dx}{d\tau}\right)+2\pi St\frac{dy}{d\tau}C_L\right]\left[\left(1-2\pi St\frac{dx}{d\tau}\right)^2+\left(2\pi St\frac{dy}{d\tau}\right)^2\right]^{0.5}+\alpha C_L^2\left(1-2\pi St\frac{dx}{d\tau}\right)\left|1-2\pi St\frac{dx}{d\tau}\right|$$ Eq. 5. 19

$$C_{VY}=\left[-2\pi St\frac{dy}{d\tau}C_{DM}+C_L\left(1-2\pi St\frac{dx}{d\tau}\right)\right]\left[\left(1-2\pi St\frac{dx}{d\tau}\right)^2+\left(2\pi St\frac{dy}{d\tau}\right)^2\right]^{0.5}$$ Eq. 5. 20

$$C_L=\hat{cL}*q/2$$ Eq. 5. 21

$$C_L^2=\hat{cL}^2q^2/4$$ Eq. 5. 22

$$C_{DM}=1.2-\alpha\frac{\hat{cL}^2}{2}$$ Eq. 5. 23

Qu,2019 proposed two sets of parameters for matching the lower and upper branch of the experimental results for low mass-damping ratio by Jauvtis & Williamson, 2004.

	κ	$\hat{c}L$	St	m*	α	ζ	(m*+Ca)ζ
General parameters	5	0.3	0.1932	7.0	2.0	0.0015	0.0117

Table 5. 1

	κ	$\hat{c}_L$	St	m*	α	ζ	(m*+Ca)ζ
General parameters	5	0.3	0.1932	2.6	2.0	0.0036	0.013

Table 5. 2

	A	ε
Lower branch	20	0.8
Upper branch	8	0.08

Table 5. 3

5.2.3. Algorithm

The diagram below 5.2 shows the programming algorithm and the diagram of the code maingeneva.m and geneva.m. It works with the codes: 'maingeneva.m', 'initialageneva.m', 'geneva.m' and 'spectrum_dos.m'. Furthermore, the code 'geneva.m' can be found in Appendix B.

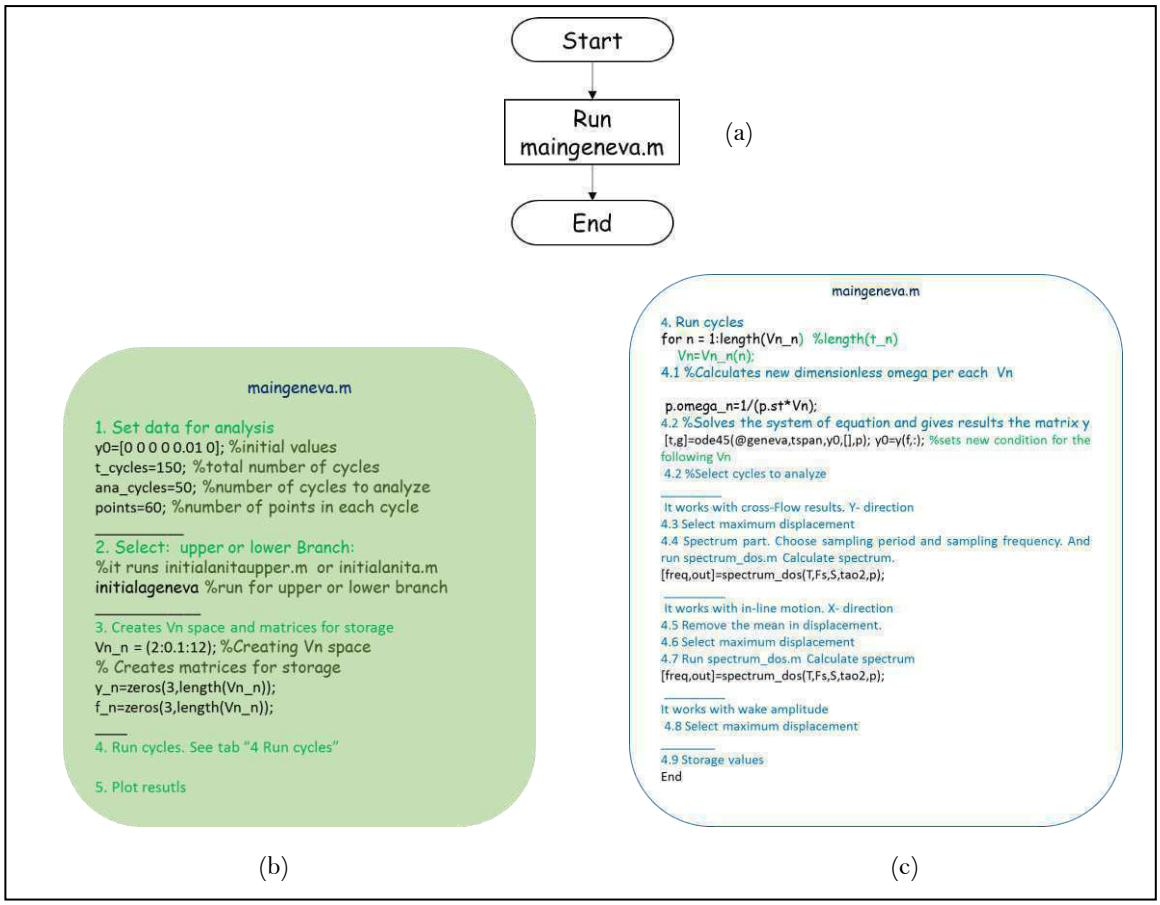

Diagram 5. 1

The main code is maingeneva.m Inside maingeneva.m there are four main parts. First, the initial data is set. Second, other parameters are called and storage in the arrangement p: the code initialgeneva.m is used for parameters for modeling the upper branch and the lower branch curves. Third, cycles, where the equation is solved with the help of the function ode45, are run for each reduced velocity (Vn) and

storage in a matrix. The cycles part is described in the part c of the diagram 5.2. Fourth, the results are plottedted.

5.2.4. Solving Equations with Function ODE45

In order to solve the differential equations, they need to be rewritten. The equation 5.24 shows how the equation is rewritten, and the equation 4.24 shows how is implemented in the code. Similar happens with equation 5.25 and equation 5.28, and equation 5.26 and equation 5.29.

$$\frac{d^2y}{d\tau^2} = -2\Omega_n\zeta\frac{dy}{d\tau} - \Omega_n^2 y + \frac{1}{m^* + C_a}\bullet\frac{1}{2\pi^3 St^2}C_{vy} \qquad \text{Eq. 5. 24}$$

$$\frac{d^2x}{d\tau^2} = -2\Omega_n\zeta\frac{dx}{d\tau} - \Omega_n^2 x + \frac{1}{m^* + C_a}\bullet\frac{1}{2\pi^3 St^2}C_{vx} \qquad \text{Eq. 5. 25}$$

$$\frac{d^2q}{d\tau^2} = -\varepsilon(q^2-1)\frac{dq}{d\tau} - q + K\frac{d^2x}{d\tau^2}q + A\frac{d^2y}{d\tau^2} \qquad \text{Eq. 5. 26}$$

$$y(2);\ -2\Omega_n\zeta\frac{dy}{d\tau} - \Omega_n^2 y + \frac{1}{m^* + C_a}\bullet\frac{1}{2\pi^3 St^2}C_{vy};\qquad \text{Eq. 5. 27}$$

$$y(4);\ -2\Omega_n\zeta\frac{dx}{d\tau} - \Omega_n^2 x + \frac{1}{m^* + C_a}\bullet\frac{1}{2\pi^3 St^2}C_{vx};\qquad \text{Eq. 5. 28}$$

$$y(6);\ -\varepsilon(q^2-1)\frac{dq}{d\tau} - q + K\frac{d^2x}{d\tau^2}q + A\frac{d^2y}{d\tau^2};\qquad \text{Eq. 5. 29}$$

Inside maingeneva.m the equation is called to be solved with the function ode45 with the line [t,g]=ode45(@geneva,tspan,y0,[],p);. In the code geneva.m the equation is defined and adjusted to be solved.

The function returns a matrix with the solution for y, dy/dt, x, dx/dt, q, dq/dt. This matrix is [tn x 6], where tn is the length of the time span. The complete code geneva.m is in appendix B. The diagram 4.2 with the function is shown below.

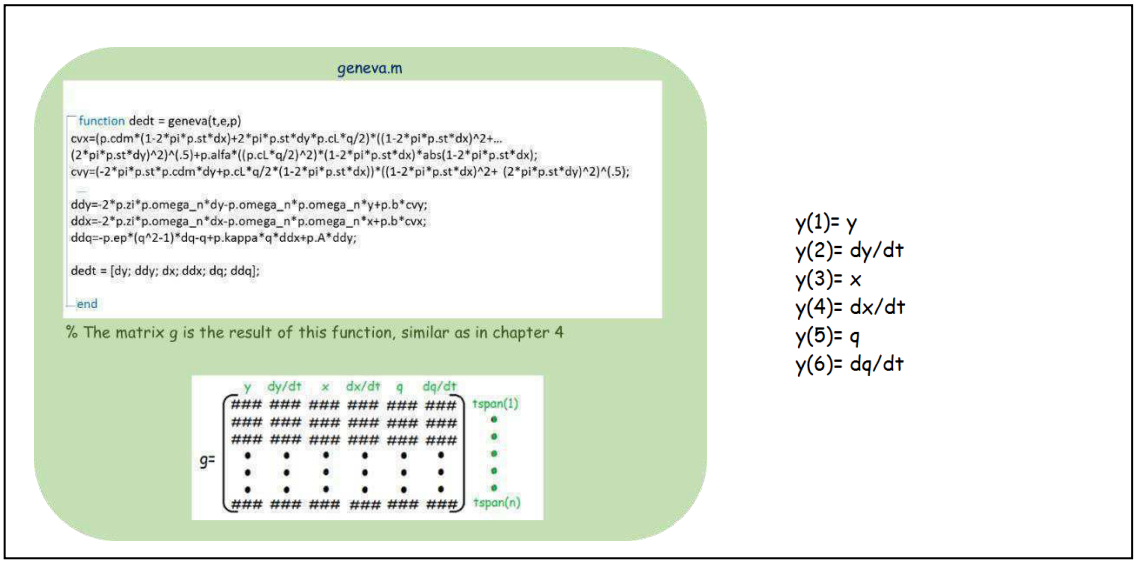

Diagram 5. 2

5.2.5. Results Free Oscillation Model

Results for m*=7.0

The parameters used for m*=7.0 are shown in tables 5.1 and 5.3

The figures 5.2a and 5.2b show the results for cross-flow direction. In both figures, we can see that the model results have the same order of magnitude that the results found by Jauvtis & Williamson, 2004.

In figure 5.2a, the cross-flow amplitude is shown. The model results have three main elevations, one at Vn=2.9 with 0.025D, other at Vn=6.9 with 1.09D and one at Vn=9.7 with 0.66D. The highest amplitude of the upper branch of the experimental results is 1.06D at Vn=6.9 and in the lower branch is about .64D at Vn=8.63, moreover the experimental results have a small hill 0.063D at Vn=3.3. Thus, the match in terms of amplitude is very similar.

The ranges of lock-in of the lower and upper branches coincide, in the experimental results the range of the upper branch is between Vn=4 to 8.27.

The figure 5.2b shows the radian frequency ratio Ωcy/Ωn. In the figure, there are three lock-in ranges one in the range between Vn=2 to 3.4, other in the range between Vn=4 to 5.8 and the third one in between Vn=5.8 to 10.8 in the model results for the lower branch, while in the experiment results apparently five lock-in ranges are found. Although these five lock-in are not properly represented by the model, the range of the general lock-in is correctly captured.

(a)

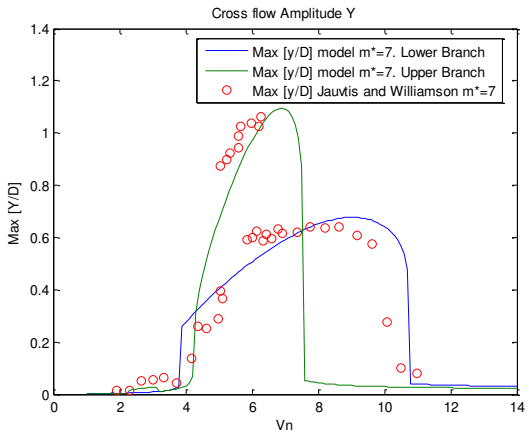

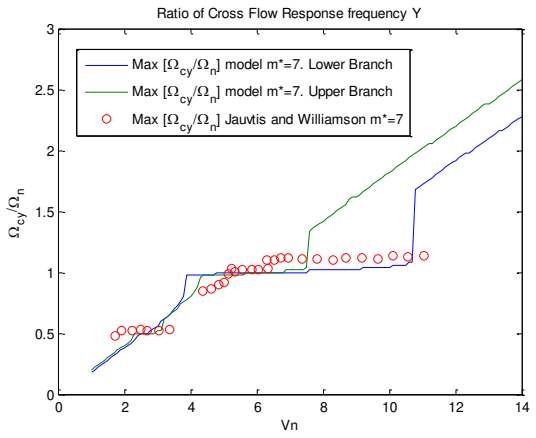

(b)

Figure 5. 2 m*=7. (a) Dimensionless Cross-flow amplitude (b) Ratio of Cross flow response frequency Ω_{cy}/Ω_n

The figures 5.3a and 5.3b show the results for the in-line direction. In both figures, we can see that the model results have the same order of magnitude that the experimental results.

In figure 5.3a, the in-line amplitude is shown. In this graph, it is possible to see that the amplitudes are much smaller than the amplitudes in the cross-flow direction. The model results represent the two curves for the lower and the upper branch. For the upper branch curve, the model an amplitude of 0.064D at Vn=7, meanwhile the experimental results have an amplitude of 0.035D at Vn=5.9. Thus, the crest of the curve of the upper branch looks more inclined towards high reduced velocities. Also, the model represents the hill in the range between Vn=2 to 4, with a similar amplitude of 0.12D as in the experimental results.

For the case of the lower branch, the lock-in range coincides between Vn=4 to 10.9. And the amplitude of the experimental results is slightly lower with 0.079D than the model results with 0.01D. Then the upper branch model represents two peaks, and the lower branch represents one peak, all three found in the experiments.

The figure 5.3b shows the radian frequency ratio Ωcx/Ωn. In this figure, there are no experimental results to compare with. However, the range of frequencies with lock-in coincides with the branches in figure 5.3a. Moreover, the model shows a peak with an amplitude of 0.98 at Vn=1.3.

(a)

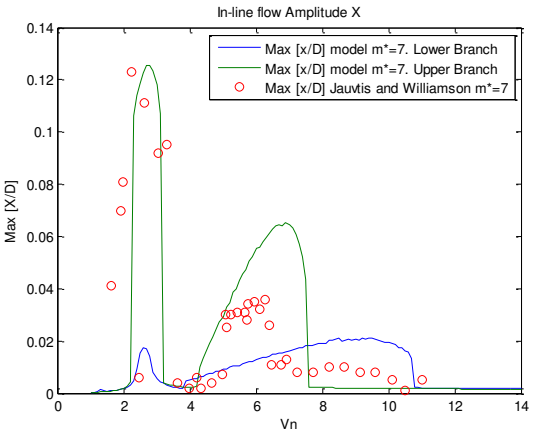

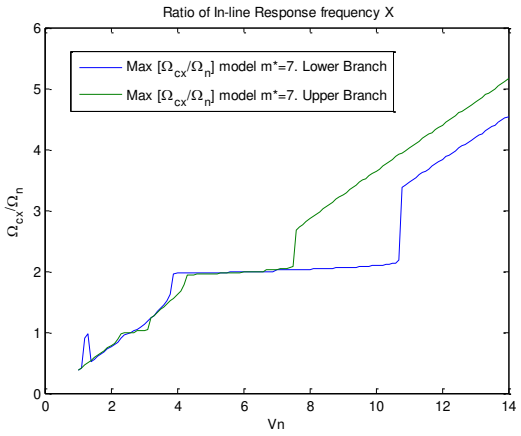

(b)

Figure 5. 3 m*=7. (a) Dimensionless In-line amplitude (b) Ratio of In-line response frequency Ω_{cx}/Ω_n.

Results for m*=2.6

The parameters used for m*=2.6 are shown in tables 5.2 and 5.3

The figures 5.4a and 5.4b show the results for cross-flow direction. In both figures, we can see that the model results have the same order of magnitude that the results found by Jauvtis & Williamson, 2004.

In figure 5.4a, the cross-flow amplitude is shown. The model results have three main elevations, one at Vn=3 with 0.05D, another at Vn=8.9 with 1.7 D, and other at Vn=10.38 with 0.7D.
The experimental results have the highest amplitude of the upper branch is 1.5D at Vn=8.7, in the lower branch is about .72D at Vn=9.86, they also have other two hills, one of 0.15D at Vn=3.3, and other of 0.16D at Vn=12.95. Thus, in terms of amplitude the match is very similar, the model represents 2 of the 4 curves found in the experiments.

The figure 5.4b shows the radian frequency ratio Ωcy/Ωn. The ranges of lock-in of the lower and upper branches coincide, in the experimental results the range of the upper branch is between Vn=4 to 8 with a value of Ωcy/Ωn~1, the range of the lower branch is between Vn=7.79 to 12.8 with a value Ωcy/Ωn=1.28. Also, an extra lock-in range is capture by the experiments in the range between Vn=2 to 4 with a value Ωcy/Ωn=0.52. From low to high reduced velocities, the model represents the three lock-in ranges.

The figures 5.5a and 5.5b show the results for in-line direction.

In figure 5.5a, the in-line amplitude is shown. The model results have three main elevations, one at Vn=2.8 with 0.12D, other at Vn=8.8 with 0.8D and one at Vn=9.8 with 0.6D. The experimental results have the highest amplitude of the upper branch is 0.31D at Vn=7.4, in the lower branch is about .06D at Vn=9.8, they also have other hills, one of 0.11D at Vn=3. Thus, the model represents the 3 curves

found in the experiments, and they match very well in terms of amplitude and lock-in ranges. Only in the upper branch curve, the peak of the model results is twisted to the right towards high reduced velocities, it looks more inclined contrary to the model curve, that it looks more vertical.

(a)

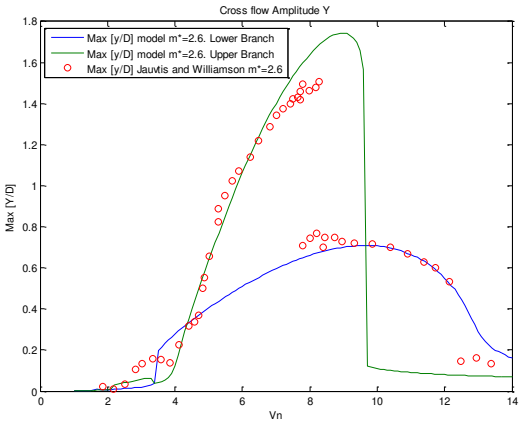

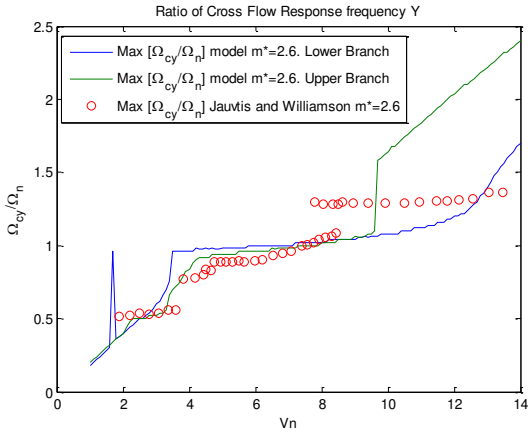

(b)

Figure 5. 4 m*=2.6. (a) Dimensionless Cross flow amplitude (b) Ratio of Cross flow response frequency Ω_{cy}/Ω_n

The figure 5.5b shows the radian frequency ratio Ωcx/Ωn. In this figure, there are no experimental results to compare with. In the model results, there are two lock-in ranges, one in the range between Vn=2 to 3.5 with a Ωcy/Ωn~1, other in the range between Vn=3.5 to 12.5 with a Ωcy/Ωn~2, and there is a peak in the range between Vn=1 to 1.6 with a peak of Ωcx/Ωn~1.

(a)

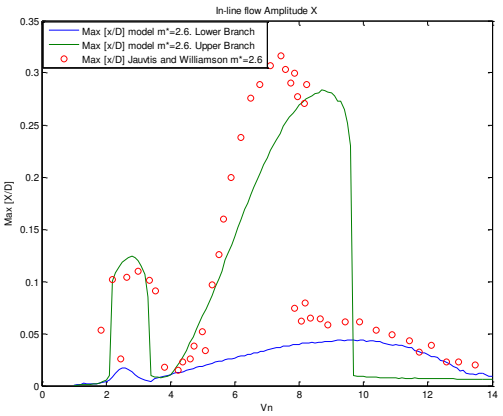

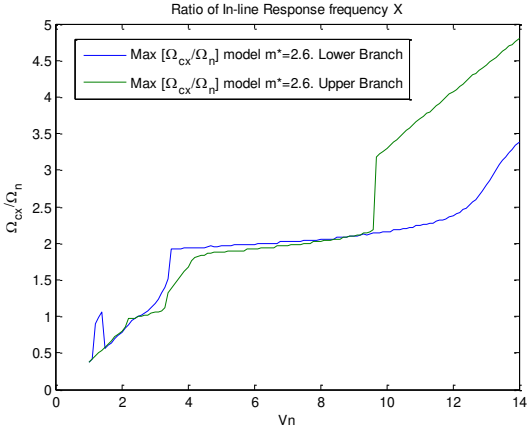

(b)

Figure 5. 5 m*=2.6. (a) Dimensionless In-line amplitude (b) Ratio of In-line response frequency Ω_{cx}/Ω_n.

5.2.6. Cylinder trajectories for the Free oscillation model

The intention of this section is to show the evolution of the shape of the cylinder trajectories on the free oscillation model.

Figure 5.6 shows the amplitude in the cross-flow direction and in the in-line direction. The figures A, B, C, D, E, F, and G show the cylinder trajectories at different reduced velocities. The cylinder trajectories plots show how is the trajectory of vibration of the cylinder. And checking its amplitude gives an idea in a real time of how it vibrates along the complete Vn range.

(a)

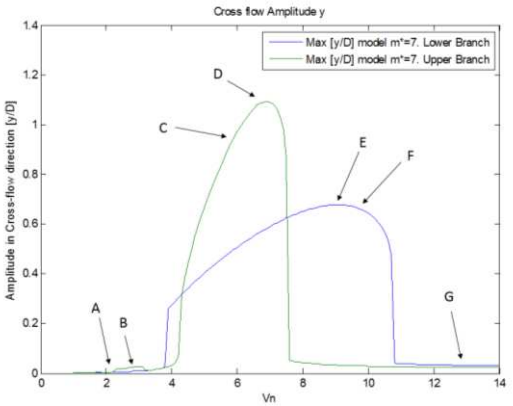

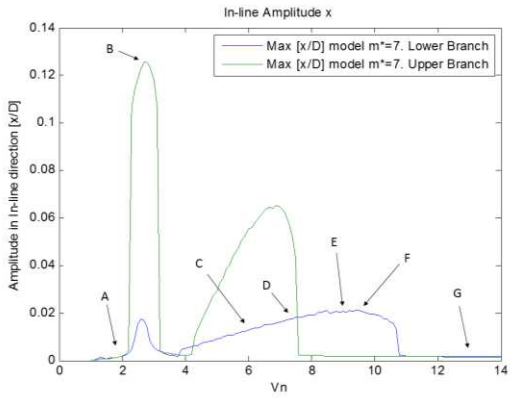

(b)

Figure 5. 6 (a) Amplitude in Cross-flow direction (b) Amplitude in In-line direction

In figure 5.7a we can see the start of the amplitude of the curve at Vn=2, and how the trajectory of the cylinder starts. And in figure 5.7B, we can see that there is a very defined eight shape, this shape is in the maximum amplitude of the first lock-in ranges at Vn=2.7. We can see that there is an amplification in the amplitudes, especially if we compare the magnitudes now of 0.02 and 0.1 with the amplitudes of figure 5.7A of 4 x10^{-3} and 1 x10^{-3}.

(a)

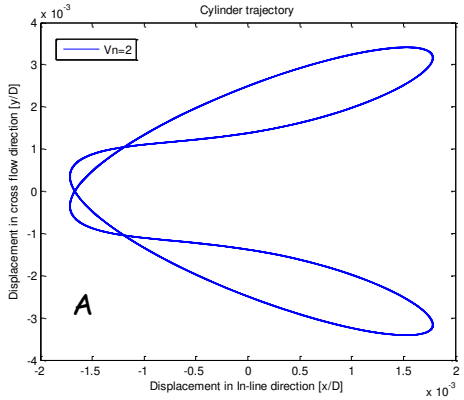

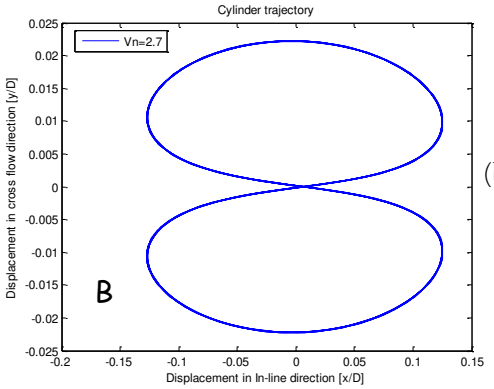

(b)

Figure 5. 7 Cylinder trajectories: (a) Cylinder trajectory. Vn=2 (b) Cylinder trajectory. Vn=2.7

In figures 5.8a and 5.8 we can see how the amplitude is growing, also this coincides with it is seen in the figures 5.6a and 6.5b. Also, it is possible to see in figure 5.8a the evolution of the shape into an eight, from the base of the hill in figure 5.6a at Vn=6, and in figure 5.8b how is the shape in the crest of the upper branch at Vn=6.9.

(a)

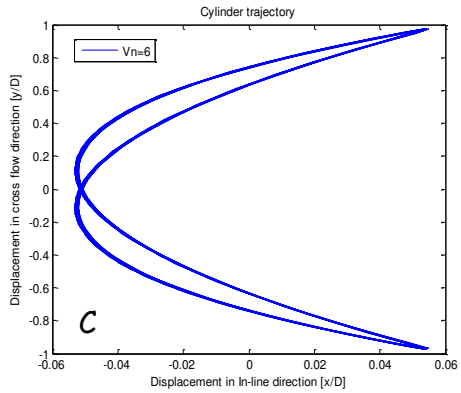

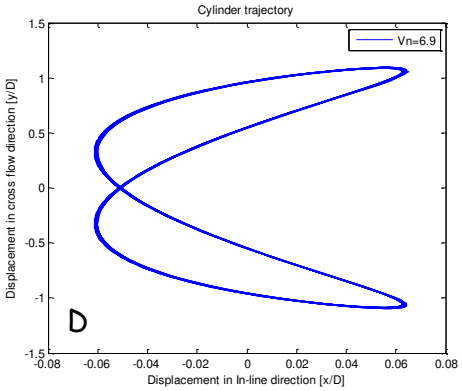

(b)

Figure 5. 8 Cylinder trajectories: (a) Cylinder trajectory. Vn=6 (b) Cylinder trajectory. Vn=6.9

In figures 5.9a and 5.9b the amplitudes of vibration have reduced as in the figures 5.6a and 6.5b in the same ranges of Vn. However, a nice eight shape showed in 5.9a is found at the crest of the lower branch at Vn=9, and the arc shape of 5.9b is found still in the lower branch but when the amplitudes have decreased at Vn=9.5.

(a)

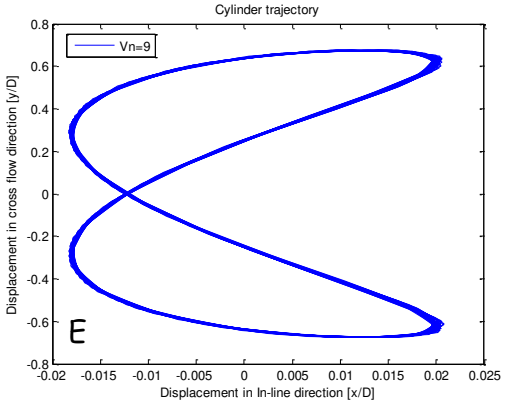

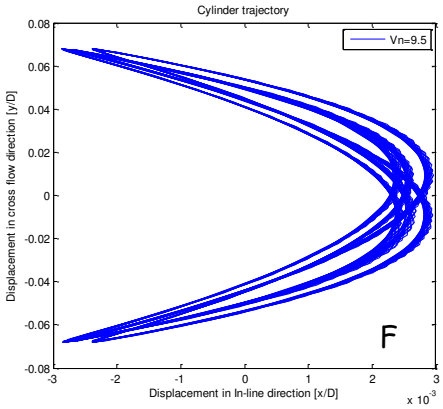

(b)

Figure 5. 9 Cylinder trajectories: (a) Cylinder trajectory. Vn=9 (b) Cylinder trajectory. Vn=9.5

Finally, in figure 5.10, an arc shape is displayed when after the lower branch finishes at Vn=13. It is possible to see how the in-line with an amplitude of 1.5 x 10^{-3} D and the cross-flow amplitude of 0.03D have diminished in comparison with the data of figure 5.7E that is in the crest of the lower branch.

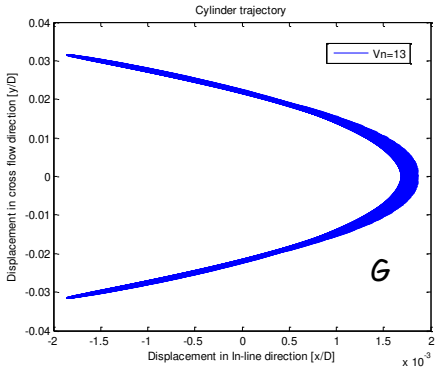

Figure 5. 10 Cylinder trajectories: Cylinder trajectory. Vn=13

A comparison in dimension can be found in the appendix C. Comparing with graphs of Jauvtis and Williamson,2004. We can notice very similar results in terms of shape.

5.3. Forced oscillation model

In this section, the new wake oscillator model by Qu,2019 is used to model forced in-line vibration experiments.

The model results are compared with the experimental results of Nishihara, 2005. Also, the implementation is explained and some comments on the results are made.

5.3.1. Implementation of the Forced oscillation model

This model is implemented to reproduce forced oscillation experiments. For this model is considered that there is a rigid cylinder inside of a fluid with a constant velocity, the cylinder is forced to vibrate in in-line direction.

Some important notes for the implementation are:

1. In this model, the cross-flow vibration (y) is restricted and its derivatives with respect to time.
2. The in-line vibration is known (x), and its derivatives with respect to time. In this case:

$$x = \hat{x}\sin(\Omega_r \Upsilon) \quad \text{Eq. 5. 30}$$
$$\dot{x} = \hat{x}\cos(\Omega_r \Upsilon)\Omega_r \quad \text{Eq. 5. 31}$$
$$\ddot{x} = -\hat{x}\sin(\Omega_r \Upsilon)\Omega_r^2 \quad \text{Eq. 5. 32}$$

3. As the cross-flow vibration is restricted or known as zero (thus, y=0, dy/dt=0, $d^2y/dt^2=0$) and the in-line vibration is imposed, thus, also known. Only the equation of the wake vibration is used for this model.
4. It is considered that a steady state is reached after some periods of oscillation, for the model for at least 400 cycles.
5. The system of equations is solved with the matlab function ODE45.
6. The reduced force velocity Vr is obtained from normalized the flow velocity with the radian frequency of oscillation ω_r.
7. The model works with the range of reduced force velocity Vr=1 to 5, with stepsize= dVr=0.1.
8. The radian frequency dimensionless is calculated for each Vr, $\Omega_r = 1/(st\ V_r)$.
9. Initial conditions for the first Vr is ini= [q dq/dt]= [0.1 0].
10. From the results of the system of equations, C_{vx}, C_{dmean}, C_{vy} (drag and lift coefficients) are calculated.
11. f_{cvy} (frequency of C_{vy}) is determined from the biggest peak in the frequency spectrum after using Fourier. Thus, $\Omega_{cvy} = 2\pi f_{cvy}$.
12. The dimensionless radian frequency for cross-flow direction is (Ω_{cvy}/Ω_r) is equal to $2\pi f_{cvy}/\Omega_r$.

5.3.2. Equations Forced oscillation model

In order to analyze the results, the following formulas have been used. The equation is in dimensionless form.

$$\ddot{q} + \varepsilon(q^2 - 1)\dot{q} + q - K\ddot{x} = 0$$ ←Equation for wake oscillator

Qu,2019 proposed two sets of parameters for matching the lower and upper branch of the experimental results.

	A	ε	κ
Lower branch	20	0.8	5.0
Upper branch	8.0	0.08	5.0

Table 5. 4

In order to analyze the results. The following formulas have been used. For further explanation see Appendix A.

Added mass coefficient (Cmass)

$$Cmass = \frac{1}{2}\frac{Cx_o \cos\varphi_x}{\Omega^2 \pi^3 St^2 x_o} \quad \text{Eq. 5. 33}$$

Added damping coefficient (Ca)

$$Ca = -\frac{1}{4}\frac{Cx_o \sin\varphi_x}{\Omega^2 \pi St^2 x_o} \quad \text{Eq. 5. 34}$$

CDmean:

$$CDmean = \frac{1}{T}\int C\hat{V}X \cdot dt \quad \text{Eq. 5. 35}$$

Cross-flow force coefficient:

$$C_{VY} = \left[C_L\left(1-2\pi St\frac{dx}{d\tau}\right)\right]\left|1-2\pi St\frac{dx}{d\tau}\right| \quad \text{Eq. 5. 36}$$

$$C_L = \hat{cL} * q/2 \quad \text{Eq. 5. 37}$$

Also, the In-line force coefficient is calculated as follows:

$$C_{V\hat{X}} = C_{VX} - 2Ca\ddot{x}\pi^3 St \quad \text{Eq. 5. 38}$$

Where:

$$C_{VX} = \left[C_{DM}\left(1-2\pi St\frac{dx}{d\tau}\right)\right]\left|1-2\pi St\frac{dx}{d\tau}\right| + \alpha C_L^2\left(1-2\pi St\frac{dx}{d\tau}\right)\left|1-2\pi St\frac{dx}{d\tau}\right| \quad \text{Eq. 5. 39}$$

$$C_{DM} = 1.2 - \alpha\frac{\hat{cL}^2}{2} \quad \text{Eq. 5. 40}$$

$$C_L^2 = \hat{cL}^2 q^2/4 \quad \text{Eq. 5. 41}$$

Where the term $2Ca\times\pi^3 St$ is equivalent in a dimensional form to $ma\ddot{x}$

$$(ma+m)\ddot{x}+c\dot{x}+kx = Fvx \quad \text{Eq. 5. 42}$$

$$m\ddot{x}+c\dot{x}+kx = Fvx - ma\ddot{x} \quad \text{Eq. 5. 43}$$

The term of the right hand side of the equation in its dimensionless form is equal to:

$$C_{VX} - 2Ca\ddot{x}\pi^3 St \quad \text{Eq. 5. 44}$$

See appendix A for further calculations.

5.3.3. Algorithm

The diagram below shows the programming algorithm and the diagram of the code mainichi.m and ichi.m. It works with the codes: 'mainichi.m', 'initiallapa.m', 'ichi.m' and 'spectrum_dos.m'. Furthermore, the code ichi.m can be found in Appendix B.

The main code is mainichi.m. Inside mainichi.m there are four main parts. First, initial data is set. Second, other parameters are called and storage in the arrangement p: the code initialgeneva.m is used for parameters for modeling the upper branch and the lower branch curves. Third, cycles where the equation is solved with help of the function ode45 are run for each reduced velocity (Vn) and storage in a matrix. The cycles part is described in the part c of the diagram 5.4. Fourth, the results are plottedted.

The code ichi.m is described in the section 5.3.4

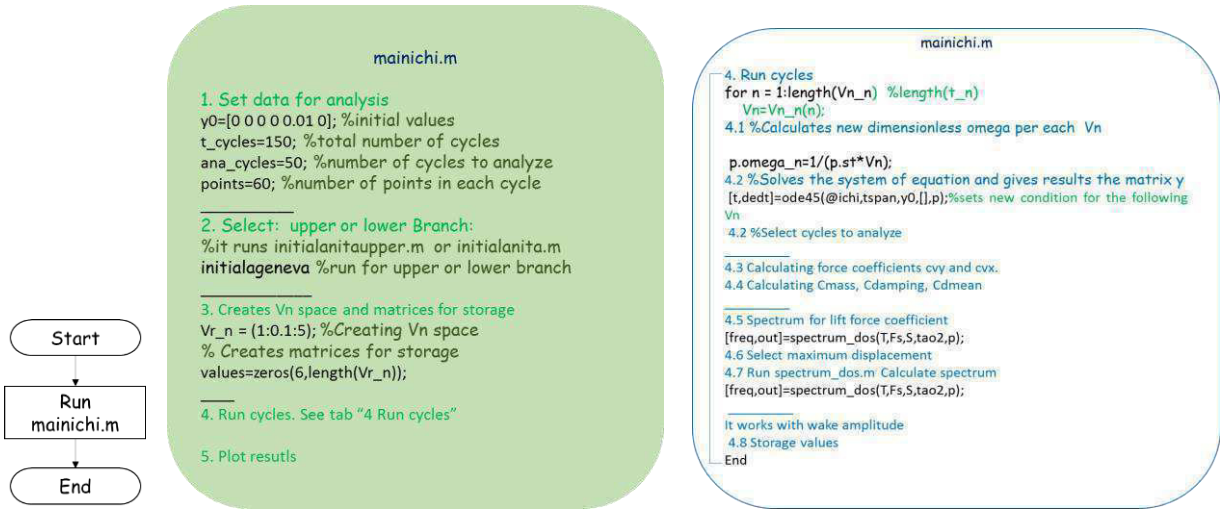

(a) (b) (c)

Diagram 5. 3

5.3.4. Solving Equations with function ODE45

In order to solve the differential equations, they need to be rewritten. The equation 5.45 shows how the equation is rewritten, and the equation 4.45 shows how is implemented in the code.

$$\frac{d^2q}{d\tau^2} = -\varepsilon(q^2-1)\frac{dq}{d\tau} - q + K\frac{d^2x}{d\tau^2}q + A\frac{d^2y}{d\tau^2} \qquad \text{Eq. 5. 45}$$

$$e(2);\ -\varepsilon(q^2-1)\frac{dq}{d\tau} - q + K\frac{d^2x}{d\tau^2}q + A\frac{d^2y}{d\tau^2};\ \qquad \text{Eq. 5. 46}$$

Inside mainichi.m the equation is called to be solved with the function ode45 with the line:

```
[t,dedt]=ode45(@ichi,tspan,y0,[],p); % dedt = [q dq];
```

In the code ichi.m the equation is defined and adjusted to be solved.

The function returns a matrix with the solution for yq, dq/dt. This matrix is [tn x 2], where tn is the length of the time span. The code ichi.m is in appendix B. The diagram 4.3 with the function is shown below.

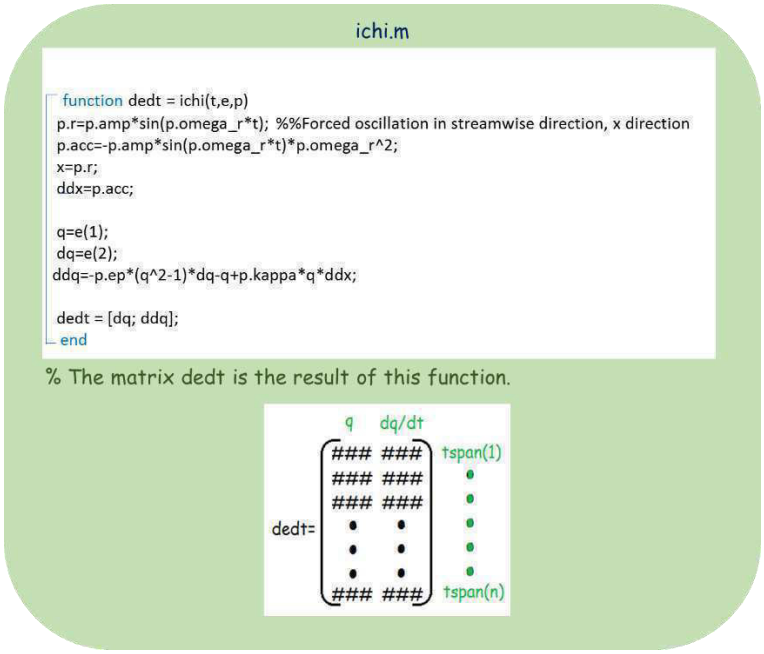

Diagram 5. 4

5.3.5. Results for Forced vibration model

In order to compare the results with respect to the forced oscillation experiments by Nishihara, 2005. The following parameters were used. The model was run for Vn in the range 1-5.

	κ	Cdmean	St	α	cL	Xo- Force amplitude	Initial values y0=[q dq];
General parameters	5	1.01	0.182	2.0	0.3	0.05	y0=[0.01 0];

	A	ε
Lower branch	20	0.8
Upper branch	8	0.08

The results are divided into two sets of graphs. Figure 5.4 shows the results for the upper branch and figure 5.5 shows the results for the lower branch.

Results for The Upper Branch

In the fig 5.11a, a hat shape is seen in the range Vn~2-3.5, also it can be seen as a range of lock-in, but with a small decrement at Vn~2.6. This also can be corroborated with the fig. 5.11b, where there is a lock-in in the range Vn~2-3.5 with $\Omega_{CVY}/\Omega_n = 0.5$.

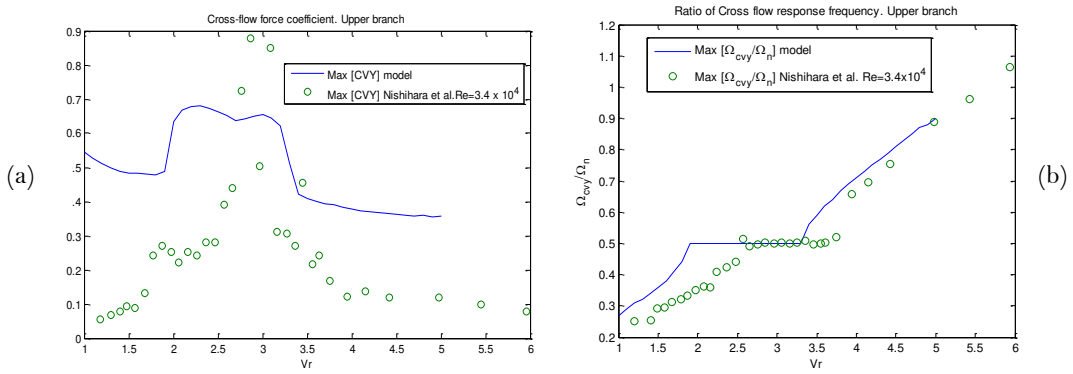

Figure 5. 11 Upper Branch (a) Cross flow force coefficient (CVY) (b) Ratio of Cross flow response frequency ΩCVY/Ωn

The figure 5.12a shows the mean of the drag force coefficient CD_{mean}. In the figure 5.12a, there is a hill between the ranges Vn=1.7 to 3.5, with a maximum amplitude of 1.5 at Vn=2.7. Similar to the experiments of Nishihara, but the peak found by Nishihara was higher by 0.2 with 1.7 at Vn=2.86.

The figure 5.12b shows the dimensionless damping coefficients. It looks like it gives energy instead of extracting. At the same time in the experiments, there is change of shape at Vn~2.7. But in the experiments the change is the opposite, however it is still in the range of the negative values.

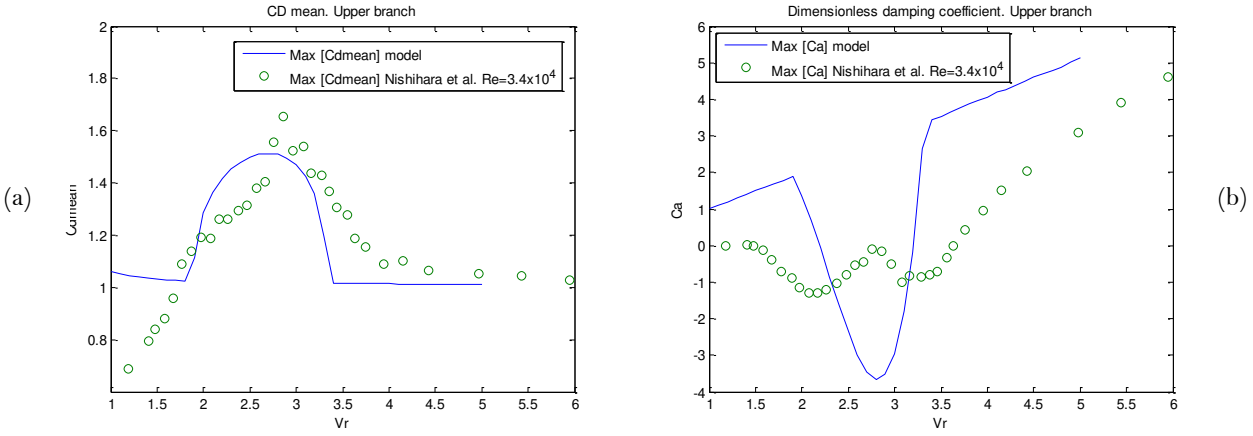

Figure 5. 12 Upper Branch (a) CDmean (b) Dimensionless damping coefficient coefficient (CVX)

In figure 5.13a, the model results and the experimental results are in the same order of magnitude. However, apart from that, there are no similarities between the results. In fact, the both curves results (model and experimental) have a different shape. The model results have an increase in magnitude in the range between Vn=1.8 to 2.2, and then a decreased until reach a value of -0.02 at Vn=3.2

In figure 5.13b, there is a range between Vn~2.3-3.5 where a small hill is formed. And during the whole range of reduced velocities, CVX decreases in magnitude.

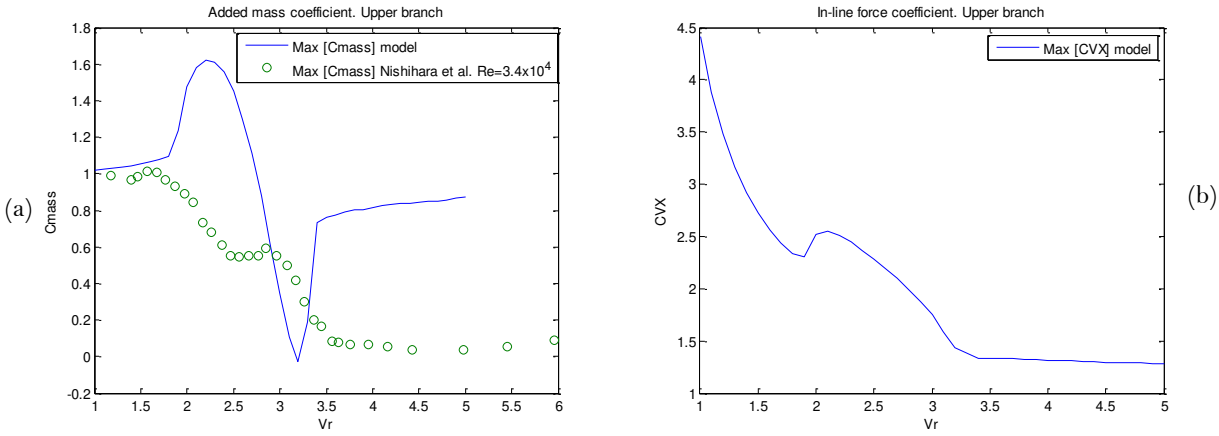

Figure 5. 13 Upper Branch (a) Added mass coefficient (b) In-line force coefficient (CVX)

Results for The Lower Branch

Now the lower Branch results are compared with the experiments of Nishihara, 2005

The fig 5.14a shows the lift force coefficient. In the graph 5.14a, there is almost a continuous value around 0.4 is in the whole range of reduced velocities. These graphs do not have similar shape.

In the fig. 5.14b, in the model results there is a lock-in in the range Vn~2 to 3.5 with Ω_{CVY}/Ω_n= 0.5 and in the experimental results there is a lock-in in the range Vn~2.5 to 4

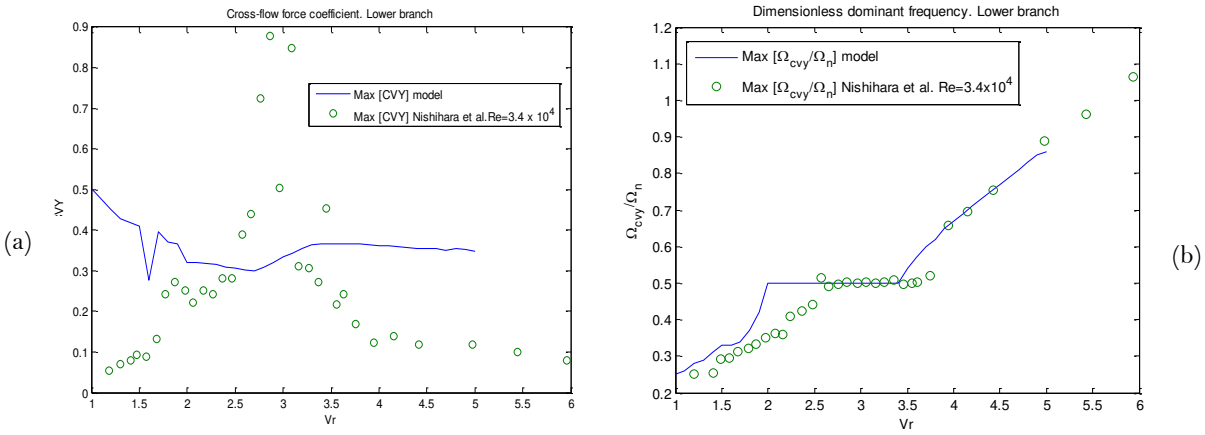

Figure 5. 14 Lower Branch (a) Cross flow force coefficient (CVY) (b) Ratio of Cross flow response frequency Ω_{CVY}/Ω_n

The figure 5.15a shows the mean of the drag force coefficient CD_{mean}. In the figure 5.15a, in the model curve, there is a hill between the ranges Vn=2.5 to 3.5, with a maximum amplitude of 1 at Vn=3.2. Like the experiments of Nishihara, but the peak found by Nishihara with 1.7 at Vn=2.86.

The figure 5.15b shows the dimensionless damping coefficient, which looks like it gives energy instead of extracting. At the same time in the experiments, there is change of shape at Vn~3. But in the experiments the change is the opposite, however the dimensionless damping coefficient is still in the range of the negative values and with the same order of magnitude.

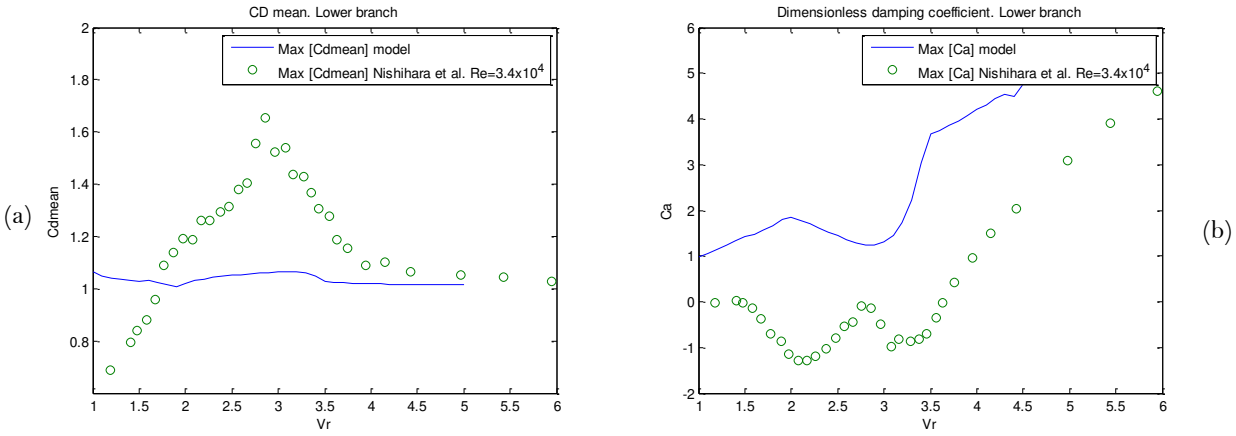

Figure 5. 15 Lower Branch (a) CDmean (b) Dimensionless damping coefficient

Figure 5.16a shows the added mass coefficient. In figure 5.16a, the model results and the experimental results are in the same order of magnitude. Both curves are in the same shape, both with positive values.

Figure 5.16b shows the in-line force coefficient. During the whole range of Vn CVX decreases in magnitude.

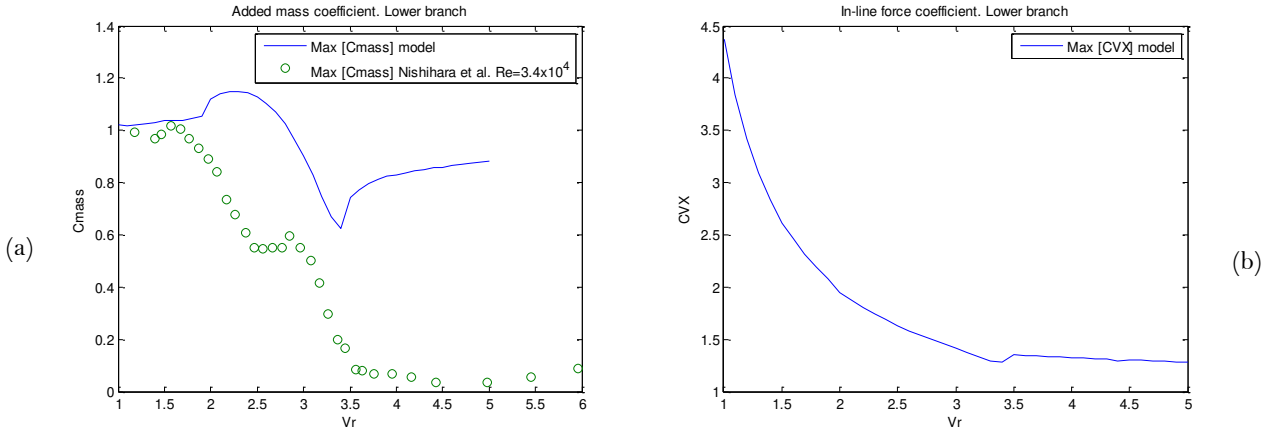

Figure 5. 16 Lower Branch (a) Added mass coefficient (b) In-line force coefficient (CVX)

5.4. Conclusions on wake oscillator model with a new coupling term in the wake equation

In this chapter the modified wake oscillator model by Qu,2019 was explored. The model was explained with its governing equations. The idea of this chapter was to investigate the advantages and drawbacks of the model. With that goal, the model was used to reproduce free oscillation experiments and forced in-line vibration experiments.

5.4.1. Comments on results of the free oscillation model

Two different mass ratio were analyzed m*=2.6 and m*=7. As it can be seen in the graphs, when m* is lower the lock-in range increases (for both cases cross-flow and in-line direction).

Talking about similarities with the experiments. For the free oscillation model. In the lower branch, for the cross-flow amplitude, the model curve and the experiment results from Govardhan & Williamson,2004 have the same shape. The curves start going up around Vn=4. However, the model curve develops higher amplitude, with a difference of 0.1 diameters. Also, there the model curve reaches its highest point at Vn~9, meanwhile the results from Govardhan & Williamson,2004 reaches its maximum point around Vr~8.5. Furthermore, in the graph of Govardhan & Williamson,2004 there is a small peak at Vn~2.7 and in the model is reflected. Then, in terms of magnitude and shape the model results and the experimental results are very similar.

On the other hand, for the frequency ratio, the shape and the start of the curves and the resonance range along Vn axis is almost the same. However, the Govardhan & Williamson,2004 experiments show that this part is extended until Vn~11, meanwhile in the model, it finishes until around Vn=10.5. Then, the model results coincide with the lock-in range of the experimental results, but they are shorter.

For lower branch in in-line vibration. The amplitude and the frequency ratio for in-line motion, show the same shape that their correspondent the cross-flow curves.

For the Upper branch curves, the behavior of the model curves has a good match with the results obtained by Govardhan & Williamson,2004.

In general, the model was able to reproduce a first lock-in range normally situated in the experiments in the range between Vn=2 to 4, physics that was not possible to reproduce in the model of chapter 4.

Then, it can be concluded that in terms of amplitude, range of lock-in frequencies and shape, the model was successful in reproducing free oscillation experiments.

5.4.2. Comments on results of forced in-line vibration model

After checking different variables in the performance of the forced in-line vibration model, it was possible to check that some graphs are close enough to imitate the results found by Nishihara, 2005, however, most of them are only similar in order of magnitude, but they are very different with respect to the experimental results.

The figures 5.11a and 5.15a both represent the mean of the drag force coefficient (for the upper and the lower branch, respectively), and in both plots, the shape of the model results and the experimental results are in correspondence, with some differences in amplitude. Similar happens when $\Omega cvy/\Omega r$ is displayed (for the upper and the lower branch).

On the other hand, the rest of the graphs have the same order of magnitude of the model results with respect to the experimental results.

Then, it can be concluded that in terms of amplitude, a range of lock-in frequencies and shape in the different measured parameters, the model still has room for improvement in terms of modelling forced in-line vibration experiments.

Finally, it is possible to conclude that, comparing the model of this chapter with respect to the model of chapter 4. The model of this chapter has an improvement reproducing the physics of VIV in free oscillation experiments. Nevertheless, in terms of reproducing force in-line vibration experiments, the model still need to be improved.

Chapter 6

Sensitivity Analysis

In chapter 5 the modified wake oscillator model by Qu,2019 was introduced. Also, in chapter 5 the model was used to model forced in-line vibration experiments and free oscillation experiments.
Identify the sensibility of the model to own parameters and to external variables is part of the objectives of this thesis. Thus, in this chapter two main cases will be investigated.

- Sensitivity to parameters of the modified wake oscillator model by Qu,2019.
- Sensitivity to external variables.

The chapter includes the results of the different analysis and comments on the results.

6.1. Sensitivity to parameters of the modified wake oscillator model by Qu,2019.

In this section, the sensitivity to parameters that work as tuning parameters is explored. Three cases are explored:

- Sensitivity to ε
- Sensitivity to A
- Sensitivity to κ

6.1.1. Sensitivity to variable ε

In this section, the sensitivity to variable ε is explored. The results are divided intoto two sections, lower branch results, and upper branch results. Also, the experimental results found by Govardhan & Williamson,2004 are plotted.

The following parameters were used for the lower and the upper branch, respectively:

	κ	$\hat{c}_L$	St	m*	α	ζ	(m*+Ca)ζ	Ca
General parameters	5	0.3	0.1932	7.0	2.0	0.00146	0.0117	1

	A	ε
Lower branch	20	variable
Upper branch	8.0	variable

Lower branch results

Usually, ε=0.8 is used for the lower branch. Figure 6.1a shows the amplitude in the cross-flow direction. In the graph the influence of ε involves a small change in the maximum amplitude, ε=0.9 gives an amplitude of 0.66, and ε=0.6 gives an amplitude of 0.74. Then, with lower ε, bigger the amplitude that is obtained. Similar happens in figure 6.1b, where ε=0.9 gives an amplitude of 0.019, and ε=0.6 gives an amplitude of 0.023. Thus, ε does not have a big influence on the results.

(a)

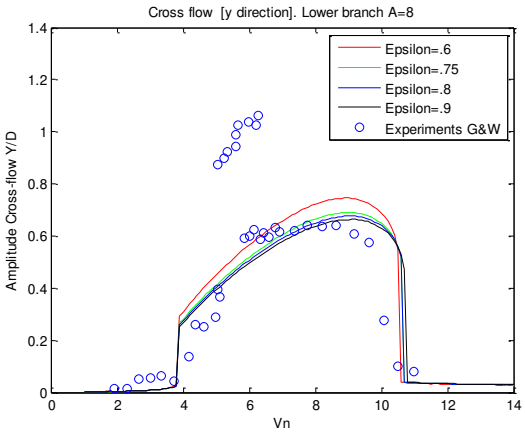

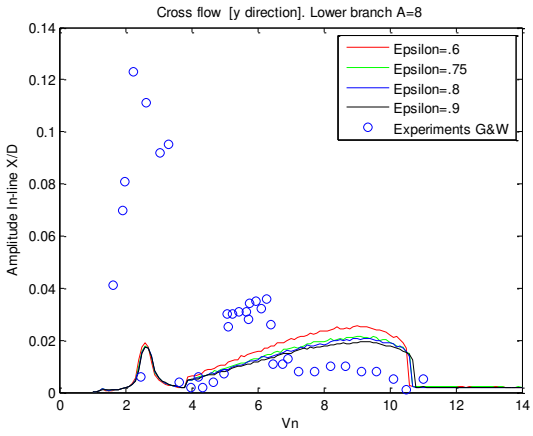

(b)

Figure 6. 1 Lower Branch (a) Dimensionless Cross flow amplitude (b) Dimensionless In-line amplitude

The figure 6.2a shows the Ωcy/Ωn, where ε has almost no influence in the results. The figure 6.2b shows the Ωcx/Ωn, similar as in figure 6.2a, ε has almost no influence in the curve.

(a)

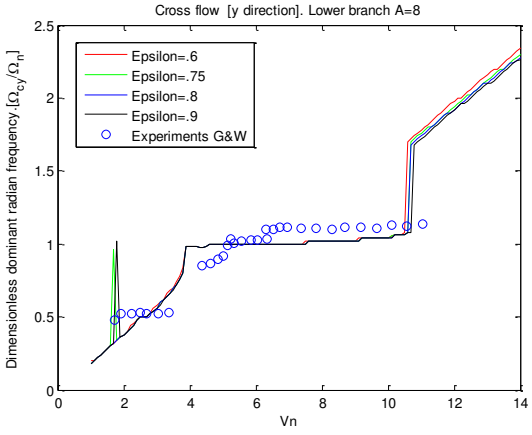

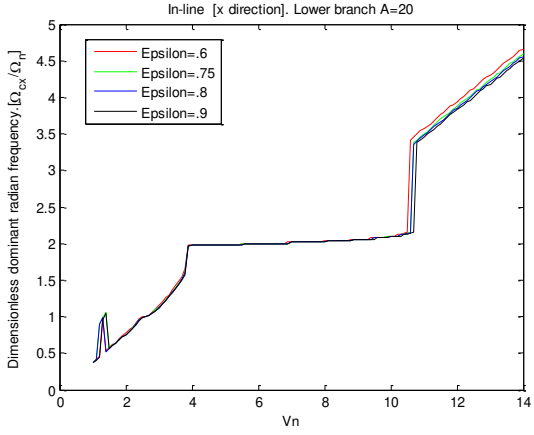

(b)

Figure 6. 2 Lower Branch (a) Ratio of Cross flow response frequency $\Omega c_y/\Omega_n$ (b) Ratio of In-line response frequency $\Omega c_x/\Omega_n$.

In figure 6.2a, there are some interesting peaks at Vn=1.8, because of that a more detailed analysis has been done to that section.

Figure 6.3 shows the amplification of figure 6.2a.

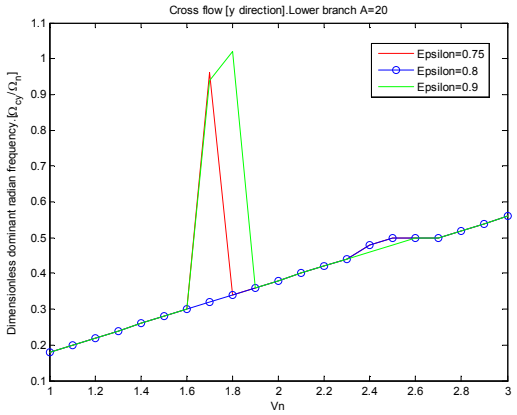

Figure 6. 3 Ωcy/Ωn vs Reduced velocity for the cross-flow direction, lower branch.

Figure 6.4 shows the frequencies that are present in that range of reduced velocities. It can be noticed that in the three plots there are two lines of frequencies, the second less strong line could be a third harmonic with resonance at 1.

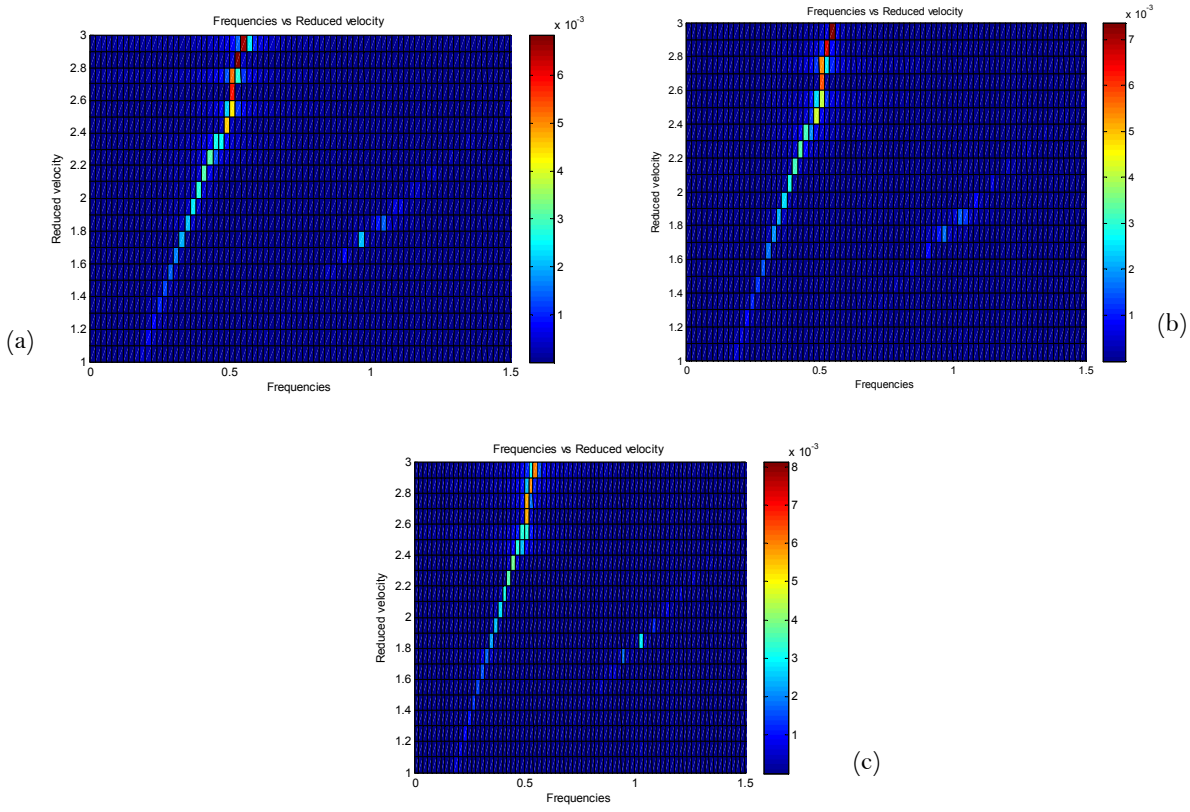

Figure 6. 4 Frequencies vs Reduced velocity. (a) Epsilon=075, (b) Epsilon=0.8 (c) Epsilon=0.9

Upper branch results

Usually, ε=0.08 is used for the upper branch. Figure 6.5a shows the amplitude in the cross-flow direction. In the graph the influence of ε involves a change in the maximum amplitude, ε=0.09 gives an amplitude of 0.98, and ε=0.05 gives an amplitude of 1.77. Thus, with low values of ε higher amplitudes are obtained.

In figure 6.5b, like the figure 6.5a, with low values ε higher amplitudes are obtained. Then, for these two plots, there is a big influence in the amplitude in both cross-flow direction and in-line direction.

(a)

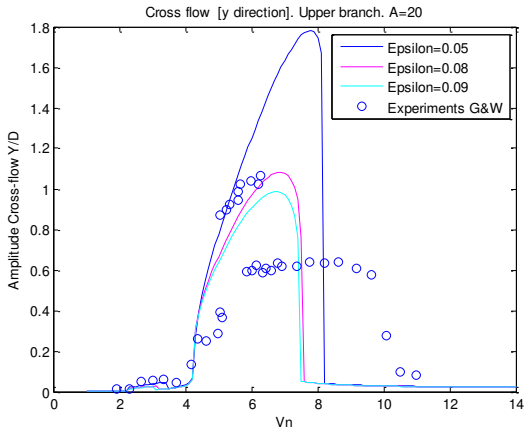

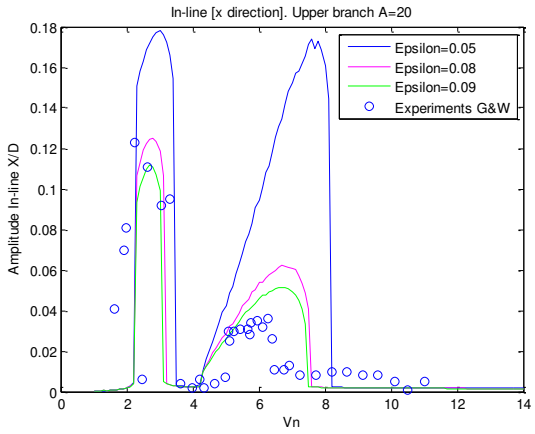

(b)

Figure 6. 5 Upper branch. Upper branch, (a)Dimensionless Cross flow amplitude (b) Dimensionless In-line amplitude

The figure 6.6a shows the Ωcy/Ωn, where low values of ε extend the lock-in range in terms of reduced velocity. The figure 6.6b shows the Ωcx/Ωn, similar as in the figure 6.6a, ε extend or reduce the lock-in range.

(a)

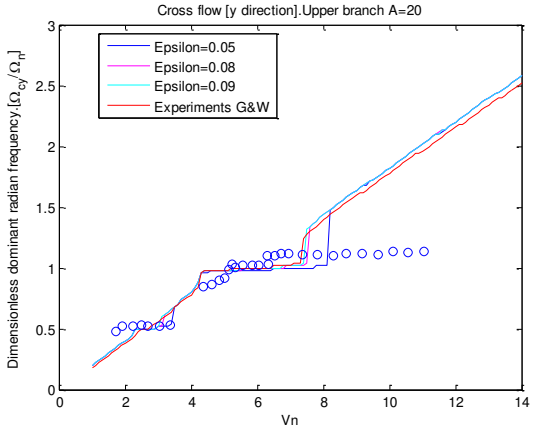

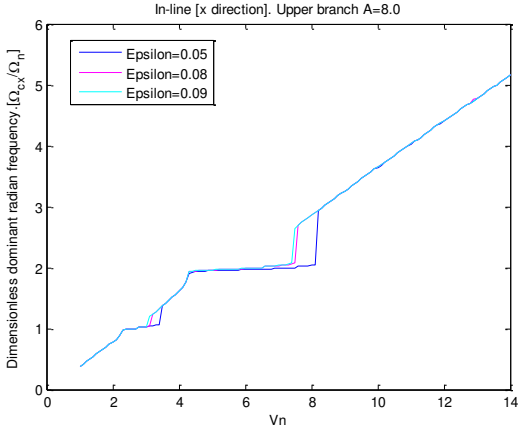

(b)

Figure 6. 6 Upper branch. (a) Ratio of Cross flow response frequency $\Omega c_y/\Omega_n$ (b) Ratio of In-line response frequency $\Omega c_x/\Omega_n$

6.1.2. Sensitivity to variable A

In this section, the sensitivity to variable A is explored. The results are divided into two sections, lower branch results and upper branch results. Also, the experimental results found by Govardhan & Williamson,2004 are plotted.

The following parameters were used for the lower and the upper branch, respectively:

	κ	ĉL	St	m*	α	ζ	(m*+Ca)ζ	Ca
General parameters	5	0.3	0.1932	7.0	2.0	0.00146	0.0117	1

	A	ε
Lower branch	Variable	0.8
Upper branch	Variable	0.08

Lower branch results

Usually A=20 is used for the lower branch. The figure 6.7a shows the amplitude in cross-flow direction. In the graph the influence of ε involves a small change in the maximum amplitude, A=19 gives an amplitude of 0.64, and A=21 gives an amplitude of 0.69. Then, with lower values of A, lower the amplitude that is obtained. Similar happens in figure 6.7b, where A=19 gives an amplitude of 0.018, and A=21 gives an amplitude of 0.021. Thus, A does not have a big influence on these results.

(a)

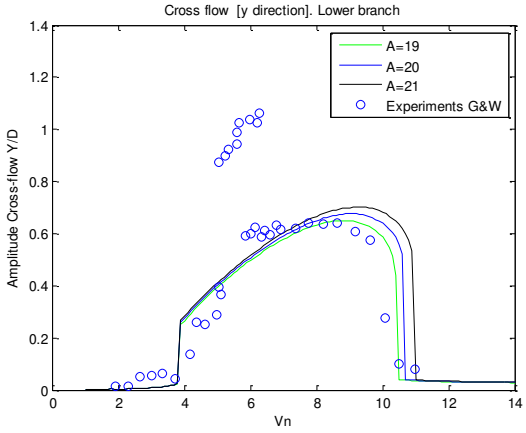

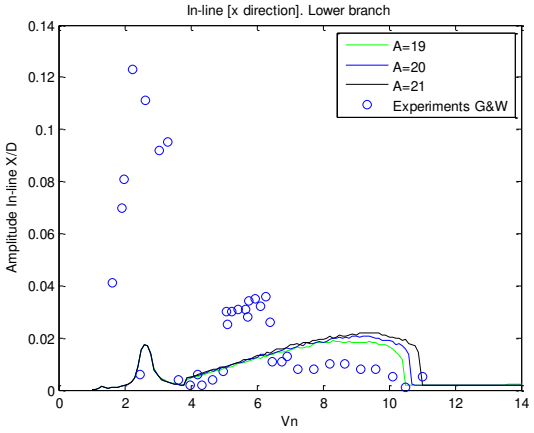

(b)

Figure 6. 7 Lower Branch (a) Dimensionless Cross flow amplitude (b)Dimensionless In-line amplitude

The figure 6.8a shows the Ωcy/Ωn, where A has almost no influence in the results. However, low values of A reduce the lock-in range. Similar happens with the figure 6.8b that shows the Ωcx/Ωn, where A extend or reduce the lock-in range.

(a)

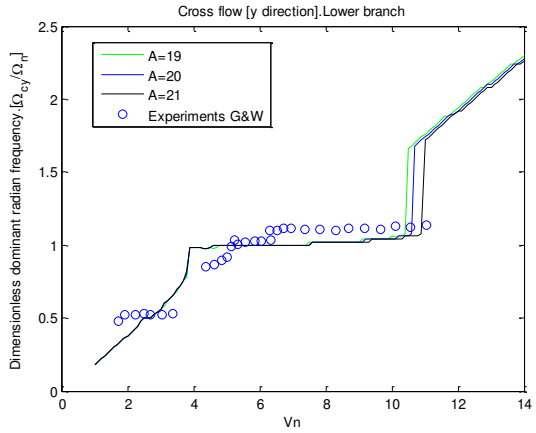

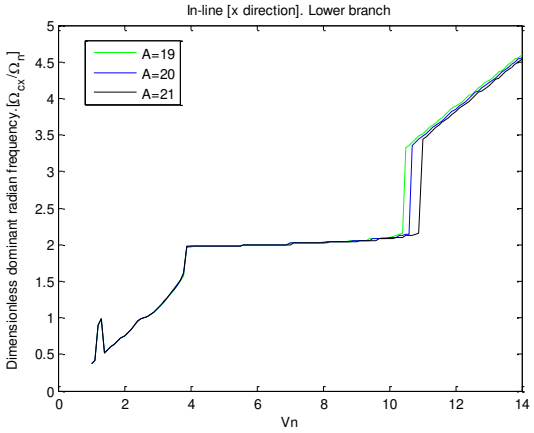

(b)

Figure 6. 8 Lower Branch (a) Ratio of Cross flow response frequency $\Omega c_y / \Omega_n$ (b) Ratio of In-line response frequency $\Omega c_x / \Omega_n$.

Upper branch results

Usually A=8 is used for the upper branch. The figure 6.9a shows the amplitude in cross-flow direction. In the graph the influence of A involves a change in the maximum amplitude, A=8 gives an amplitude of 1.18, and A=9 gives an amplitude of 2.19. Also, the range of reduced velocities where the upper branch is situated is extended with higher values of A. Thus, the amplitude and the range of reduced velocities is highly influenced by the variation of A between the values of 8 and 9.

In the figure 6.9b, a similar thing happens to the figure 6.9a, the amplitude and the range of reduced velocities is highly influenced by the variation of A between the values of 8 and 9.

(a)

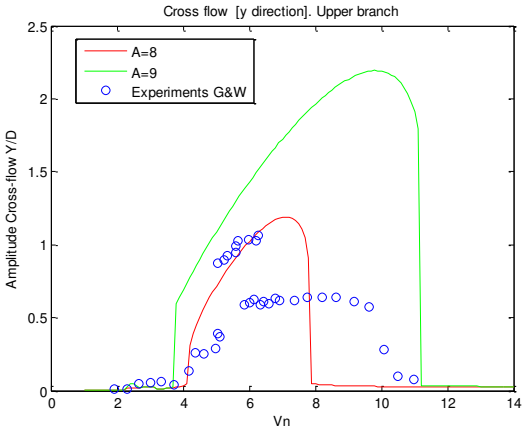

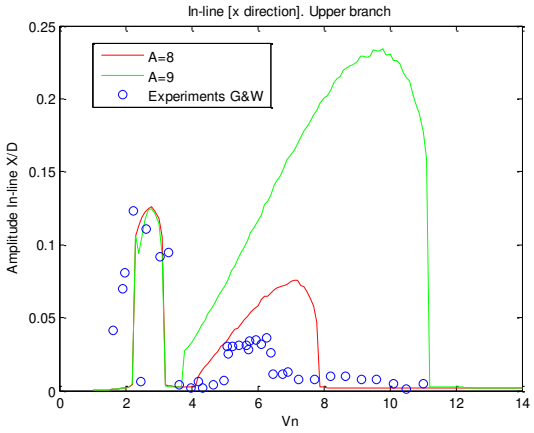

(b)

Figure 6. 9 Upper Branch (a) Dimensionless Cross flow amplitude (b) Dimensionless In-line amplitude

The figure 6.10a shows the Ωcy/Ωn. Low values of A reduce the lock-in. Similar happens with the figure 6.10b that shows the Ωcx/Ωn, where higher values of A extend the lock-in range.

(a)

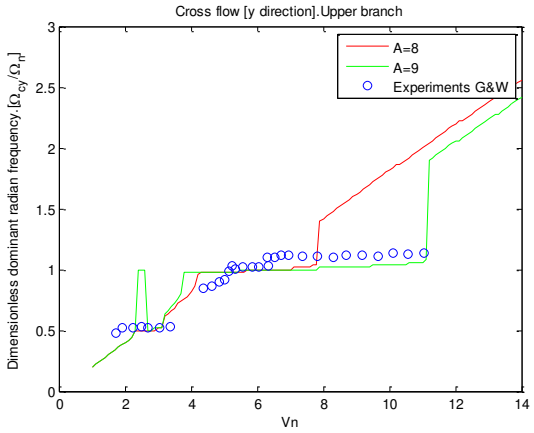

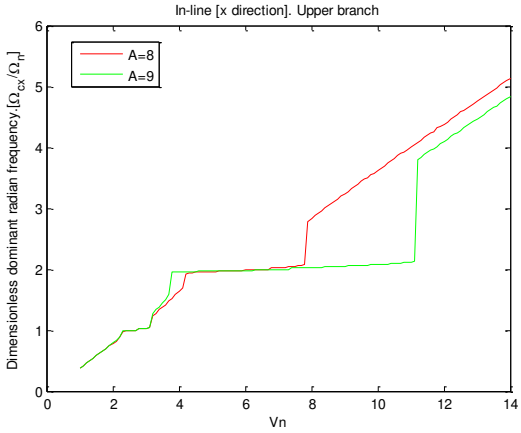

(b)

Figure 6. 10 Upper Branch (a) Ratio of Cross flow response frequency $\Omega c_y/\Omega_n$ (b) Ratio of In-line response frequency $\Omega c_x/\Omega_n$

6.1.3. Sensitivity to variable κ

In this section, the sensitivity to variable **κ** is explored. The results are divided into two sections, lower branch results and upper branch results. Also, the experimental results found by Govardhan & Williamson,2004 are plotted. It is important to notice that having negative values of **κ** means that, the physics of the model changes, because the term $-\kappa\ddot{x}q$ will change.

The following parameters were used for the lower and the upper branch, respectively:

	κ	ĉL	St	m*	α	ζ	(m*+Ca)ζ	Ca
General parameters	Variable	0.3	0.1932	7.0	2.0	0.00146	0.0117	1

	A	ε
Lower branch	20	0.8
Upper branch	8	0.08

Lower branch results

Usually, **κ**=5 is used for the modeling of the lower branch and the upper branch. Figure 6.11 shows the amplitude in the cross-flow direction. In the graph, the influence of **κ** involves a small change in the amplitude of the lower branch. With smaller values of **κ** lower amplitudes are obtained. Similarly happens in figure 6.11b. Also, the range of reduced velocities where the lower branch is situated is slightly extended towards higher Vn.

(a)

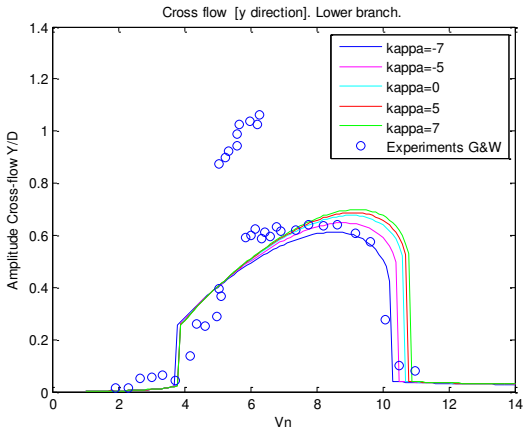

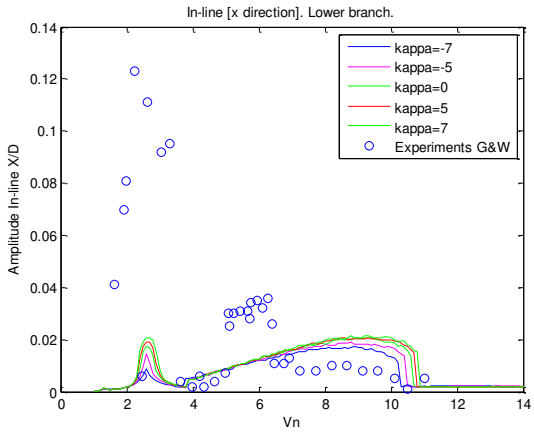

(b)

Figure 6. 11 Lower Branch (a) Dimensionless Cross flow amplitude (b)Dimensionless In-line amplitude

Figure 6.12a shows Ωcy/Ωn. In congruence to figure 6.11 the lock-in range is slightly extended to higher Vn. For example, with **κ**=-7 the lower branch finishes at Vn=10.3 and for **κ**=7 the lower branch finishes at Vn= 10.8. In terms of Ωcy/Ωn, the **κ** value does not represent any change. The same happens with figure 6.12b, where lower values of **κ** slightly decrease the boundary in terms of Vn where the lower branch finishes.

(a)

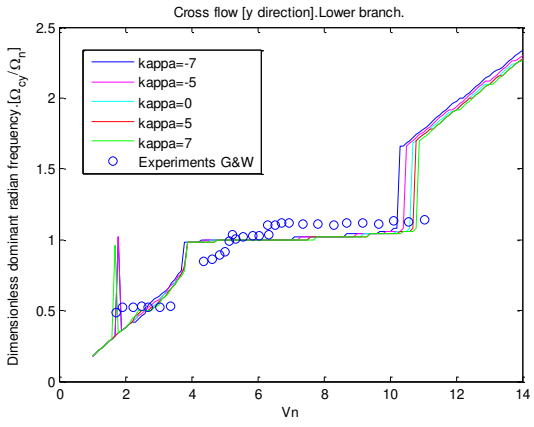

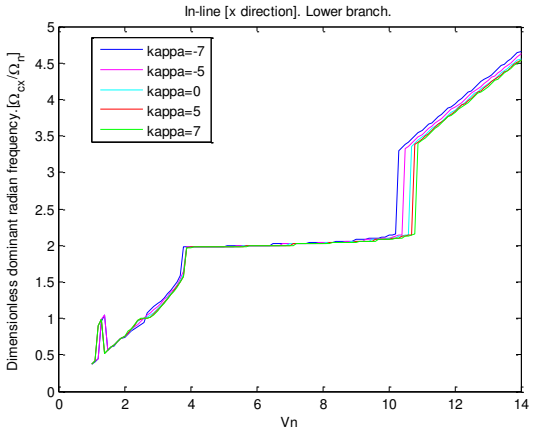

(b)

Figure 6. 12 Lower Branch (a) Ratio of Cross flow response frequency $\Omega c_y/\Omega_n$ (b) Ratio of In-line response frequency $\Omega c_x/\Omega_n$

Upper branch results

Usually, κ=5 is used for the lower branch and the upper branch. Figure 6.13 shows the amplitude in the cross-flow direction. In the graph, the influence of κ involves a big change in the amplitude of the upper branch. With smaller values of κ lower amplitudes are obtained. Similarly happens in figure 6.13b. Also, the range of reduced velocities where the upper branch is situated is significantly extended towards higher Vn.

(a)

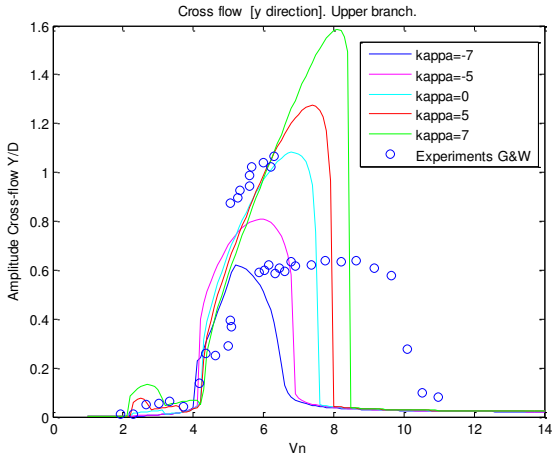

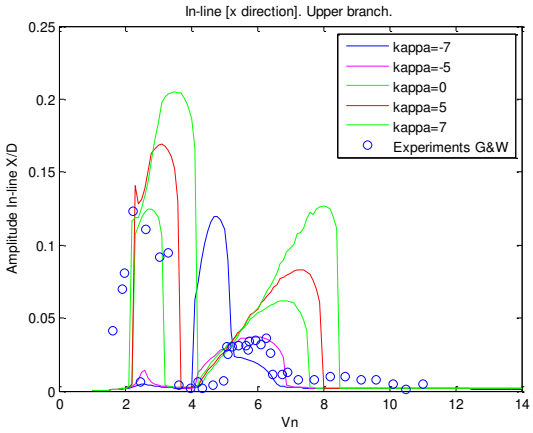

(b)

Figure 6. 13 Upper Branch (a) Dimensionless Cross flow amplitude (b)Dimensionless In-line amplitude

The figure 6.14a shows the Ωcy/Ωn. In congruence to figure 6.13 the lock-in range is significantly extended to higher Vn. For example, with κ=-7 the upper branch finishes at Vn=6.5 and for κ=7 the lower branch finishes at Vn= 8.4. In terms of Ωcy/Ωn, the κ value does not represent any change. The same happens with figure 6.14b, where lower values of κ significantly increases boundary in terms of Vn where the upper branch finishes.

(a)

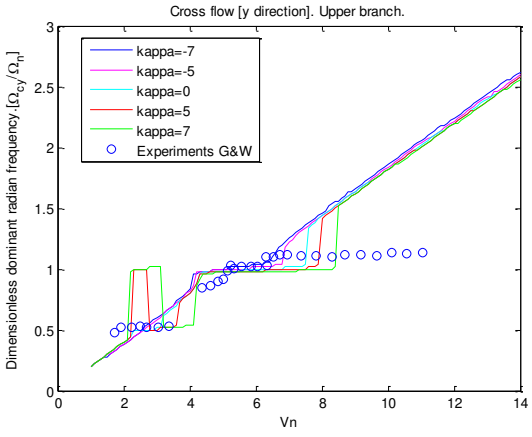

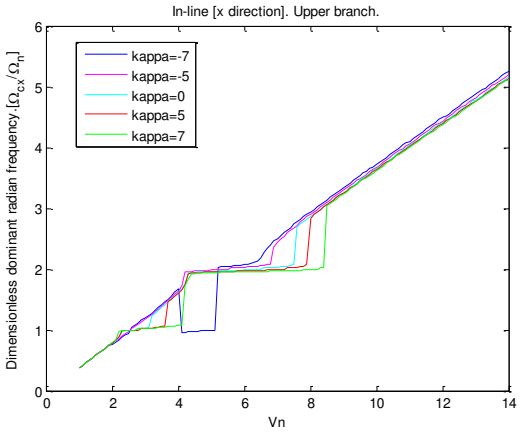

(b)

Figure 6. 14 Upper Branch (a) Ratio of Cross flow response frequency $\Omega c_y/\Omega_n$ (b) Ratio of In-line response frequency $\Omega c_x/\Omega_n$

6.2. Sensitivity to external variables

In this section, the sensitivity to external variables is explored. Two cases are explored:

- Sensitivity to m*
- Sensitivity to ζ

6.2.1. Model with variable Dimensionless Mass (m*)

In this section, the sensitivity to m^* is explored. The results are divided into two sections, lower branch results and upper branch results. Also, the experimental results found by Govardhan & Williamson,2004 are plotted.

The following parameters were used for the lower and upper branch, respectively:

	κ	$\hat{c}_L$	St	m*	α	ζ	Ca
General parameters	5	0.3	0.1932	Variable	2.0	0.00146	1

	A	ε
Lower branch	20	0.8
Upper branch	8	0.08

Lower branch results

The figure 6.15a shows the amplitude in cross-flow direction. In the graph the influence of m* involves a significant change in amplitude and in the range of Vn where the lower amplitude is situated.
The figure 6.15b shows the amplitude in In-line direction. Also, the amplitude and the range of lock-in is significantly influenced by the variation of m*. Where lower values of m* increase the amplitude of the lower branch. For example for m*=11, there is a maximum amplitude of 0.02, and for m*=1.3 it reaches an amplitude of 0.07.

(a)

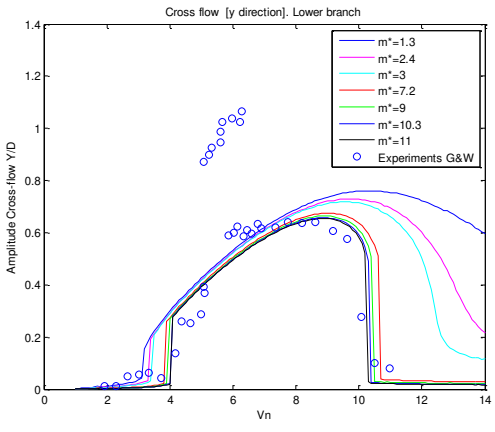

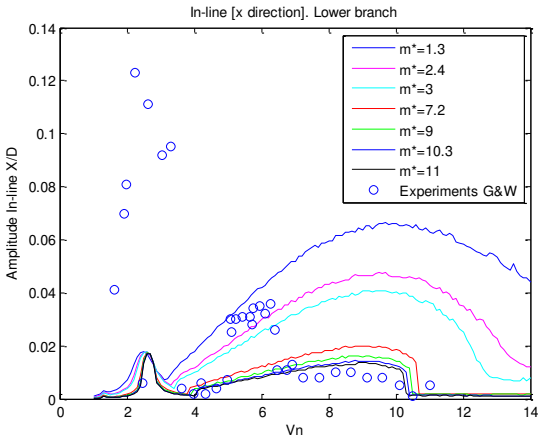

(b)

Figure 6. 15 Lower Branch (a) Dimensionless Cross flow amplitude (b) Dimensionless In-line amplitude

The figure 6.16a shows the Ωcy/Ωn. In the figure 6.16a the lock-in range is significantly extended to higher Vn. For example, with m^*=2.4 the lower branch ends at Vn~13 and for m^* =11 the lower branch ends at Vn= 10.2.

The figure 6.16b shows the Ωcx/Ωn. The lock-in range is significantly extended to higher Vn For example, with m^*=2.4 the lower branch ends at Vn~13 and for m^* =11 the lower branch ends at Vn= 10.2.

(a)

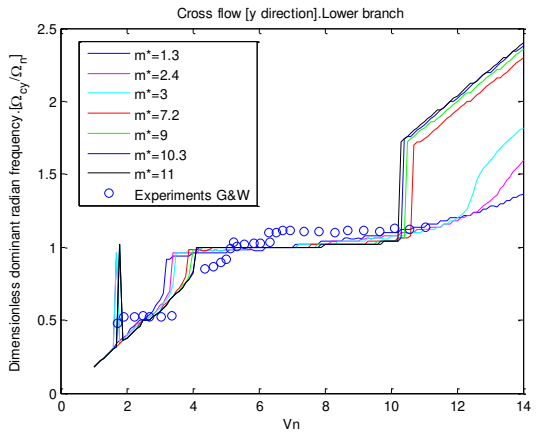

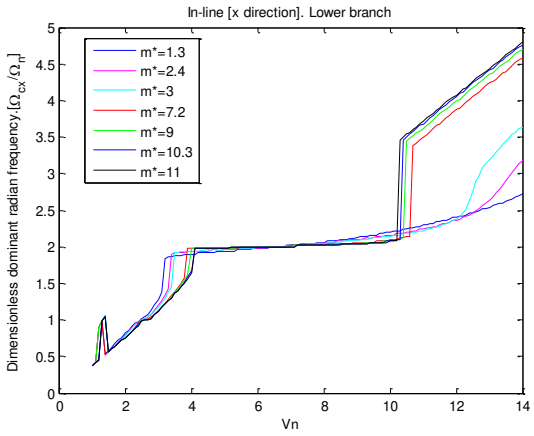

(b)

Figure 6. 16 Lower Branch (a) Ratio of Cross flow response frequency $\Omega c_y / \Omega_n$ (b) Ratio of In-line response frequency $\Omega c_x / \Omega_n$.

Upper branch results

The figure 6.17a shows the amplitude in cross-flow direction. In the graph the influence of m* involves a significant change in amplitude and in the range of Vn where the upper branch amplitude is situated. A variation in amplitude of almost 1.

The figure 6.17b shows the amplitude in In-line direction. Also, the amplitude and the range of lock-in is significantly influenced by the variation of m*.

(a)

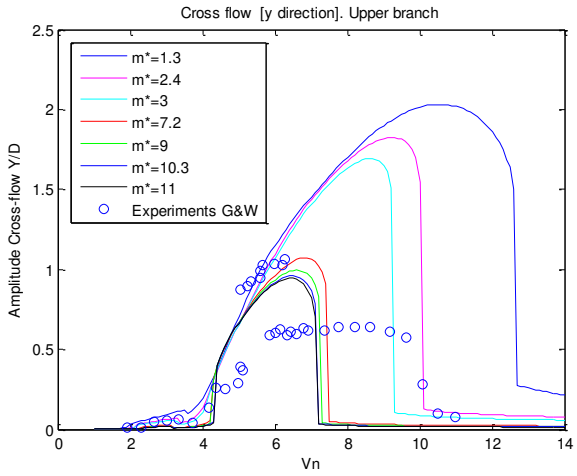

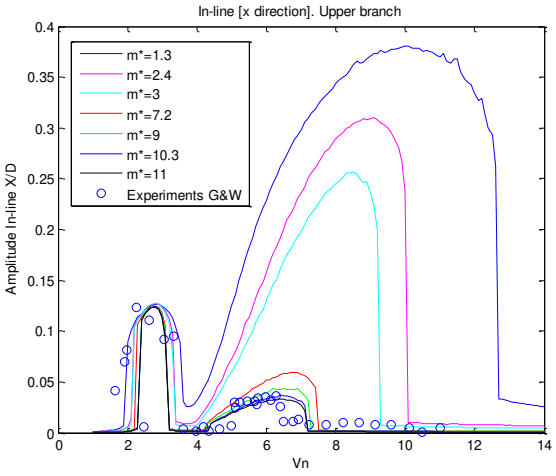

(b)

Figure 6. 17 Upper Branch (a) Dimensionless Cross flow amplitude (b) Dimensionless In-line amplitude

The figure 6.18a shows the Ωcy/Ωn. In the figure 6.16a the lock-in range is significantly extended to higher Vn. For example, with m^* =11 the upper branch finishes at Vn=7.2 and for m^* =1.3 the lower branch finishes at Vn=12.6.

In terms of values of Ωcy/Ωn, the m^* value does not represent a significant change.

The figure 6.18b shows the Ωcx/Ωn. Also, the lock-in range is significantly extended to higher Vn.

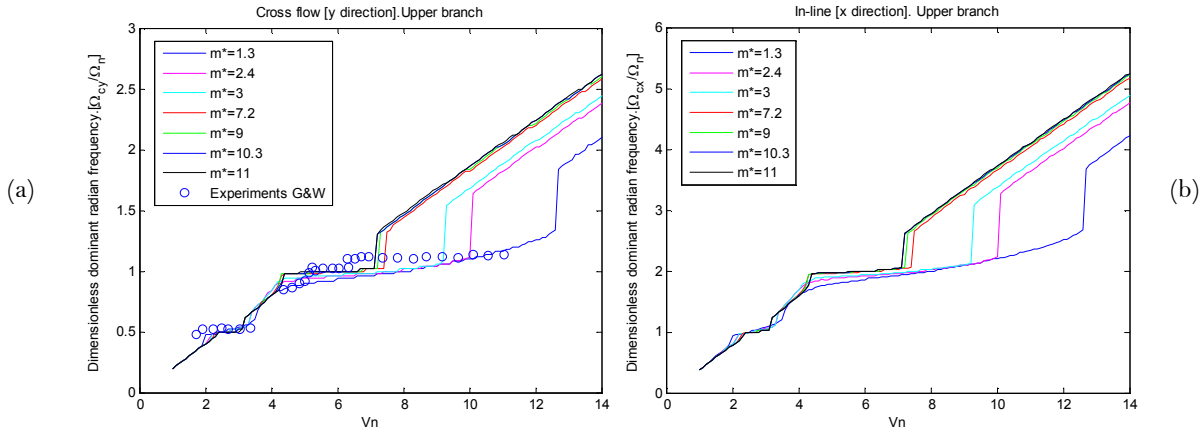

Figure 6. 18 Upper Branch (a) Ratio of Cross flow response frequency $\Omega c_y/\Omega_n$ (b) Ratio of In-line response frequency $\Omega c_x/\Omega_n$.

The figure 6.19 shows an amplification of the figure 6.16a.

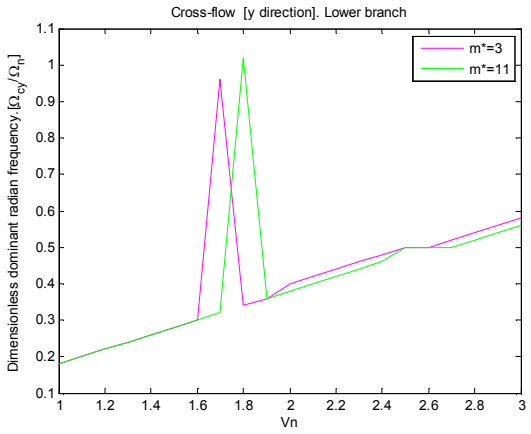

Figure 6. 19 Ωcy/Ωn vs Reduced velocity for cross-flow direction, lower branch.

The figure 6.20 show the frequencies that are present in that range of reduced velocities. It can be noticed that in the two plots there are two lines of frequencies, the second less strong line could be a third harmonic, that has resonance at 1.

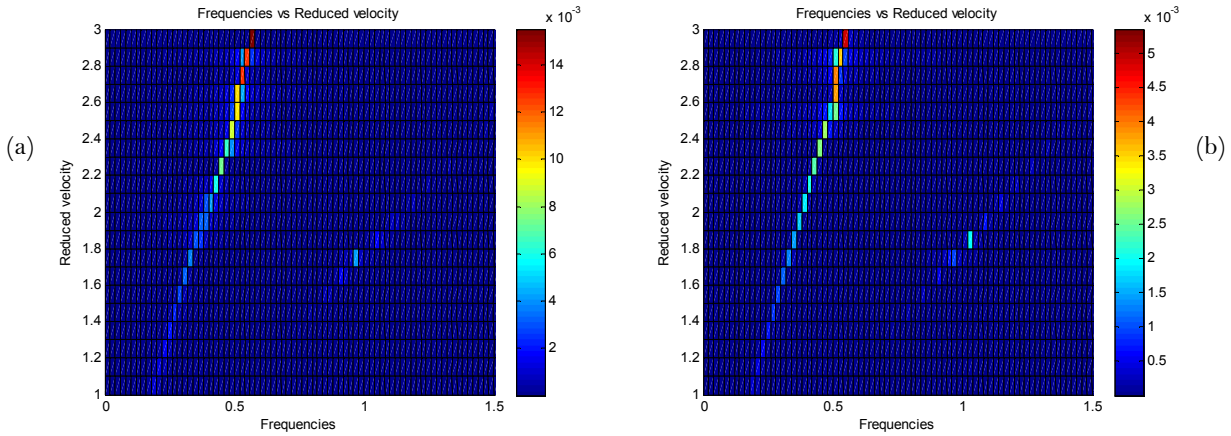

Figure 6. 20 Frequencies vs Reduced Velocity, (a) m*=3, (b) m*=11.

6.2.2. Model with ζ variable

In this section, the sensitivity to ζ is explored. The results are divided into two sections, lower branch results and upper branch results. Also, the experimental results found by Govardhan & Williamson,2004 are plotted.

The following parameters were used for the lower and upper branch, respectively:

	κ	m̂L	St	m*	α	ζ	Ca
General parameters	5	0.3	0.1932	7.0	2.0	Variable	1

	A	ε
Lower branch	20	0.8
Upper branch	8	0.08

Lower branch results

Figure 6.21a shows the amplitude in the cross-flow direction. In the graph, the influence of ζ does not represent any significant variation in the lower branch.
The figure 6.21b shows the amplitude in In-line direction. Similarly, as the figure 6.21a in the graph 6.21b, the influence of ζ does not represent any significant variation in the lower branch in the in-line direction.

(a)

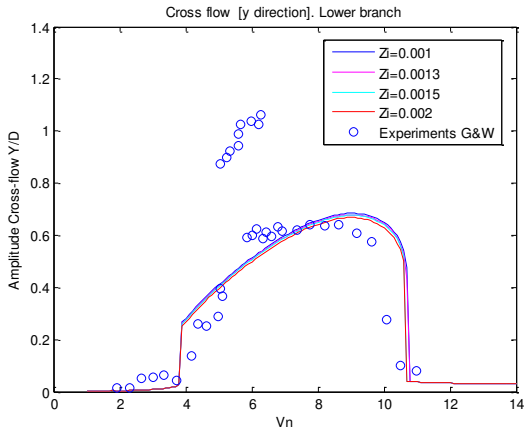

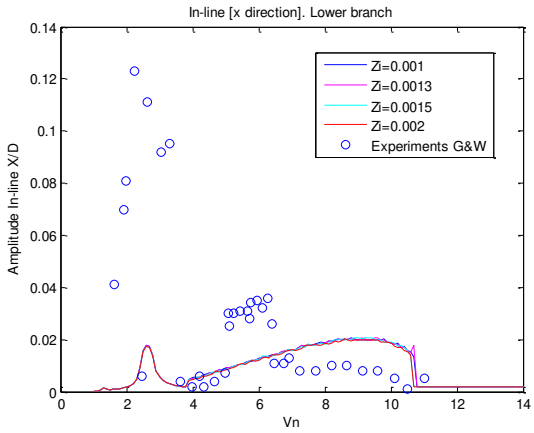

(b)

Figure 6. 21 Lower Branch (a) Dimensionless Cross flow amplitude (b) Dimensionless In-line amplitude

Figure 6.22a shows Ωcy/Ωn. In the graph, the influence of ζ does not represent any significant variation in the lower branch.
Figure 6.22b shows Ωcx/Ωn. The influence of ζ does not represent any significant variation in the lower branch in the in-line direction.

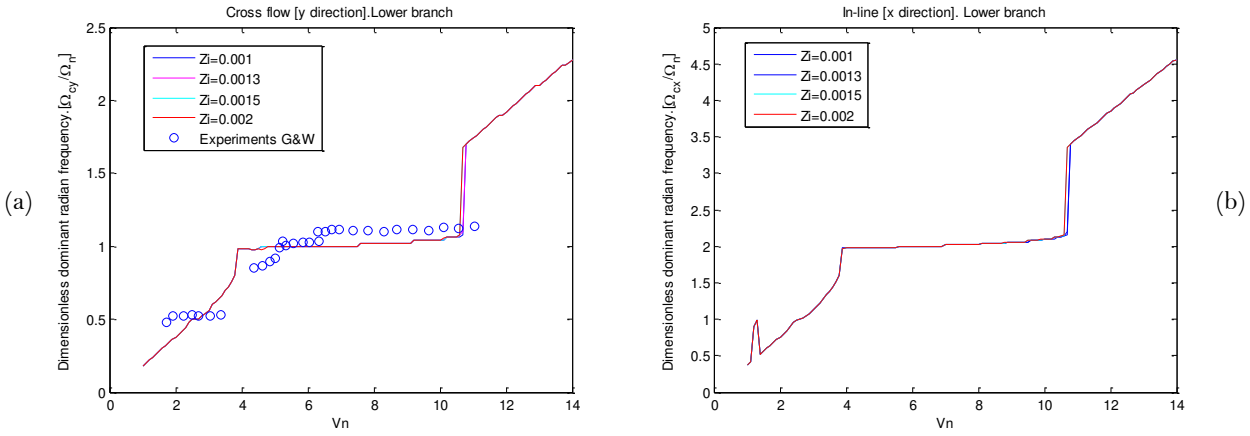

Figure 6. 22 Lower Branch (a) Ratio of Cross flow response frequency $\Omega c_y/\Omega_n$ (b) Ratio of In-line response frequency $\Omega c_x/\Omega_n$.

Upper branch results

Figure 6.23a shows the amplitude in the cross-flow direction. In the graph, the influence of ζ represents a slight increase in amplitude in the upper branch.
The figure 6.23b shows the amplitude in In-line direction. Similarly, as the figure 6.23a in the graph 6.23b, the influence of ζ does not represent any significant variation of amplitude in the upper branch.

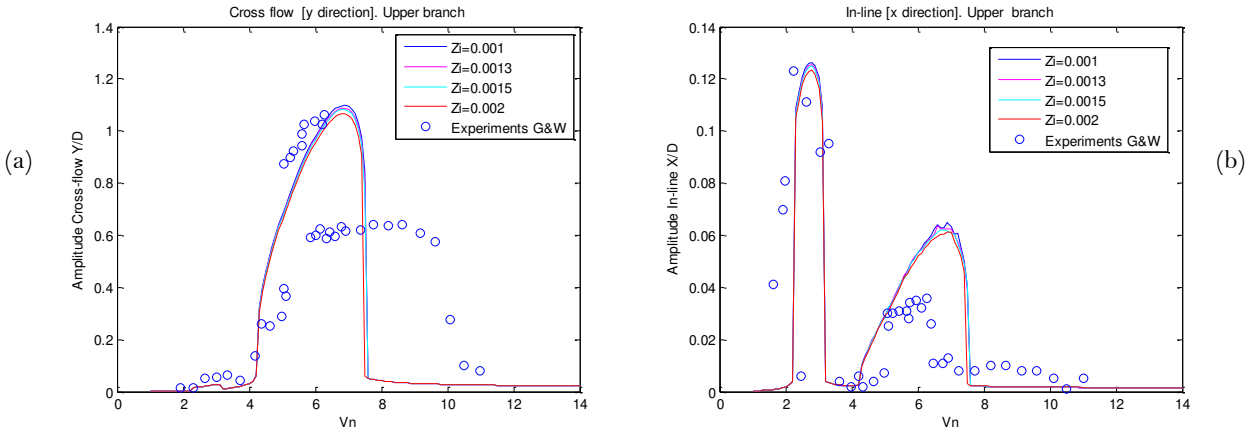

Figure 6. 23 Upper Branch (a) Dimensionless Cross flow amplitude (b) Dimensionless In-line amplitude

Figure 6.24a shows $\Omega cy/\Omega n$. In the graph, the influence of ζ does not represent any variation in the upper branch. Figure 6.24b shows $\Omega cx/\Omega n$. The influence of ζ does not represent any variation in the upper branch.

(a)

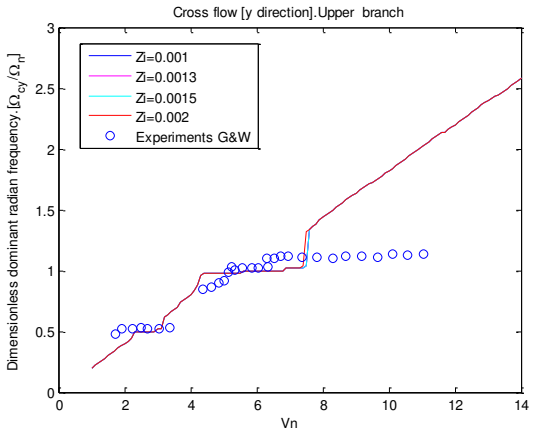

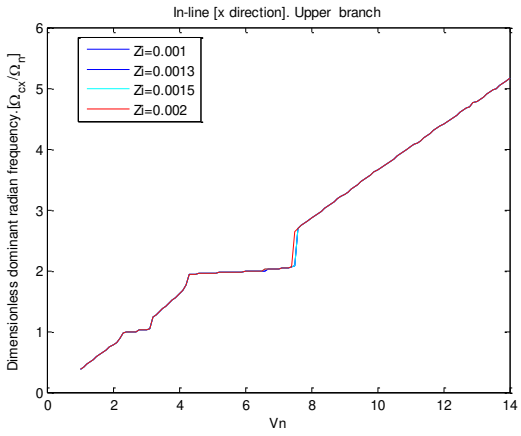

(b)

Figure 6. 24 Upper Branch (a) Ratio of Cross flow response frequency $\Omega c_y/\Omega_n$ (b) Ratio of In-line response frequency $\Omega c_x/\Omega_n$.

6.3. Conclusions on sensitivity analysis

In this chapter, the sensitivity of the model to two kinds of parameters was analyzed. For tunning parameters and for external parameters.

First, the comments on sensitivity to tuning parameters are mentioned.

In terms of ε. It can be concluded that the upper branch model has a significant sensibility to this parameter. In such a way, that it can increases the amplitude of the branch up to 2 times with a difference of 0.03 in the value of ε. Not the same happens with the upper branch that it is almost not affected with variation of the value of ε.

With respect to the sensibility to A. The model is not significantly sensitive to the value of A for the lower branch. However, for the upper branch, it is very significant with a difference in amplitude of almost 3 times when there is a difference of 1 in the value of A. Not only the amplitude is sensitive, also the lock-in range is affected.

After analyzing the influence of κ on the model. In can be concluded that, there is a slight variation in the range of lock-in and in terms of amplitude, that applies to both branches. But the upper branch is more sensitive to the variation of κ.

In terms of external parameters, the following is of importance.

After study the influence of m* on the model is possible to conclude that, with smaller m* the range of lock-in is extended towards higher reduced velocities, and higher amplitudes are obtained. In other words, the hill of the branches is extended towards the right side.

No significant sensitivity was found in the moment of changing ζ. The response in terms of frequency and of amplitude remain almost the same, that applies to both branches.

In conclusion, most of the tuning parameters have a slight influence in the lower branch results, but a relevant influence on the upper branch results.

Therefore, the model looks reliable for the following three reasons:

1. Its low sensitivity to tuning parameters that are already stablished.
2. Good response to external parameters as m*, that usually is known.
3. Not much sensibility to ζ, that is a parameter usually is supposed or unknown.

Chapter 7

Conclusions and Recommendations

By means of modelling of the vortex-induced vibrations with a single wake oscillator coupled to both cross-flow and in-line motions it was possible to reach a better understanding of the VIV phenomenon. The main findings are related to the behavior of the system in the in-line direction. In this chapter, final conclusions are given, and some recommendations for future research are suggested.

The wake oscillator model with a coupling term in the in-line direction works well in terms of reproducing the free oscillation experiments. It was found that, in the in-line direction, the amplitude curves for lower and upper branches have similar shape to their corresponding cross-flow amplitude curves in their respective branches.

Also, it was discovered that the 8 shape is preserved during different reduced velocities, and that it tends to disappear at the higher reduced velocities, meaning that it tends to form a shape similar to letter C.

Concerning the behavior of the new model with respect to the forced oscillation experiments, even though the different predictions are of the same order of magnitude when compared to the experimental results, the model results do not match with the shapes that were obtained by Nishihara, 2005.

In the model for the forced oscillation experiments, the frequency of vibration has a good match, in terms of the range of the reduced velocity. Additionally, similar amplitudes of the cross-flow force are obtained. However, the calculations do not give similar results to those obtained by Nishihara, 2005. This result is interesting because the model has a good performance with respect to the free oscillation experiments, but not a good match with the forced in-line oscillation experiment. It could be possible that something is not considered right from the results of Nishihara, 2005.

An important recommendation is to compare the forced in-line oscillation results of the model with the results of other researchers, because to compare just with one set of data does is not reliable. Another option is to perform a new set of the forced in-line oscillation experiments.

Furthermore, in experimenting with free oscillation tests, it would be advisable to measure the oscillation frequency of the in-line motion, because not much data of this kind is available in the literature.

In terms of sensitivity, the model showed to be reliable according to the analysis performed in chapter 6.

In summary, the model by Yang Qu is concluded to be a perceptible improvement in terms of modelling the free oscillation experiments in which both the cross-flow and in-line motions are enabled. However, reasons for an unsatisfactory prediction of the forced in-line vibrations need to be investigated further.

A reasonable direction of investigation seems to be the one into a new set of the coupling terms in the equation for the wake.

Bibliography

Robert D. ***Blevins***, Charles S. ***Coughran***. *Experimental Investigation of Vortex-Induced Vibration in One and Two Dimensions With Variable Mass*, Damping, and Reynolds Number. Journal of Fluids Engineering, Octuber 2009, Vol. 131/101202-1, DOI: 10.1115/1.3222904, https://fluidsengineering.asmedigitalcollection.asme.org on 11/19/2018.

N. ***Jauvtis*** and C. H. K. ***Williamson***. *The effect of two degrees of freedom on vortex-induced vibration at low mass and damping*. Journal of Fluid Mechanics, 509:23–62, June 2004. doi:10.1017/S0022112004008778, 2004.

Dimitrios ***Livanos***. *Investigation of Vortex Induced Vibrations on Wind Turbine Towers*. Master of Science Thesis at the Delft University of Technology. October 29, 2018.

Achilleas ***Mina***, *Modeling the vortex-induced vibrations of a multi-span free standing riser*. Delft University of Technology, Master Offshore and Dredging Engineering, Faculty of Mechanical, Maritime and Materials Engineering, April 15, 2013.

Akira ***Nakamura,*** Atsushi ***Okajima*** and Takashi ***Kosugi***. *Experiments on Flow-Induced In-Line Oscillation of a Circular Cylinder in a Water Tunnel (2nd Report, Influence of the Aspect Ratio of a Cantilivered Circular Cilinder)* Series V, Vol. 44, No.4, 2001.

T. ***Nishihara***, S. ***Kaneko***, T. ***Watanabe***. *Characteristics of Fluid Dynamic Forces Acting on a Circular Cylinder Oscillated in the Streamwise Direction and its Wake Patterns*. Journal of Fluids and Structures 20(2005) 505-518,www.elsevier.com/locate/jfs.

R.H.M. ***Ogink***, A.V. ***Metrikine.*** *A wake Oscillator with Frequency Dependent Coupling for the Modeling of Vortex-Induced Vibration*. Delft University of Technology, Faculty of Civil Engineering and Geosciences, Stevinweg 1, 2628 CN Delft, The Netherland. Journal of Sound and Vibration 329 (2010) 5452-5473. doi:10.1016/j.jsv.2010.07.008. 2010.

Yang ***Qu***. *Modeling of Coupled Cross-Flow/In-Line Vortex-Induced Vibration of an Elastically Supported Rigid Cylinder*. Delft University of Technology, Department of Hydraulic Engineering, Stevinweg 1, 2628 CN Delft, The Netherland. 2019.

Yang ***Qu***, Andrei ***Metrikine***, A single wake oscillator model for coupled cross-flow and in-line vortex-induced vibration of marine structures. (a) Department of Hydraulic Engineering,(b) Department of Structural Engineering, Delft University of Technology, Stevinweg 1, 2628CN Delft, The Netherlands. January 7, 2019.

Morten ***Slingsby***. Dynamic *Interaction of Subsea Pipeline Spans due to Vortex-Induced Vibrations*. Master's Thesis, Delft University of Technology. June 4, 2015.

Narakorn ***Srinil***, Hossein ***Zanganeh***. *Modeling of coupled cross-flow/in-line vortex-induced vibrations using double Duffing and van der Pol oscillators*. Department of Naval Architecture & Marine Engineering, University of Strathclyde, Henry Dyer Building, Glasgow G4 0LZ, Scotland, UK. Ocean. Engineering 53 (2012) 83–97. June, 2012.

Jiayao ***Sun***. *Scale test facility for measuring vortex induced vibrations*. Thesis to obtain the degree of Master of science In Offshore and dredging engineering at the Delft university of technology 2017-06-19.

C.H.K. ***Williamson,*** R. ***Govardhan***. *Vortex-Induced Vibrations*. Annu. Rev. Fluid Mech. 2004. 36:413–55, doi: 10.1146/annurev.fluid.36.050802.122128. www.annualreviews.org.

Tim de ***Zwart***. *Vortex-induced vibrations in OTEC an analysis of VIV of a cold water pipe for OTEC plants*. Thesis to obtain the degree of Master of Science at the Delft University of Technology, to be defended publicly on Thursday December 21, 2017 at 11:00 AM. http://repository.tudelft.nl/.

Appendix

A

$$\omega = \omega_n = \Omega \frac{2\pi st V_r}{D}$$

$$\omega = 2\pi f$$

$$f = \frac{\omega}{2\pi} = \frac{\omega_s \Omega}{2\pi} = \frac{\Omega}{2\pi} \cdot \frac{2\pi st \cdot V_r}{D}$$

$$f = \frac{\Omega \cdot st \cdot V_r}{D} \rightarrow \frac{1}{f} = \frac{D}{\Omega \cdot st \cdot V_r}$$

Added damping coefficient (Ca)

$$Ca' = \frac{F_I}{\omega A}$$

$$Ca' = \frac{-1/2\, \rho D V^2 C x_o \sin \varphi_x}{\left(\Omega \frac{2\pi st V_r}{D}\right) x_o D}$$

$$Ca = \frac{Ca'}{\rho D^2 f}$$

$$Ca = \frac{-1/2\, \rho D V^2 C x_o \sin \varphi_x}{\left(\Omega \frac{2\pi st V_r}{D}\right) x_o D} \frac{1}{\rho D^2} \frac{D}{\Omega st V_r}$$

$$Ca = -\frac{1}{4} \frac{C x_o \sin \varphi_x}{\Omega^2 \pi st^2 x_o}$$

$$st = \frac{f_s \cdot D}{V} \rightarrow f_s = \frac{st \cdot V_r}{D}$$

$$\omega_s = \frac{2\pi st V_r}{D}$$

$$\Omega = \frac{\omega_n}{\omega_s} \rightarrow \omega_n = \Omega\, \omega_s$$

$$\omega = \omega_n = \Omega\, \omega_s$$

$$\omega = \omega_n = \Omega \frac{2\pi st V_r}{D}$$

Cmass=Added mass coefficient

$$ma' = \frac{FM}{\omega^2 A} \qquad ma_o = \frac{\pi \rho D^2}{4}$$

$$Cmass = \frac{ma'}{ma_o}$$

$$Cmass = \frac{\frac{FM}{\omega^2 A}}{\frac{\pi \rho D^2}{4}} = \frac{FM}{\omega^2 A} \frac{1}{\pi \rho D^2 1/4}$$

$$Cmass = \frac{1/2\, \rho D V_r^2 C x_o \cos \varphi_x}{\left(\Omega^2 \frac{4\pi^2 st^2 V_r^2}{D^2}\right) x_o D} \frac{1}{\pi \rho D^2 1/4}$$

$$Cmass = \frac{1}{2} \frac{C x_o \cos \varphi_x}{\Omega^2 \pi^3 st^2 x_o}$$

$$C x_o \cos \varphi_x = \frac{2}{T} \int_o^T C\hat{V}X \cdot \sin(\Omega_r \cdot t)\, dt$$

$$C x_o \sin \varphi_x = \frac{2}{T} \int_o^T C\hat{V}X \cdot \cos(\Omega_r \cdot t)\, dt$$

B

```
%%%In case of doubts with the code, please email the author:
isis_galia_zazueta@hotmail.com
```

Code vdp2.m

```
function dydt = vdp2(t,y,p)
%epsilon*omegas=y(3) ---> miu1
%omegas*omegas= y(4) ---->miu2


dydt = [y(2); p.miu1*(1-y(1)^2)*y(2)-p.miu2*y(1)+p.A*sin(p.omega*t)];
```

Code anita.m

```
function dydt = anita(t,y,p)

deal1=p.cd0*(p.sina-p.pist2*y(2));
deal2=p.cl0/2*y(5)*(p.cosa-p.pist2*y(4));
deal3=(p.cosa-p.pist2*y(4))^2;
deal4=(p.sina-p.pist2*y(2))^2;
deal5=p.cd0*(p.cosa-p.pist2*y(4));
deal6=p.cl0/2*y(5)*(p.sina-p.pist2*y(2));
cvy=(deal1+deal2)*(deal3+deal4)^0.5;
cvx=(deal5-deal6)*(deal3+deal4)^0.5;

 dydt = [y(2); -2*p.zi*p.omega_n*y(2)-p.omega_n*p.omega_n*y(1)+p.b*cvy;
     y(4); -2*p.zi*p.omega_n*y(4)-p.omega_n^2*y(3)+p.b*cvx; y(6);
     -p.ep*(y(5)^2-1)*y(6)-y(5)+p.A*(p.cosa*(-2*p.zi*p.omega_n*y(2)...
      -p.omega_n^2*y(1)+p.b*cvy)-p.sina*(-2*p.zi*p.omega_n*y(4)...
       -p.omega_n^2*y(3)+p.b*cvx))];

%    dydt = [y(2);-2*p.zi*p.omega_n*y(2)-p.omega_n*p.omega_n*y(1)+...
%     p.b*cvy;y(4);-2*p.zi*p.omega_n*y(4)-p.omega_n*p.omega_n*y(3)+...
%     p.b*cvx;y(6);-p.ep*(y(5)^2-1)*y(6)-y(5)+p.A*(...
%     (-2*p.zi*p.omega_n*y(2)-p.omega_n*p.omega_n*y(1)+p.b*cvy)*p.cosa-...
%     (-2*p.zi*p.omega_n*y(4)-p.omega_n*p.omega_n*y(3)+p.b*cvx)*p.sina)];
 end
```

Code geneva.m

```
function dedt = geneva(t,e,p)


%%%code Geneva
```

```
y=e(1);
dy=e(2);
x=e(3);
dx=e(4);
q=e(5);
dq=e(6);

%considering angle of attack or alfa = zero

cvx=(p.cdm*(1-2*pi*p.st*dx)+2*pi*p.st*dy*p.cL*q/2)*((1-2*pi*p.st*dx)^2+...
    (2*pi*p.st*dy)^2)^(.5)+p.alfa*((p.cL*q/2)^2)*(1-2*pi*p.st*dx)*abs(1-
2*pi*p.st*dx);

cvy=(-2*pi*p.st*p.cdm*dy+p.cL*q/2*(1-2*pi*p.st*dx))*((1-2*pi*p.st*dx)^2+...
    (2*pi*p.st*dy)^2)^(.5);

ddy=-2*p.zi*p.omega_n*dy-p.omega_n*p.omega_n*y+p.b*cvy;
ddx=-2*p.zi*p.omega_n*dx-p.omega_n*p.omega_n*x+p.b*cvx;

%ddq=-p.ep*(q^2-1)*dq-q+p.kappa*q*ddx/(1+ddx^2)+p.A*ddy;

ddq=-p.ep*(q^2-1)*dq-q+p.kappa*q*ddx+p.A*ddy;

%ddq=-p.ep*(q^2-1)*dq-q+p.A*ddy;%+p.kappa*q*ddx);

 dedt = [dy; ddy; dx; ddx; dq; ddq];

 end
```

Code ichi.m

```
function dedt = ichi(t,e,p)
 p.r=p.amp*sin(p.omega_r*t); %%Forced oscillation in streamwise direction, x
direction
 p.acc=-p.amp*sin(p.omega_r*t)*p.omega_r^2;
  x=p.r;
 ddx=p.acc;
 q=e(1);
 dq=e(2);
 % ddq=-p.ep*(q^2-1)*dq-q+p.kappa*q*ddx/(1+ddx^2)+p.A*ddy;
ddq=-p.ep*(q^2-1)*dq-q+p.kappa*q*ddx;
  dedt = [dq; ddq];
 end
```

C

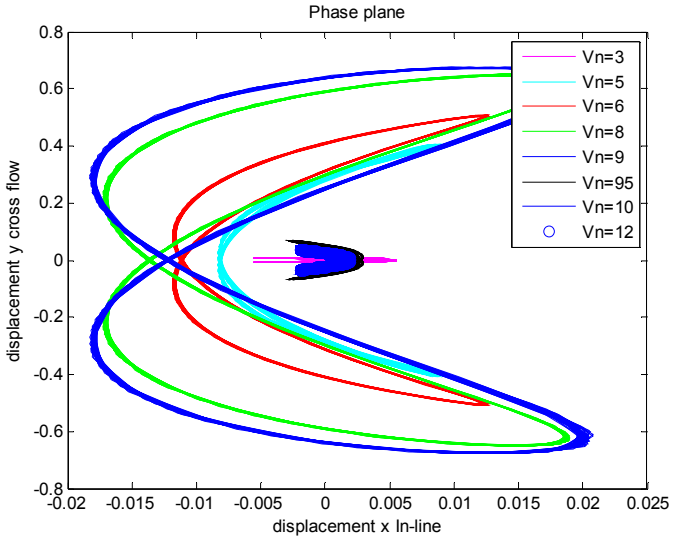

Phase plane. Lower Branch.

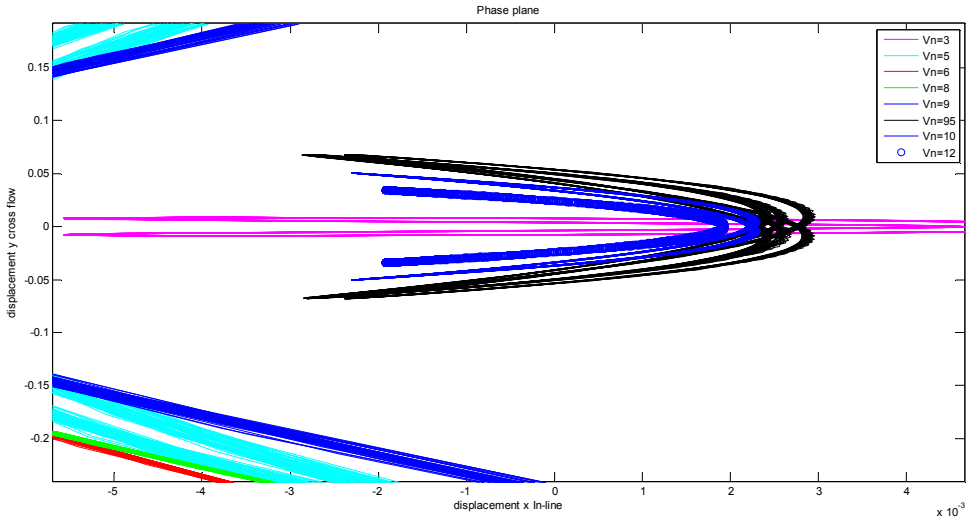

Phase plane. Lower Branch. Zoom for smaller shapes

D

Vortex force decomposition

$$C_{VL} = \frac{F_{VL}}{\frac{1}{2}\rho D V^2}$$

$$C_{VD} = \frac{F_{VD}}{\frac{1}{2}\rho D V^2}$$

Where:

C_{VD}=Vortex drag force coefficient

F_{VD}=Vortex drag force

C_{VL}=Vortex lift force coefficient

F_{VL}=Vortex lift force

ρ= density kg/m^3

D=diameter in m

V=Velocity of the fluid in m/s

E

Results of wake oscillator model in chapter 4.

m*=7.0

(a)

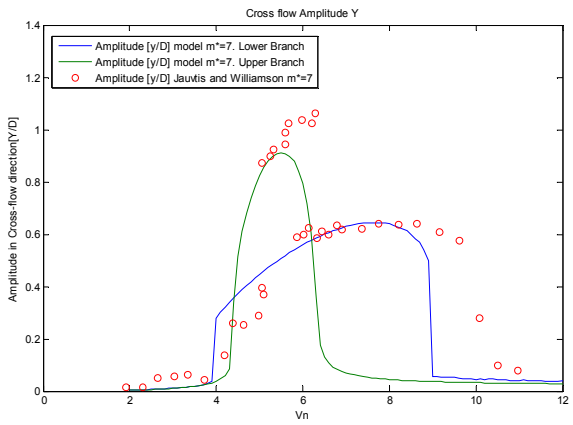

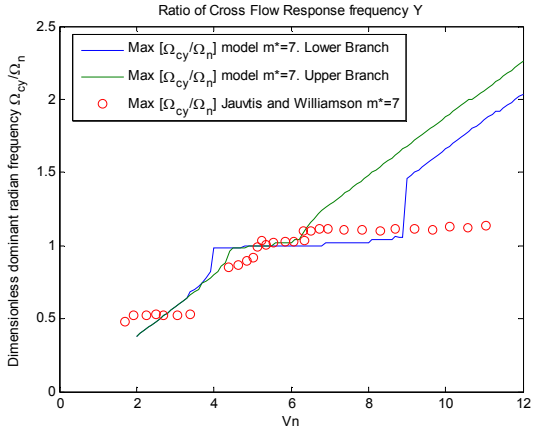

(b)

Figure E.1 m*=7. (a) Dimensionless Cross flow amplitude (b) Ratio of Cross-flow response frequency Ωcy/Ωn.

(a)

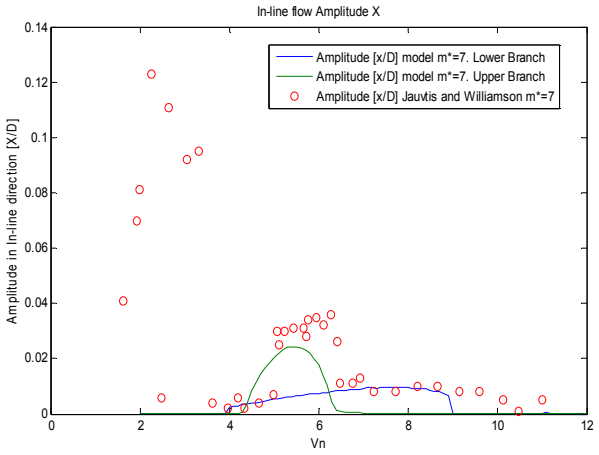

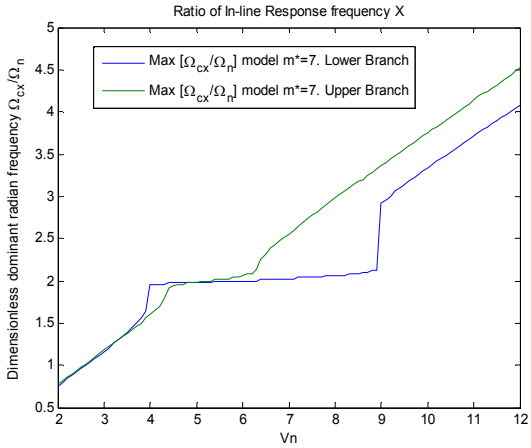

(b)

Figure E.2 m*=7. (a) Dimensionless In-line amplitude (b) Ratio of In-line response frequency Ωcx/Ωn.

m*=2.6

(a)

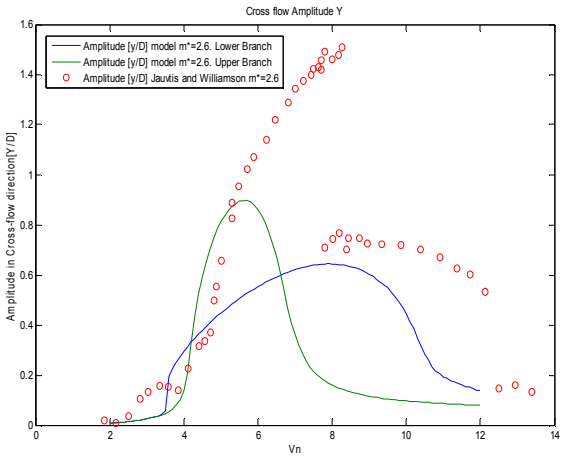

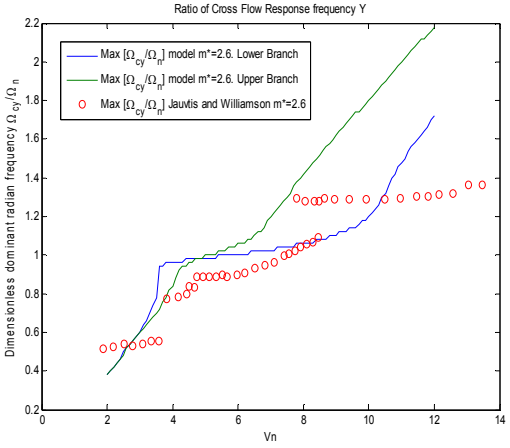

(b)

Figure E.3 m*=2.6. (a) Dimensionless Cross flow amplitude (b) Ratio of Cross-flow response frequency Ωcy/Ωn.

(a)

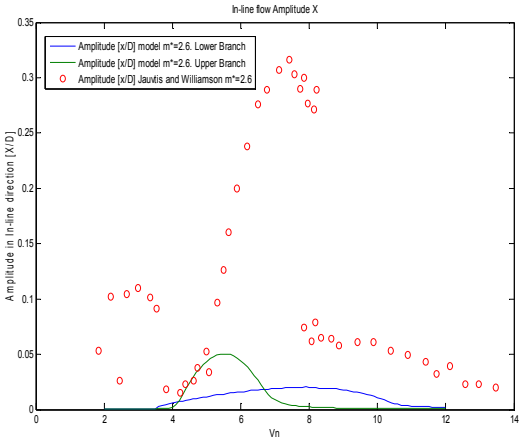

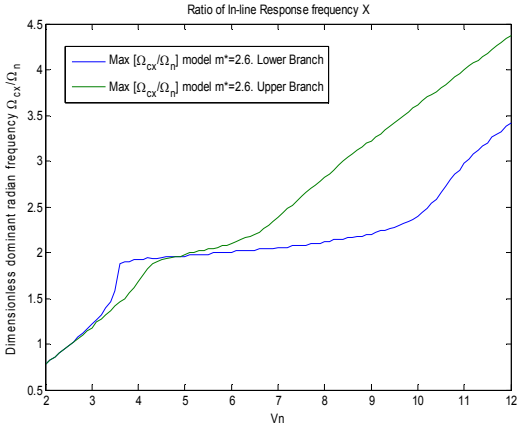

(b)

Figure E.4 m*=2.6. (a) Dimensionless In-line amplitude (b) Ratio of In-line response frequency Ωcx/Ωn.

F

Results of wake oscillator model with a new coupling term in chapter 5.

m*=7

The parameters used for m*=2.6 are shown in tables 5.1 and 5.3

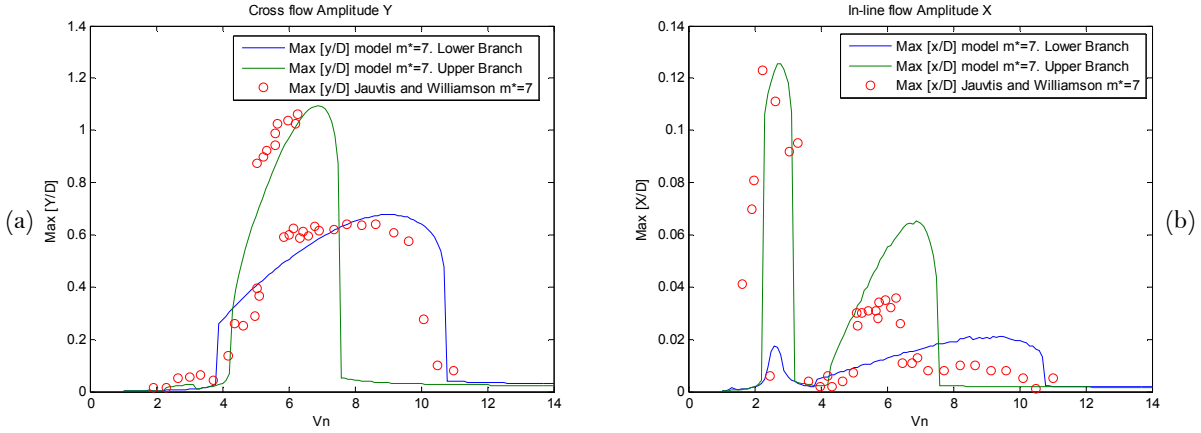

F.1 m*=7. Left- Dimensionless Cross-flow amplitude. Right- Ratio of Cross flow response frequency Ω_{cy}/Ω_n

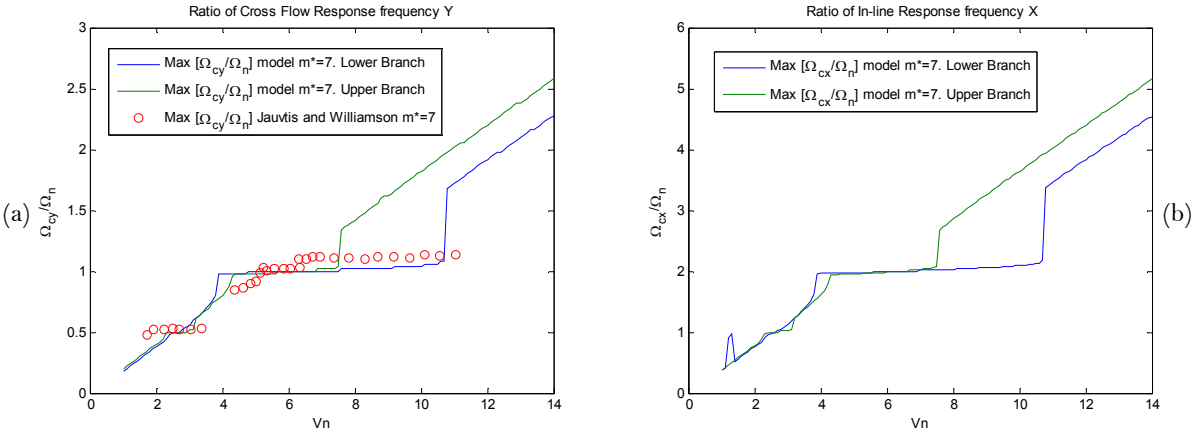

Figure F.2 m*=7. Left. Dimensionless In-line amplitude. Right. Ratio of In-line response frequency Ω_{cx}/Ω_n.

m*=2.6

The parameters used for m*=2.6 are shown in tables 5.2 and 5.3

(a)

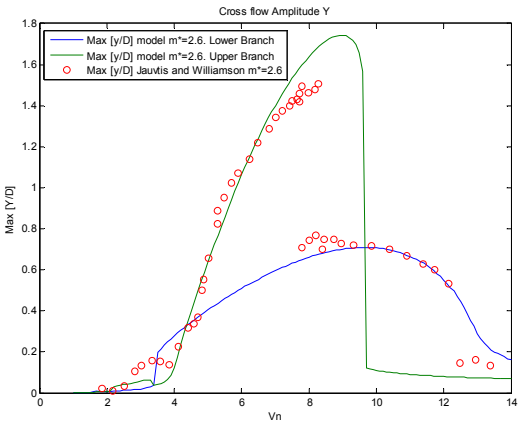

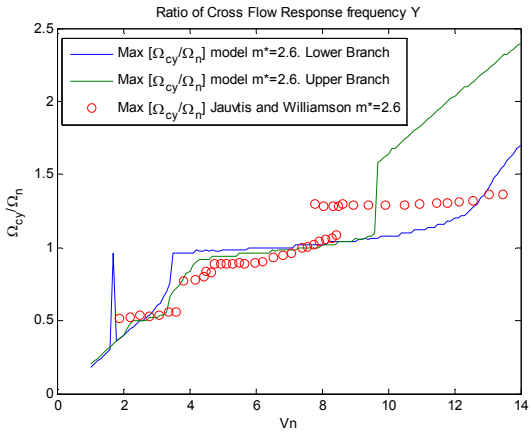

(b)

Figure F.3 m*=2.6. (a) Dimensionless Cross flow amplitude (b) Ratio of Cross flow response frequency Ω_{cy}/Ω_n

(a)

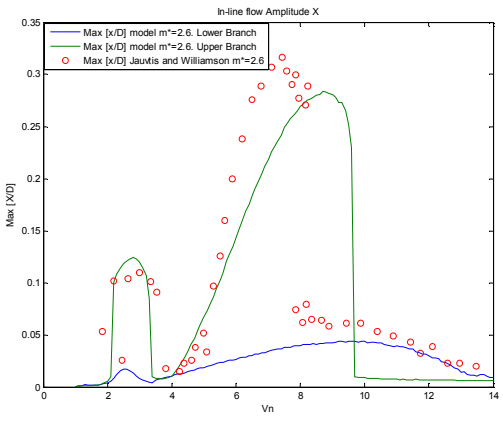

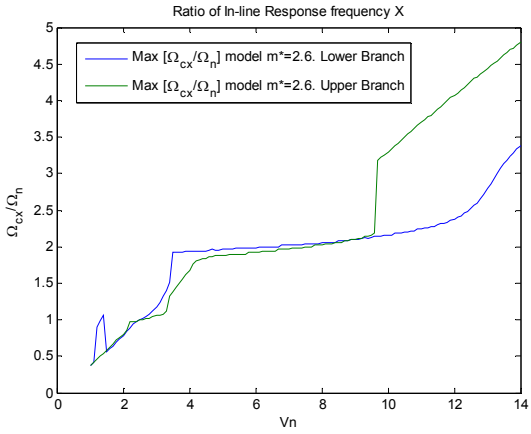

(b)

Figure F.4 m*=2.6. (a) Dimensionless In-line amplitude (b) Ratio of In-line response frequency Ω_{cx}/Ω_n.

G

```
%%%In case of doubts with the code, please email the author:
isis_galia_zazueta@hotmail.com

-----------------------------------------
```

Code maingeneva.m

```
clc;
clear all;
close all;

tic

%main genva
y0=[0 0 0 0 0.01 0]; %initial values
%tspan=[0 300];
t_cycles=150; %total number of cycles
ana_cycles=50;
%cycles=t_cycles-ana_cycles;
points=30; %number of points in each cycle


branch=2; %2 = upper branch, 1=lower branch

p.zi=0.0015; %For md=7
be=0.0117;  % be=(md+Ca)*zi For md=7

% p.zi=0.0036; %For md=2.6
% be=0.013;  % be=(md+Ca)*zi For md=2.6

%p.md=2.6; %mass dimensionless
initialgeneva %



% %%% Vn
Vn_n = (1:0.1:14); %%%Creating Vn space

%Vn_n = (14:-0.1:1);%%Go in reverse

y_n=zeros(3,length(Vn_n));
f_n=zeros(3,length(Vn_n));

%%Before changes
for n = 1:length(Vn_n)%length(t_n)
    Vn=Vn_n(n);
    p.omega_n=1/(p.st*Vn);
 tspan=0:2*pi/p.omega_n/points:(2*pi/p.omega_n*t_cycles);
%tspan=0:2*pi/p.omega_n/points:(2*pi/p.omega_n*n_cycles);
    [t,g]=ode45(@geneva,tspan,y0,[],p);
    [f,c]=size(g);
    y0=g(f,:);

    %Selecting the cycles to analyze
```

```
    ini=[2*pi/p.omega_n*(t_cycles-ana_cycles)];
    %ini=[2*pi/p.omega_n*(cycles)];
    ini=find(t>ini,1);
    fin=length(t);



    %%%%%%%%Cross flow
    S=g(:,1); %displacement in y
    S=S(ini:fin); %segment to be analyzed
    maxy1=max(S);

    %%%Spectrum
    tao2=t(ini:fin); %tao

    T=tspan(1,2); %sampling period
    Fs=1/T; %sampling frequency

    [freq,out]=spectrum_dos(T,Fs,S,tao2,p);
    freq=2*pi*freq/p.omega_n; %omega_c/omega_n
    %freq2=2*pi*freq; %omega_c
    maxi=max(out);
    pos = find(out==maxi);
    value1=freq(1,pos);

%
%     %%%%%%%In-flow direction


%     S=g(ini:fin,:3);

    S=g(ini:fin,3)-mean(g(ini:fin,3)); %displacement in x

%     S=S(ini:fin); %segment to be analyzed
%     S=g(:,3)-mean(g(:,3)); %displacement in x
    %S=g(:,3); %displacement in x

    maxx1=max(S);

%
%     %Frequency spectrum
    %S=g(:,3)-mean(g(:,3)); %Only for displacement in x

    [freq,out]=spectrum_dos(T,Fs,S,tao2,p);

    freq=2*pi*freq/p.omega_n; %omega_c/omega_n
    %freq2=2*pi*freq; %omega_c
    maxi=max(out);
    pos = find(out==maxi);
    value2=freq(1,pos);

    %%%%%%% Wake oscillator
    S=g(:,5); %displacement in q
    fin=length(t);
    S=S(ini:fin);
    maxq1=max(S);
```

```
%       %%%%Saving values of the spectrum

    val=[value1 value2 0];
    f_n(:,n)=val; %maxima recurrent
    s=[maxy1 maxx1 maxq1];
    y_n(:,n)=s; %maxima recurrent

    %hola=n


%     figure
%     subplot(3,1,1)
%     plot(t,y(:,1))
%     ylabel('displacement y');
%     subplot(3,1,2)
%     plot(t,y(:,5))
%     ylabel('Displacement q');
%     xlabel('t')
%     title('Coupled wake oscillator')
%     subplot(3,1,3)
%     plot(t,y(:,3))
%     ylabel('displacement x');
%     xlabel('t')
    %h = msgbox('Hola Isis');
    disp(n);
end

figure; plot(Vn_n,y_n(1,:))
%  figure; plot(Vn_n,y_n(1,:),Vn_n,f_n(1,:))
 xlabel('Vn');
 title('Cross flow y');

 figure; plot(Vn_n,f_n(1,:))
 xlabel('Vn');
 title('Cross flow response frequency y');

 %figure; plot(Vn_n,y_n(2,:),Vn_n,f_n(2,:))
 figure; plot(Vn_n,y_n(2,:))
 xlabel('Vn');
 title('In-line vibration x');

figure; plot(Vn_n,y_n(2,:),Vn_n,f_n(2,:))
 xlabel('Vn');
 title('In-line response frequency x');


 figure; plot(Vn_n,f_n(2,:))
 xlabel('Vn');
 title('In-line response frequency x');

 disp('Done')
 toc
```